

MARCH, 1965

INSTRUMENTATION DESIGN STUDY FOR TESTING A HYPERSONIC RAMJET ENGINE ON THE X-15 A-2

Volume 2

FACILITY FORM 802	N 65-21464	
	(ACCESSION NUMBER)	(THRU)
	190	7
	(PAGES)	(CODE)
CR-62183	14	
(NASA CR OR TMX OR AD NUMBER)	(CATEGORY)	

PRELIMINARY DESIGN OF

IN-FLIGHT THRUST/DRAG MEASURING DEVICE

By

GPO PRICE \$ _____

D.J. DeMichele

OTS PRICE(S) \$ _____

Dr. R.M. Mains

Hard copy (HC) \$ 5.00

R.L. George

Microfiche (MF) \$ 1.25

N.H. Wood

PREPARED UNDER CONTRACT NO. NAS 4-715

For

NATIONAL AERONAUTICS & SPACE ADMINISTRATION

ADVANCED ENGINE AND TECHNOLOGY DEPARTMENT



CINCINNATI, OHIO 45215

FOREWORD

The preliminary design of the in-flight thrust/drag device constitutes 40% of the instrumentation design study of a hypersonic ramjet engine for testing on the X-15 A-2 aircraft project. This report contains the contributions from the Advanced Technology Laboratory of the General Electric Company who were responsible for this portion of the total project. We also gratefully acknowledge the efforts of all of those who contributed to this project by their knowledge in specialized fields.

TABLE OF CONTENTS

	<u>Page</u>
1.0 INTRODUCTION.	1
2.0 SUMMARY.	3
3.0 DISCUSSION OF DESIGN STUDY.	7
3.1 Structural Attachment. (Engine to Aircraft)	7
3.2 Identifiable Design Problem Areas	7
3.2.1 Forces, Lift, Yaw, Thrust, Drag	7
3.2.2 Thermal Expansion.	8
3.2.3 Local Aerodynamic Heating	8
3.2.4 Jettison Requirement.	8
3.3 System Configuration and Attachment.	9
3.3.1 Attachment to the Aircraft.	9
3.3.1.1 Rigid Attachment.	10
3.3.1.1.1 Strain Detection	10
3.3.1.1.2 Displacement Detection.	10
3.3.1.2 Flexible Attachment.	10
3.3.1.2.1 Rollers.	11
3.3.1.2.2 Beam or Plates.	11
3.3.1.2.3 Link.	11
3.3.1.2.4 Flexural Pivots.	11
3.3.1.2.5 Fluid Bearing.	11
3.3.2 Jettison Arrangement.	12
4.0 PROMISING SUSPENSION SYSTEM CONCEPTS.	13
4.1 Flexible Attachment.	13
4.2 Four Flexure Concepts	13
4.3 Two Point Suspension Roller Element	16
4.4 Two Point Suspension Fluid Bearing	16
5.0 RESULTS OF SUSPENSION SYSTEM ANALYSIS.	20
5.1 Sensing Element Configuration.	20
5.2 Arrangement I (Roller Element Forward).	20
5.3 Arrangement II (Roller Element Aft).	24
5.4 Oil Bearing System.	26
5.4.1 Assumptions.	26
5.4.2 Bearing Design Loads.	27

Table of Contents (Continued)

	<u>Page</u>
5.4.3 Description of Design.	27
5.4.4 Conclusion and Recommendations	31
6.0 RESULTS OF JETTISON DYNAMIC ANALYSIS	33
7.0 AXISYMMETRICAL VS TWO DIMENSIONAL ENGINE.	34
8.0 RECOMMENDATION FOR "FOLLOW UP".	35
8.1 Compatibility Study of Attachment.	35
8.2 Single Prototype Thrust Element Evaluation.	36
8.3 Complete Prototype Thrust Measuring System Evaluation.	37
8.4 Design and Manufacture of Flyable System.	38
9.0 APPENDICES.	41
I ANALYSIS OF SENSOR BLOCK.	41
1.1 Block Concept	41
1.1.1 Strain Detection.	41
1.1.2 Displacement Detection	43
1.2 Spring Constant of Displacement Block	44
1.2.1 Displacement Block Fixed to Ramjet	44
1.2.2 Displacement Block to Measure Friction Forces.	45
1.2.3 Effect of Axial Load on Spring Constant.	45
1.3 Effect of Moment Applied to Base of Blocks.	49
II ANALYSIS OF SUSPENSION SYSTEM WITH ROLLERS AT REAR SUPPORT.	51
2.1 Forces and Moments Applied to Ramjet	51
2.2 Forces and Moments Applied to Sensor-Specific Case.	56
III ANALYSIS OF SUSPENSION SYSTEM WITH ROLLERS AT FRONT SUPPORT.	69
3.1 Forces and Moments Applied to Ramjet.	69
3.2 Forces and Moments Applied to Sensor-Specific Case	73
IV FLUID BEARING ANALYSIS.	81
4.1 Gas Lubricated Configuration.	81
4.2 Oil Lubricated Configuration.	82
4.3 Oil Lubricant.	85

INSTRUMENTATION DESIGN STUDY FOR TESTING

A HYPERSONIC RAMJET ENGINE

ON THE X-15 A-2

PRELIMINARY DESIGN OF IN-FLIGHT THRUST/DRAG

MEASURING DEVICE

By

D. J. DeMichele
R. L. George
Dr. R. M. Mains
N. H. Wood

PREPARED UNDER CONTRACT NO. NAS 4-715

GENERAL ELECTRIC COMPANY
ADVANCED ENGINE & TECHNOLOGY DEPT.
Cincinnati, Ohio 45215

For

NATIONAL AERONAUTICS & SPACE ADMINISTRATION

Table of Contents (Continued)

	<u>Page</u>
V JETTISON ANALYSIS.	86
5.1 Dynamics of Guide System - General Expression	86
5.2 Specific Case Where the Front Roller is at Station 465	89
5.3 Peel-off Jettison Study	91
VI MATHEMATICAL MODEL DYNAMIC ANALYSIS OF SUSPENSION SYSTEM.	94
6.1 Fuel-Line Stiffness	94
6.2 Electrical-Line Stiffness	94
6.3 Static Load Stresses.	94
6.4 Method of Stiffness Compilation.	95
6.5 Results for Peel-off Design.	106
6.6 Results for Fore and Aft Design	106
6.7 Study of the Flexure as a Flexible Support.	119
VII RAMJET THERMAL ANALYSIS.	125
7.1 Ramjet Support Temperature Rise	125
7.2 Thermodynamic Protection Considerations.	125
7.3 Thermal Protection of the Deflection Block	127
VIII SENSOR EVALUATION.	128
8.1 Strain Measurement.	128
8.2 Force Measurement.	128
8.3 Deflection Measurement.	132
8.4 Linear Variable Differential Transformer (LVDT)	132
8.4.1 Principles of Operation.	132
8.4.2 Linearity and Linear Range.	136
8.4.3 Sensitivity and Output.	138
8.4.4 Resolution.	138
8.4.5 Excitation.	138
8.4.6 Phase Characteristics	138
8.4.7 Mounting the Transformer Body.	140
8.4.8 Mounting the Transformer Core.	140
8.4.9 Elevated Temperature.	140
IX ELECTRICAL CIRCUITING.	141
X ACCELEROMETER.	145
XI RANGE EXTENDER	149
XII LITERATURE SEARCH AND REFERENCES	152
REFERENCE AND BIBLIOGRAPHY.	173

TABLES

		<u>Page</u>
6-1	Load Vectors - Case 1 -----	108
6-2	Data Sheet Log - Case 1 -----	109
6-3	Relative Z Motion of Masses 13 and 14 -Case 1 -----	110
6-4	Summary of Stresses - Case 1 -----	111
6-5	Data Sheet Log - Case 2 -----	113
6-6	Load Vectors - Case 2 -----	114
6-7	Relative Z Motion of Masses - Case 2 -----	115
6-8	Summary of Stresses - Case 2 -----	117
6-9	Normal Frequencies - Case 2 -----	118
10-1	Comparison of Common Accelerometers -----	146

PRELIMINARY DRAWINGS

	<u>Page</u>
AFT Deflection Block Assembly	177
Arrangement I - 421D905	
Forward Deflection Block Assembly	178
Arrangement I - 421D892	
AFT Deflection Block Arrangement	179
454C613	
X-15 Axi-Symmetrical Ramjet	180
Thrust/Drag Instrumentation	
587E440	
X-15 Ramjet Thrust/Drag	181
Instrumentation 587E430	
AFT Hydraulic Support	182
Bearing Arrangement 421D904	

1.0 Introduction

Considerable interest exists within the Government in research programs aimed at developing safe, reliable and efficient hypersonic air-breathing engines. A previous feasibility and preliminary design study (reference 1) showed it was feasible to flight test experimental ramjet engines on the X-15 airplane. To aid in such an experimental ramjet test program a list of desired flight test measurements was identified by the NASA Flight Research Center (reference 2). In September 1964, the General Electric Company was awarded a four-month contract, NAS 4-715 to evaluate these measurements and to specifically:

- a) provide a conceptual design of a thrust/drag measuring device
- b) define and provide conceptual designs of other advanced instrumentation requiring development
- c) identify commercially available components
- d) formulate an overall plan to provide the flight instrumentation for ramjet tests.

This report covers the results of a preliminary design study for the thrust drag device to measure net ramjet nacelle thrust or drag transmitted to the X-15 A-2 aircraft.

The design had to fulfill the following requirements.

1. Overall range - 6000 to +6000 lbs.
2. Measurement range - 6000 to +6000 lbs.
- 500 to + 500 lbs.
3. Accuracy - 2%.
4. Dynamic Response 100 cps.
5. Flight test range Mach 3 to Mach 8.
6. Consideration of heating and aerodynamic leakages.

7. Consideration of extraneous aerodynamic forces.
8. Minimum weight and physical size.
9. Compatibility to NASA Edwards data acquisition system.
10. Jettisoning of the ramjet nacelle without impingement on the X-15-2 airplane.
11. Structural integrity at the attachment points on the X-15 aircraft with a safety factor of 1.5.

2.0 Summary

The preliminary design study has produced the following results:

- a) A thrust/drag device can be built to measure the thrust and drag forces to the required accuracy and with the required frequency response.
- b) The ramjet should be suspended from the X-15 from two widely spaced points of attachment to reduce internal axial force errors, friction forces and temperature effects.
- c) One of the attachments should be rigidly attached to the ramjet to provide the required stiffness and support the applied loads.
- d) The second attachment point should be made flexible in the fore and aft direction to provide for thermal growth of the ramjet engine and minimize the effect of extraneous forces.
- e) The thrust and drag forces of the ramjet will produce deflections in deflection block sensors at both points of support. These deflections will be sensed by linear variable differential transformers (LVDT).
- f) Rollers were selected for the flexible point of support because thermal expansion is not a limiting factor in their design and they are of low weight. Fluid bearings considered for this purpose were too heavy.
- g) To determine the effects of assumptions, verify computations, and minimize weight, a full size model simulating dynamic characteristics of the ventral fin suspension, deflection blocks, and ramjet is recommended to measure frictional forces, to determine effects of thermal gradients, to test electrical circuitry, to determine resonance frequencies, and to verify calculations.
- h) If a ramjet other than the 188 inch two dimensional ramjet considered in this study is to be used, the results of these calculations and designs should be reviewed but methods used are appropriate.
- i) The thrust/drag device can be developed with a follow-on program consisting of 4 phases. Development can be completed by mid-calendar year 1967 if started now.

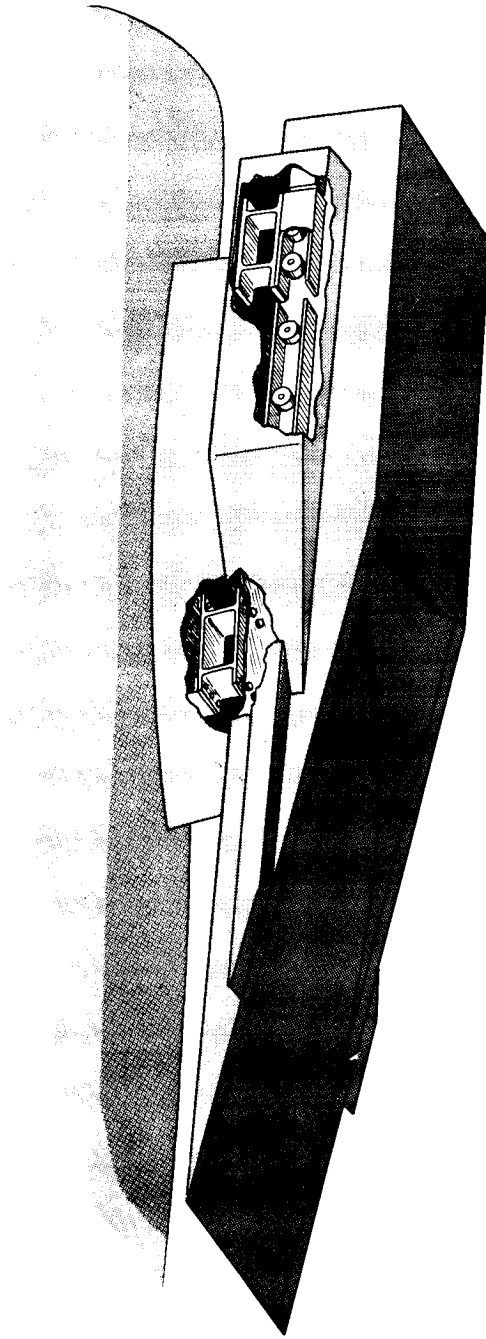
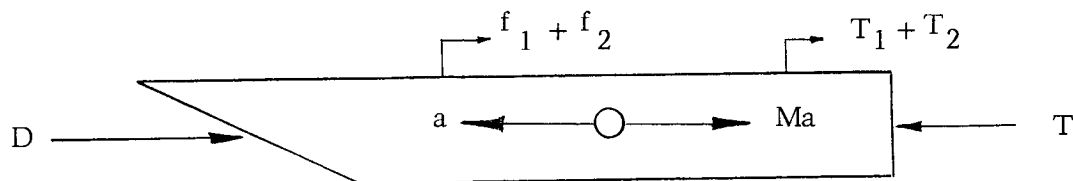


Figure 1 Artist Conception of Thrust-Drag Measurement System

- j) Figure 1 shows an artist conception of the thrust drag measuring device. It can be noted that the flexible support is mounted aft. It is, however, recommended that in the final design the flexible support be placed forward.

The thrust/drag measuring system as designed consists of the following measurements which will result in the final net thrust developed by the engine, (1) thrust and drag by the fixed aft deflection blocks; (2) the roller friction force at the forward flexible deflection blocks; (3) the inertial force recorded by an accelerometer mounted on the ramjet .

The analysis as shown below from the free body diagram illustrates the procedure by which the net thrust is obtained. This can be done either electronically or by computation. (See Figure 2)



$$(T_1 + T_2) + (f_1 + f_2) - T + D + Ma = 0$$

$$-D = (T_1 + T_2)_c + (f_1 + f_2)_c + Ma$$

$$T = (T_1 + T_2)_h + (f_1 + f_2)_h + D + Ma$$

$$T_m = T - D_e$$

(c) Denotes cold
(h) Denotes hot

T = engine thrust
D = engine drag
f = tare forces at flexible support
M = engine weight
a = acceleration forces

Figure 2

The drag (D_e) will be recorded during cold flow engine tests in-flight. The thrust (T) will be recorded with the engine hot to obtain the necessary information. Calibration to determine drag characteristics of the engine is also necessary by testing the ramjet in a wind tunnel.

The study also indicated that the measurement of internal thrust either by electro-mechanical system or by pressure probing is impractical in a two dimensional engine.

3.0 DISCUSSION OF DESIGN STUDY

3.1 Structural Attachment - Engine to Aircraft

A major objective of this portion of the design study program was to devise a means of coupling the measurement sensors (described in Section 5.1) to the engine and the aircraft such that the required thrust and drag forces could be measured.

Principle factors which influenced the design of the thrust/drag measurement system include the following:

- (a) Structural support and stability under extreme aerodynamic loads.
- (b) Frequency response of 100 cps
- (c) Environmental protection against loads and temperatures expected at Mach 8 flight conditions.
- (d) System sensitivity of 10 pounds of thrust or drag.
- (e) Provision for jettison of engine under any flight condition.

3.2 Identifiable Design Problem Areas

The structural support and connection system function can be accomplished in a number of different ways, each way representing different approaches to the major identifiable problem areas. The following problem areas were determined those most critical and solutions were generated for each which are feasible, and warrant development.

3.2.1 Forces: Lift, Yaw, Thrust & Drag. Two configurations of engine are contemplated for the application, two dimensional and axisymmetric. Of the two, the two-dimensional engine represents the most severe problem from the load aspect. Therefore, effort was concentrated on this engine with the philosophy that if an acceptable solution could be generated for the extreme condition, then a ready solution for the less extreme condition would be relatively simple.

From the approximate drag coefficients and areas, it has been determined that a 60,000 pound lift force is generated on the inlet ramp. This force produces extremely large moments and resulting compressive and tensile loads at points of engine support. For a selected two point suspension, resulting loads were 120,000 lb. compressive at the front support and 60,000 lb. tensile at the aft support. The thrust system must be designed to accommodate the loads without resulting system error.

Considering engine weight and the requirement for a frequency response of 100 cps, the stiffness of the thrust sensing elements becomes quite high ($k = 3-4 \times 10^6$ lbs/in.).

With a sensing element of this nature, and a sensitivity of 10 pounds, the strain or deflection, which ever is measured will be extremely small.

Thus with small values of "sensing" signal to work with, the effect of other extraneous forces, yaw, bending moments, friction and temperature differential generated forces must be given serious consideration.

3.2.2 Thermal Expansion. The actual degree of thermal expansion cannot be predicted with any degree of accuracy. Temperatures of the X-15 at Mach 6 provide some information, but there is no information available for expected engine temperatures. The flight profile provides useful information, in that under the procedure, the actual time in the "measurement mode" will be short, thus reducing the effect of transient temperature rises. While this tends to minimize the effect of temperature on the actual measurement, the long term effect must be the governing criteria to preserve the integrity of the system for subsequent use. It is anticipated that the engine length change between attachment points could be quite large compared to the X-15 length change at the same points of attachment.

The basic problem therefore, becomes that of providing means of accommodating this length change without affecting the measurement sensing system accuracy.

3.2.3 Local Aerodynamic Heating. A third critical problem area is that of protection of the measurement system from adverse effects of hot gas. The flow field of the aircraft/engine combination is unknown and will probably not be known to any real degree of accuracy until actual flight. It is, therefore, necessary to assume that a maximum of protection must be provided. The protection provided however, must not in anyway produce a "negative" effect or error in the measurement system. For example, physical contact of ablative protection would produce friction forces felt by the sensor as thrust or drag which would appear as part of the total force measured, but inseparable as error.

The specific problem is that of providing protection of the measurement system from hot gas flow such that:

- a. Physical contact does not exist which will produce an immeasurable error force.
- b. Hot gas leakage does not produce a temperature rise in the sensor elements that is not "cancellable" or detectable during the measurement portion of mission profile, and,

- c. Does not produce a total temperature rise which would exceed the "life" temperature limit of the sensing system.

3.2.4 Jettison Requirement. The fourth major problem area is the selection of a means of jettison of the engine from the aircraft during an emergency which will not impair the function of the measurement system during the measurement mode of the mission profile. While full scale consideration of the actual means of jettison is not actually a part of the scope of the design study of the instrumentation, the requirement of sensing system compatibility necessitated detailed consideration of the means of jettison. The actual means of jettison imposes a definite limit on the approaches which can be taken toward solution of a number of the above problems, particularly the support system and hot gas protection considerations.

3.3 System Configuration and Attachment

During the course of the study, a number of means of support and jettison of the engine were considered. From detailed consideration of these configurations the following conclusions were drawn:

- a. A two point support system should be used with one point fixed and one "flexible" to accommodate an appreciable length change.
- b. Axial forces resulting from sources other than engine drag or thrust (friction, thermal expansion, etc.) must be measured and an appropriate correction provided. A two point suspension system provides opportunity to cancel these forces because of the resulting equal and opposite effect between support points.

It is on this premise, and within the limits of available structure information that the proposed system has been developed.

3.3.1 Attachment to the Aircraft. The possible points of attachment of the ramjet to the aircraft are relatively limited. Three choices exist - (1) Direct attachment to the X-15 structural members, completely independent of the ventral fin assembly using the fin assembly only as a protective device. (2) Attachment to the ventral fin assembly, transmitting all loads from the engine to the aircraft through the fin structure, or (3) A combination of 1 and 2.

No specific preference is expressed at this point, but the later appears the most likely arrangement. In any event, a new ventral fin assembly with the lower ventral hydraulic drive system removed will undoubtedly be required, with structural stiffening required at the forward support location.

From examination of the aircraft structure the areas between stations 483-495 and between 557 (approx.) and 565 appear to be the only points capable of withstanding the loads which will be imposed by the two point system. This should be confirmed by the aircraft designer since it is beyond the scope of this program.

The load distribution on the engine is also a consideration in making the choice of 1, 2 or 3 above. While a single support direct to the fuselage independent of the fin at STA. 483-495 is possible, such an arrangement may pose a severe loading on the engine. The areas between fuselage stations 483-565 provide possible location for strong points of attachment from the ramjet to the ventral fin area. These points provide support at approximately the center and extreme aft end of the 188 inch ramjet. Because of the expected relative thermal expansion between the ramjet and X-15 support structure, one support will be rigidly attached and the other designed to allow for thermal expansion.

3.3.1.1 Rigid Attachments. The force sensing element is bolted securely to the ramjet providing a direct thrust-drag force path to the sensor. At jettison this joint is severed by explosive bolts. This force sensing element is designed to support all aerodynamic forces and detect a horizontal force of less than 500 pounds with 10 pounds accuracy and less than 6000 pounds with 120 pound accuracy. Two candidate methods of measuring the horizontal force are to measure either the strain in an element or the relative displacements in a supporting structure.

3.3.1.1.1 Strain Detection. Strain detection method is analyzed and discussed in Appendix I. It is concluded that with wire or foil gages with a threshold strain of 10×10^{-6} in/in and the specification of a frequency response of 100 cps, the supporting structure cannot be designed to both support all aerodynamic forces and provide a measuring system to satisfy the required accuracy. If semi-conductor strain gages could be used with a threshold strain of 1×10^{-6} , it would be feasible to design a structure at fuselage station 565 that supports all forces and satisfies accuracy requirement. However, the state-of-the-art of semi-conductor gages must be further developed before they could be used for this application.

3.3.1.1.2 Displacement Detection. A deflection block (see Figure 1-1 of Appendix I, Section 9.0) consisting of two vertical plates rigidly attached to a stiff base and top plate has been designed to transfer horizontal forces to the X-15. These forces will be measured by recording the displacement between the top and bottom plates with a linear variable differential transformer (LVDT).

3.3.1.2 Flexible Attachment. A flexible attachment is necessary in order to support aerodynamic loads and provide for thermal growth of the ramjet engine. Ideally, axial forces at this attachment point less than 10 pounds would not affect the overall measurement accuracy. It is estimated that relative motion differences between the X-15 and the ramjet will be on the order of 1/4 inch. (Based on maximum temperature difference between aircraft and engine of 500-600°F)

3.3.1.2.1 Rollers. A rolling element between the ramjet and X-15 provides a flexible attachment with unlimited horizontal travel. Temperature differences between the X-15 and ramjet are not a primary factor in its design. The horizontal friction force, however, will be greater than 10 pounds and must be measured either with strain gages or LVDT's. Since LVDT's must be used in the rigid attachment, they are recommended here for compatibility of instrumentation.

3.3.1.2.2 Beam or Plates. A plate rigidly attached to the X-15 and ramjet can be designed as a flexible attachment; flexible in comparison to the spring constant of the deflection block. The most favorable location for a plate support is at fuselage station 565 because of the reduced forces. A plate 12 inches long and 6 inches wide would have a thickness of about 0.20 inches if the material had an ultimate strength of 150,000 psi. When the deflection approaches the beam thickness, the stresses in the plate and spring constant become non-linear. Since the expected maximum deflections exceed the thickness, operation in the non-linear region is expected. The non-linearity complicates the calibration.

The large axial force applied to the beam will produce a bending moment in the beam of the same order of magnitude as that produced by the drag force if the beam is deflected 1/4 inches. This moment introduces an error to the force measuring system that must be measured if the accuracy requirements are to be met. To measure this error the axial load and deflection of the beam must be known. This data can be obtained if strain gages are mounted at two points along the beam and the beam is calibrated.

3.3.1.2.3 Link. A rigid member attached to a pivot on the ramjet and X-15 provides a flexible attachment. Because of the friction in the pivots a force sensing element similar to the deflection block has to be included between the link and X-15. Also, as such a link becomes inclined to the vertical under a high lift load, a horizontal component of force is generated as a function of the angle. For accurate error compensation, both the lift force and the angle must be measured.

3.3.1.2.4 Flexural Pivots. The arrangement of the flexible support is the same as that of the link except flexural pivots are used for the pivots instead of bearings. It was the intention of this pivot that no force sensor be required. It was not possible to design a flexural pivot that will support the aerodynamic loads and provide a 1/4 inch deflection without producing a horizontal force of 10 pounds. Therefore a force sensing element, either strain or displacement gages must be included that also measures the lift force and deflection of the ramjet with respect to the X-15.

3.3.1.2.5 Fluid Bearing. An ideal flexible attachment can be designed with a fluid bearing. Expected friction forces would be less than the threshold force measured by the deflection block. The rear suspension point is the better location for the bearing because of the reduced loading and increased space available for mounting.

3.3.2 Jettison Arrangement. Two basic methods for jettisoning the ramjet with which the suspension system must be compatible have been considered in this study. They are the fore-aft slider arrangement and peel off. The fore-aft arrangement has rollers or slides mounted on the ramjet and guided by a track or way built into the ventral fin extension. Only the rollers in contact with the deflection block touch the track when the ramjet is in the measurement mode. The new ventral fin must be designed to withstand the forces encountered during jettison which adds weight to the over-all system. Weight is also added by the jettison rollers and slides required to guide the ramjet during jettison. It is estimated that the weight of the fore-aft jettison system will be greater than the peel off system. The ejection force to the ramjet may be supplied either by a explosive charge or hydraulic means once the structural suspension system has been severed from the ramjet.

The peel off system has the ramjet pivoted at the rear support and an ejection force supplied by an explosive charge at the front support until the engine has rotated about 7° . At this point the ramjet swings clear of the pivot and the aerodynamic forces push the ramjet from the X-15. This system does not require the ventral fin extension to carry the jettison guide force and, therefore, can be made lighter in weight. However, the ramjet must have the strength to withstand the ejection forces. The rear pivot must be extremely strong to prevent swaying of the ramjet once the suspension system releases the ramjet. This jettison system was reviewed with NASA and rejected. No further development of this system was done once this decision was reached.

To obtain the frequency response of 100 cps, at least one suspension point must be firmly fastened to the ramjet. This point must be extremely stiff in the fore-aft direction and released at jettison. Explosive bolts, hydraulic ball joints, and fractureable structural members can be used to form this rigid joint. The explosive bolts are double fused and even double charged if required to obtain the reliability of performance required for this system. Failure of the bolt occurs between the ramjet and suspension component producing a clean break with minimum resistance to jettison. The hydraulic ball joints were not considered adequate to supply the drawing force required to produce a strong joint. Structural elements that are fractured by the main ejection force transmitted through the ramjet was not considered satisfactory because of possible premature failure of the ramjet. Other means of structural failure require an explosive charge.

4.0 PROMISING SUSPENSION SYSTEM CONCEPTS

The rigid and flexible methods of attachment were integrated to form a suspension system compatible with fore-aft and/or the peel off mode at jettison. As a preliminary means of evaluation, a free body diagram of the forces acting in each component was analyzed to determine the forces being measured and those to be kept low. Each of the four systems considered had attachment points to the X-15 between stations 483 and 495 and at 565 as discussed in section 3.

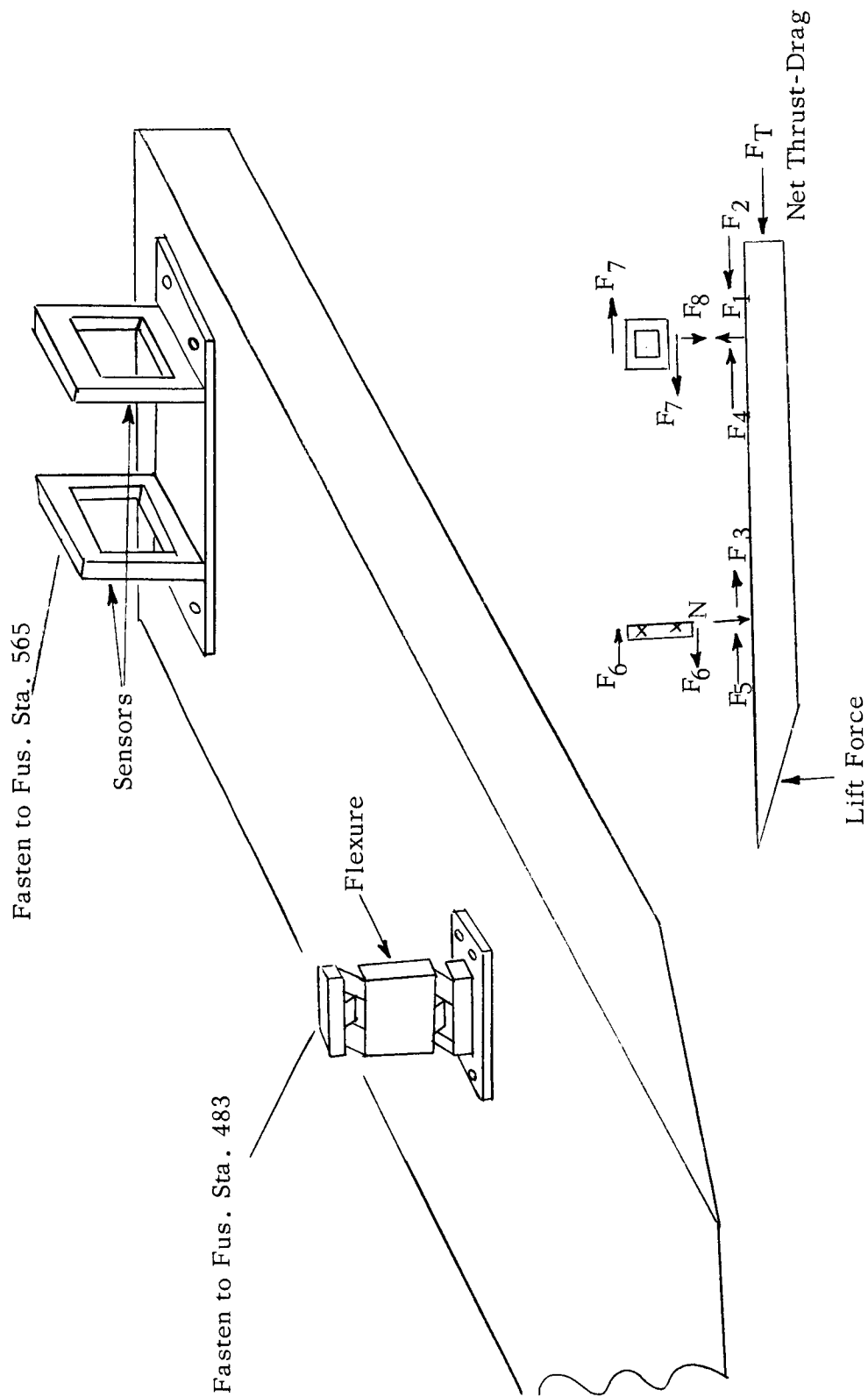
4.1 Flexible Attachment at 483 and Fixed Attachment at 565

This suspension system is shown schematically in Figure 3 with a flexural pivot (discussed in section 3.1.2.4) located at X-15 fuselage station 483 and deflection blocks at fuselage station 565. The system is compatible with either the fore-aft and peel off mode of jettison. For fore-aft jettison, the ejection force system is located between the two rear deflection blocks. At jettison the explosive bolts fastening flexible and rigid attachments to the ramjet are ignited releasing the ramjet simultaneously with the fore-aft ejection force. For peel off the ejection force is applied vertically at fuselage station 483 and a pivot about which the ramjet rotates is located between the two rear deflection blocks and the ramjet. At jettison the explosive bolts fastening the front attachment are ignited releasing the front of the ramjet.

From the force analysis shown in Figure 3 the deflection blocks measure the thrust/drag force plus the horizontal force acting on the flexible attachment. A flexible attachment using rollers, beams, links and flexure pivot can not be designed to withstand the large forces resulting from the lift force and accomodate a 1/4 inch deflection with a horizontal force of less than 10 pounds. The same conclusion is reached if the flexible attachment is at fuselage station 565 when the lift loads are reduced. It is, however, possible to include a fluid bearing as the flexible attachment. If used, the flexible attachment must be at fuselage station 565 instead of 483 to reduce the loads acting on the bearing.

4.2 Four Flexure Concept

The four flexure concept shown in Figure 4 was conceived primarily for



F_2 & F_3 result from thermal expansion

$$F_2 = F_3 \text{ (equal \& opposite)}$$

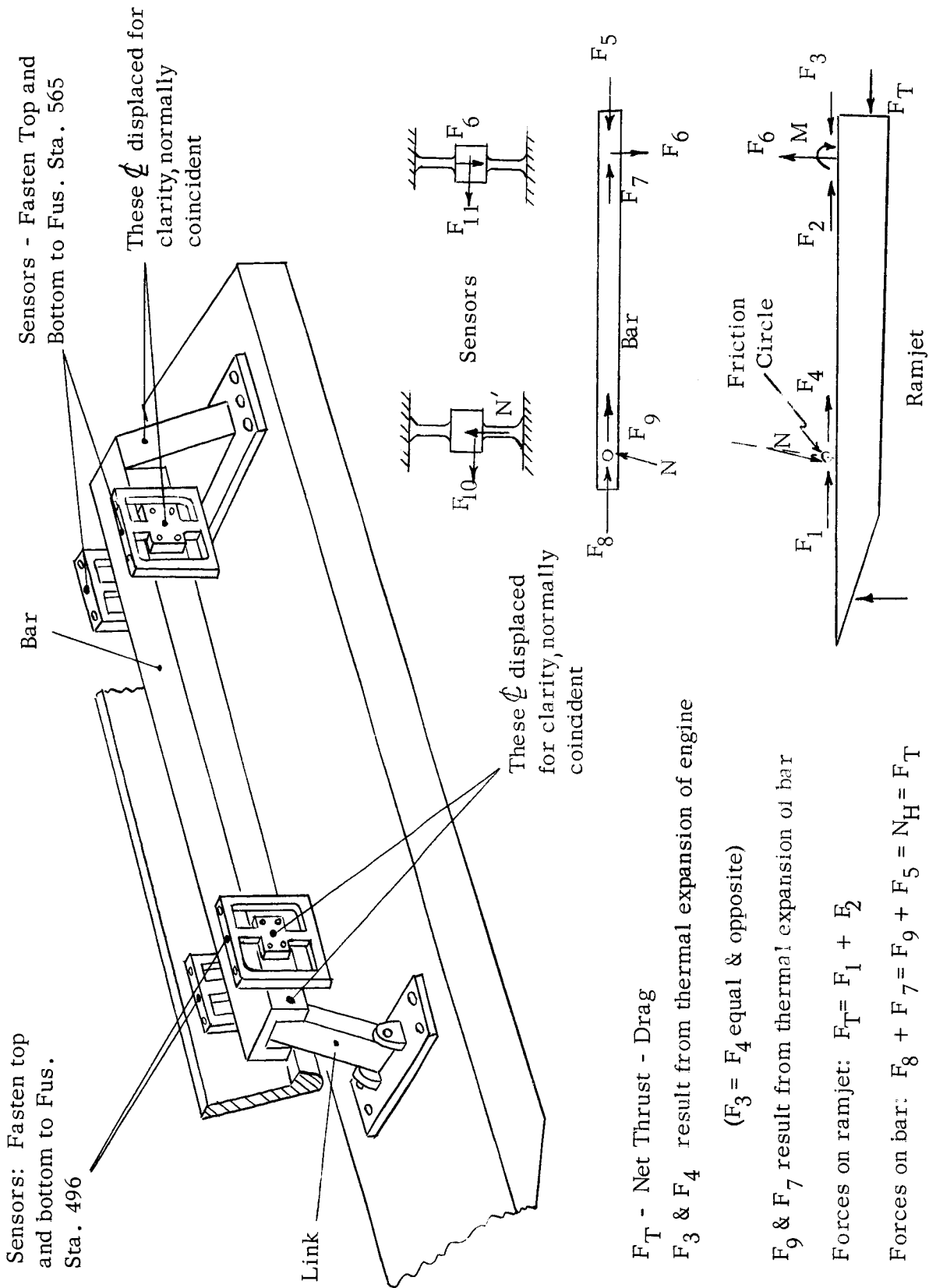
$$F_T = F_5 + F_4 + F_3 - F_2 = F_5 + F_4$$

Measure F_7

$$F_7 = F_4 - F_2 = F_M \therefore F_M = F_T - F_5 - F_2 = F_T - F_5 - F_3 = F_T - F_6$$

Flexure Force F_6 must be less than 2% F_T

Figure 3 Flexible Attachment



Sensors: Fasten top and bottom to Fus. Sta. 496

Sensors - Fasten Top and Bottom to Fus. Sta. 565

These displaced for clarity, normally coincident

These displaced for clarity, normally coincident

F_T - Net Thrust - Drag
 F_3 & F_4 result from thermal expansion of engine

($F_3 = F_4$ equal & opposite)

F_9 & F_7 result from thermal expansion of bar

Forces on ramjet: $F_T = F_1 + E_2$

Forces on bar: $F_8 + F_7 = F_9 + F_5 = N_H = F_T$

Measure F_{10} & F_{11} : $F_8 + F_7 = F_{10} + F_{11} = F_T$

Figure 4 Four Flexure Concept

the peel off jettison system but can be made compatible with the fore-aft jettison. At the front support is a link to allow for thermal expansion and also serves a cylinder piston construction providing the ejection force for peel off jettison. The pivot for jettison is located between the rear support and the ramjet. A bar running the length of the ventral fin will change length due to thermal expansion but this expansion will be appreciably less than that of the ramjet thus reducing excessive deflection of the flexures. This expansion produces equal and opposite forces to the sensors which are connected to cancel this effect. To insure frequency response the sensors must measure deflection as discussed in section 3.1.1.

From the force analysis shown in Figure 4 the effect of thermal-expansion can be successfully subtracted from the force reading if the horizontal force is measured at the front and rear suspension points. This system also compensates for the horizontal force error induced by an inclined link under a large axial force. Development of this system was dropped when peel off mode of jettison was rejected.

4.3 Two Point Suspension Roller Element

A suspension system using rolling elements as the flexible means of attachment is shown in Figure 5 with the flexible element at the front suspension point. The result of this discussion also applies to a system with the flexible support in the rear. This system is readily adaptable to the fore-aft mode of jettison but can easily be made compatible with peel off jettison. The ejection force system is located between the aft deflection blocks. At jettison explosive bolts release the rear support and the ejection force is applied. The rolling element of the front attachment point also serves as guides for the ramjet.

From the force analysis also included in Figure 5 it is concluded that thermal expansion effects can be eliminated if the friction of the rollers are measured. This system was selected for further development because it compensated for thermal expansion and the magnitude of this expansion is not a limiting factor, and the estimated weight of the entire system was lower than other systems giving the same performance.

4.4 Two Point Suspension Fluid Bearing

It was pointed out in sections 3.1.2.5 and 4.1 that a fluid bearing would

provide such a low friction support that it would not have to be measured. A system incorporating a fluid bearing is shown in Figure 6 with the bearing at 565. This location is preferred because of the reduced forces from the lift force and larger space inside the ventral fin available for mounting. Further development of a fluid bearing was undertaken and is reported in section 5.4.

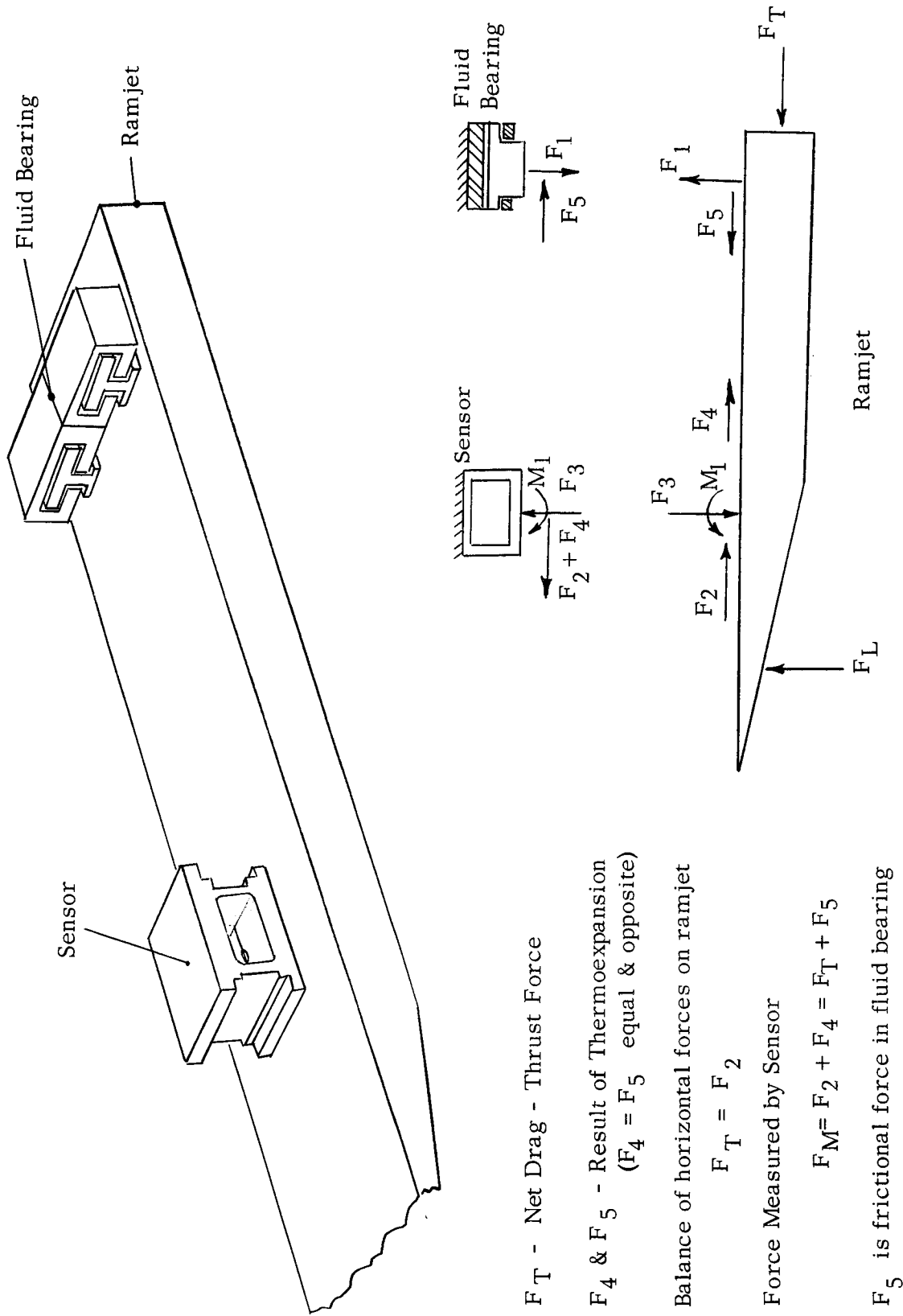


Figure 6 Two Point Suspension Fluid Bearing

5.0 RESULTS OF SUSPENSION SYSTEM ANALYSIS

Suspension systems using rolling elements as the flexible means of attachment and a deflection block as the rigid attachment were further developed. This concept was chosen because (1) the extent of thermal expansion is not a limiting factor in its design, (2) the force sensing element is easily made compatible with the deflection block of the rigid attachment point, and (3) the suspension system weight is as low as other concepts.

Also receiving further development was an arrangement using a fluid bearing as the flexible point of attachment. The fluid bearing has the advantage that no force sensing instrumentation is required because of its low frictional properties. Weight, however, is a major problem.

5.1 Sensing Element Configuration

A common component in all suspension systems considered for further development is the force sensing element. As discussed in Section 3.1 and Appendix I, the rigidly attached sensing element must measure displacements instead of strain to insure specified accuracy of the measuring system. A "deflection block" housing a LVDT and accelerometers and consisting of two vertical plates separated 4 inches and rigidly attached to stiff top and bottom plates has been designed as a rigid attachment shown in Dwg. 454C613. For system compatibility the frictional force in the rollers will also be measured by sensing displacement. A "deflection block" similar to that shown in Dwg. 454C613 with a slightly different spring constant is capable of measuring friction forces of at least 10 pounds.

Errors can be introduced into the force measurement by large applied moments to the deflection block, relative thermal expansion between the top and bottom plate, and shifting of assembled components from vibration environment. The lift force and stiffness of the ramjet produces a large applied moment about an axis of the LVDT creating compressive forces in one vertical plate and tensile forces in the other (y axis in Figure 1-1 in Appendix I). LVDT's are insensitive to rotations and radial translations of the armature in the stator. An error, however, is introduced if the center of the LVDT does not coincide with the exact center of rotation of the base plate. Tolerances on the LVDT location will be about 0.001 inches based on the analysis in Appendices II and III. This tolerance could be widened if the lift force and its point of application in front of the forward suspension point are reduced or a flexible

joint is introduced between the deflection block and ramjet to reduce moments transmitted to the deflection block. The flexible joint, however, can only be used if its fore-aft spring constant is 10 times greater than that of the deflection block. Further development of the joint should be considered if the engine manufacturer requires a reduction of applied moments.

A thermal gradient may exist across the deflection block causing the base plate to expand relative to the top plates. The change in length causes the two vertical plates of exact dimensions to deflect in equal and opposite directions. Considering a free body diagram, any change in length of the top or base plates will produce equal and opposite deflections in the vertical plates. Therefore, when thermal expansion does exist the armature suspended between the two vertical plates undergoes either a uniform tension or compression force but its center is not displaced relative to the center of the top or bottom plates. An error can be introduced if the LVDT is not mounted symmetrically in the deflection block and the armature is not suspended between the two vertical plates.

Joints required for assembly of the deflection block must be pinned and bolted to eliminate any shifting of components in a vibrating environment.

5.2 Arrangement I (Roller Element Forward)

The suspension system designated as arrangement I (G.E. Dwg. 587E430) consists of a flexible support of rollers at fus. sta. 483-495 and a rigid support at fus. sta. 565. There are two roller assemblies mounted at the front support on either side of the ramjet in the extended ventral fin area. An assembly is shown in greater detail in Dwg. 421D892 where all supporting structure attaching the deflection block to the X-15 is conceptual. The deflection block is shown mounted in the side of the ventral fin extension that is aerodynamically designed for minimum drag and providing space for suspension system mounting. It is possible to relocate the deflection blocks to the lateral section of the ventral fin extension as shown in view D arrangement II (G.E. Dwg. 587E430) raising the rollers to the top of the ramjet. No preferred point of attachment is recommended in this study. Selection of such a point must be based on ventral fin structural design, ramjet structure, and deflection block design.

Rollers 4 inches in diameter are required to reduce the contact stresses to reasonable levels. (See Appendix II). These rollers, attached to the ramjet with 1 3/4 inch shafts, have hardened rims that roll on hardened steel ways mounted to a deflection block and isolated from the surrounding ventral fin

structure. Also rolling on this guide way are lateral bearings, one on each side of ramjet, that provides lateral support. One of the lateral bearings is spring loaded to cover manufacturing tolerances. Fore and aft friction forces are measured by the deflection block and displacement between the ramjet and ventral fin is isolated from the force measured. In the measurement mode, the only guide rollers in contact with the guide rail are those in contact with the deflection block.

Two deflection blocks located at fus. sta. 565 are rigidly attached to the ramjet and separated symmetrically about the center line of the ramjet to provide lateral support to the mounting system and space for the jettison cylinder as shown in Dwg. 421D905. Accelerometers are shown attached to the deflection block to measure the "g" forces between the X-15 and ramjet.

Also shown are the service lines, fuel, electrical, and coolant conduits connected to the ramjet adjacent to deflection block to minimize the effect of their stiffness and thermal expansion on the force measurements. The spring constant of the service lines are to be at least 1/100 less than that of the rigidly attached deflection block or 4×10^4 #/in.

The arrangements shown in G.E. Dwg. 587E430 are with a two dimensional ramjet 188 inches long 24 inches wide and 21 inches high. With a ventral fin height of 15 inches measured at the center line of the X-15 skin, there will be a ground clearance of 6" at landing

At jettison the double fused explosion bolts holding the rear deflection blocks are released and the explosive charge in the jettison cylinder is ignited. The piston slowly moves to take up the space between the piston head and pad provided for thermal expansion. When the piston strikes the pad mounted to the ramjet, the second charge of the two charge propellant is ignited giving the ramjet its initial jettison push. An analysis of the ramjet dynamics during jettison was made in Appendix V resulting in the requirement that the ramjet must be guided until its nose is past fus. sta. 565 if a lift force of 60,000 pounds acts during jettison. If not completely guided, the ramjet will strike the ventral fin if jettisoned with a drag force of 6000 pounds and a lift force of 60,000 pounds (Mach 8 conditions). Instead of using rollers at the ramjet's nose, a guide skid coated with ablative teflon is used that extends from the most forward ramjet position into the guide way of the ventral fin extension. This guide skid serves also as a plug to prevent high velocity air from entering the guide ways. Service connectors must be adequately supported to enable a clean disconnect at jettison. The fuel lines are equipped with quick disconnect that shuts the fuel flow off when disconnected.

The maximum forces and moments applied to the suspension system are computed in Appendix III. In this analysis a lift force of 60,000 pounds acting at fus. sta. 425, a lateral force of 10,000 pounds uniformly distributed along the side due to a yaw angle, and a 6,000 pound drag force acting at the center of the ramjet were taken as the maximum loads that the suspension system must resist. The ramjet is assumed to be a beam with constant EI along its length where the moment of inertia, I, was computed assuming the engine consisted of two plates, top and bottom, 1/2 inches thick, 24 inches wide, and weighing 500 pounds resulting in an I of 2280 in⁴. The analysis was conducted by first writing the force and moment equations of equilibrium. Where a statically indeterminate beam existed, a differential equation for the moment at any point in the ramjet was written and solved applying boundary conditions. The resultant loading on the rigidly attached front deflection block is shown in Figure 3-2 and on the rear deflection blocks is shown in Figure 3-1. This loading produces a maximum stress of 78,570 psi in the front deflection block and 43,115 psi in the rear. Applying the safety factor of 1.5, the ultimate strength of the material must be at least 118,000 psi. It is recommended that 17-4PH stainless steel be used for all deflection blocks because its ultimate strength is 157,000 psi at 800°F and exhibits low hysteresis characteristics. Temperature measurements made on the existing X-15 ventral fin shows the temperature does not exceed 400°F at Mach 6. Therefore with the deflection block mounted in the ventral fin, the temperature at Mach 8 is not expected to exceed 800°F.

Having computed the applied forces and moments to the deflection blocks, it is possible to estimate the tolerances in positioning the LVDT that must be held if error due to applied moments to the deflection block discussed in Section 5.1 is to be kept within specified accuracy. From the results of Appendix III, the rigidly attached deflection block must have the LVDT located within 0.00236 inches of the rotation center of the deflection blocks base. The deflection block measuring friction must have its LVDT located within 0.00167 inches of the rotation center. The tolerance in the rigidly attached deflection block can be increased by including a flexible joint between the deflection block and ramjet. This joint must have no horizontal backlash and a horizontal stiffness that is at least 10 times that of the deflection block while being flexible when subjected to moment.

The error induced by applied moments on the deflection block measuring friction force is a result of load transmission by the rollers to the guide ways because of relative thermal expansion between the ramjet and the ventral fin structure. The tolerances may be increased if the load were uniformly distributed along the base of the deflection block. This load distribution is achieved by substituting linear roller bearings for the two rollers. An arrangement with

linear roller bearings is shown in Dwg. 421D892. The use of this bearing allows the guide ways to be reduced in height because the distribution of load relaxes the constant stresses so smaller rollers can be used.

The force sensing instrumentation is protected from the high velocity air by mounting the deflection blocks in the ventral fin. Exposed areas of the instrumentation are the rollers and the base of the rear deflection block. The teflon coated guide skid is expected to divert the high velocity air from entering the guide channel in the ventral fin extension. High velocity air will enter the space between the ventral fin and ramjet. The flow field and pressure in this area were not included in this study. If required, this flow may be diverted from the base of the fixed deflection block by mounting a reflector between the ramjet and ventral fin in front of this deflection block. The spring constant should be 1/100 that of the deflection block to eliminate errors. It may also be possible to design a flow reflector along the ventral fin's leading edge to divert the major part of the flow from entering the space between the ventral fin and ramjet.

5.3 Arrangement II (Roller Element Aft)

The suspension system designated as "Arrangement II", G. E. Dwg. 587E430, consists of a flexible support of rollers in the vicinity of fus. sta. 565 and a rigid support between fus. stat. 483-495. There are two roller assemblies mounted at the rear support on either side of the ramjet in the extended ventral fin area. An assembly is shown in greater detail in Dwg. 421D892 where all supporting structure attaching the deflection block to the X-15 and ramjet is conceptual. If required, the deflection blocks may be positioned inside the existing ventral fin profile if the ramjet can accommodate the mounting of the rollers and space for guide channel. Rollers attached to the ramjet must be 2 inches in diameter to reduce the contact stresses to reasonable levels (see Appendix II). These rollers have hardened rims and roll on hardened steel ways to reduce the coefficient of friction. Also rolling on the guide ways mounted to the deflection block are lateral bearings that provide lateral support mounted with the same manner as those in Arrangement I. Fore and aft friction forces are measured by the deflection block and displacement sensor while any effect of thermal expansion between the ramjet and ventral fin is omitted from the force measurement because the guide way mounted to the deflection block is isolated from the ventral fin structure. In the measurement mode, the only rollers in contact with the guide way are those in contact with the deflection block.

One deflection block is located between fus. sta. 483 and 495 and is rigidly attached to the ramjet similar to method identified in Dwg. 421D905. Also shown are the service lines connected to the ramjet in the vicinity of the rigidly mounted deflection block to reduce errors induced by their stiffness. Accelerometers are shown attached to the deflection block to measure the accelerations of the ramjet and X-15. The "g" forces are factored into the thrust-drag reading.

The ground clearance will be the same as that of Arrangement I, 6 inches.

At jettison the double fused explosive bolts holding the front deflection block are ignited, fracturing the pads separating the deflection block and ramjet permitting the guide rollers to contact the guide channel. Simultaneously one explosive charge in the jettison cylinder is ignited slowly moving the piston to take up the space between the piston head and pad. Note that the clearance required in Arrangement II is larger than that required in Arrangement I because the distance from the rigidly mounted deflection block is greater which permits a larger thermal displacement. When the piston strikes the pad mounted to the ramjet, the second and more rapidly burning explosive of the 2 propellant charges is ignited giving the ramjet its initial jettison push. The requirements in guiding the ramjet are the same as Arrangement I.

The forces and moments applied to the suspension system are computed in Appendix III. In this analysis the external forces acting on the ramjet, the stiffness of the ramjet, and methods used in the analysis are the same as that used in analysis of Arrangement I. The resultant loading on the rigidly attached front deflection block is shown in Figure 2-1 and on the rear deflection blocks is shown in Figure 2-2. This loading produces a maximum stress of 99,645 psi in the front deflection block and only 25,391 psi in the rear. Applying the safety factor of 1.5, the ultimate strength of the material must be at least 150,000 psi. It is recommended as in Arrangement I that 17-4PH stainless steel be used for both deflection blocks.

Having computed the applied forces and moments to the deflection block, it is possible to estimate the tolerances that must be held if the error due to applied moment to the deflection block as discussed in Section 5.1 is to be kept within specified limits. From the results of Appendix II, the rigidly mounted deflection block must have its LVDT located within 0.0003 inches of the center of rotation of the deflection block's base. The deflection block measuring friction must have its LVDT located within 0.003 inches of the center of rotation. This tolerance is based on an analysis in which it was assumed that all the energy supplied to the deflection block by the moment is put into strain energy of tension and compression of the vertical plates. However, some energy goes into bend-

ing the side plates which was assumed negligible for small rotations. If bending is large the tolerances on the LVDT location should increase. The tolerances can also be increased by including a flexible joint between the deflection block and ramjet if the stiffness of the joint in the fore aft plane is 10 times that of the deflection block and if it has no backlash.

The error induced by applied moments on the deflection block measuring friction force is a result of load shifting as discussed for Arrangement I. This error can be reduced by a more uniformly distributed load as obtained by a linear roller bearing. Linear roller bearings are shown in G.E. Dwg. 587E430 Arrangement II aft suspension and Dwg. 421D892 in greater detail.

The instrumentation is protected by the same methods as discussed for Arrangement I.

5.4 Oil Bearing System

As described in detail in Appendix IV, feasibility of two hydrostatic (sometimes called "externally pressurized") bearing systems was examined. One used a supply of high pressure gas to support the aft engine attachment member, and the other used a circulating high pressure oil system. Of the two, only the oil bearing design proved to be feasible in this application.

The principle of the hydrostatic bearing is to admit a fluid under high pressure into a small clearance (order of 0.005 inch) between a stationary and moving element. When the clearance is filled, the pressure in the film times the area of the bearing represents a force equal and opposite to an external load. The stationary and moving members are therefore separated by an oil film. The only source of friction is shear of this film, and at low velocities this is generally negligible. A coefficient of friction of 0.00001 is typical.

5.4.1 Assumptions:

- a) To simplify the hydraulic circuitry in general, and the high pressure pump in particular, it was assumed to be feasible to heat the hydraulic system and bearing structural members to 0°F during the period of exposure to a soaking temperature of -65°F.
- b) The oil to be used in the bearing system is MIL-H-5606 red hydraulic fluid. Although this oil is being used in other hydraulic systems on the aircraft, the bearing system is to be completely independent, with its own pumps, reservoirs, filters, valves, and other components.

- c) The oil will be collected and scavenged upon flowing out the ends of the bearings. It will not be exposed to high temperatures or open flame.
- d) The bearing parts exclusive of the oil reservoir and supply pump must fit in an envelope roughly 23 inches long, 20 high, and 24 wide. The reservoir and pump can be located in the fuselage of the aircraft.

5.4.2 Bearing Design Loads.

- a) The major load on the bearing system is a downward force of approximately 47,000 lbs. (see equation 2-37 Appendix II), tending to separate the rear of the test engine from the bottom of the aircraft.
- b) A 4000 lb. side load on the engine at the axial location of the supporting bearings results in a couple transverse to the direction of flight. If two bearings are used, each 7-1/2 inches from the axial center line of the engine, one bearing will have an upward load of 25,000 lbs., and the other a downward force of the same magnitude, due to this couple.
- c) The bearings cannot support any axial loads in the line of flight.

5.4.3 Description of Design.

- a) First Preliminary Design

Using the approximate analytical procedure described in Appendix IV, detailed calculations were performed on an assumed design, to examine its feasibility. The major dimensions of this design are given in the sketch of Figure 7.

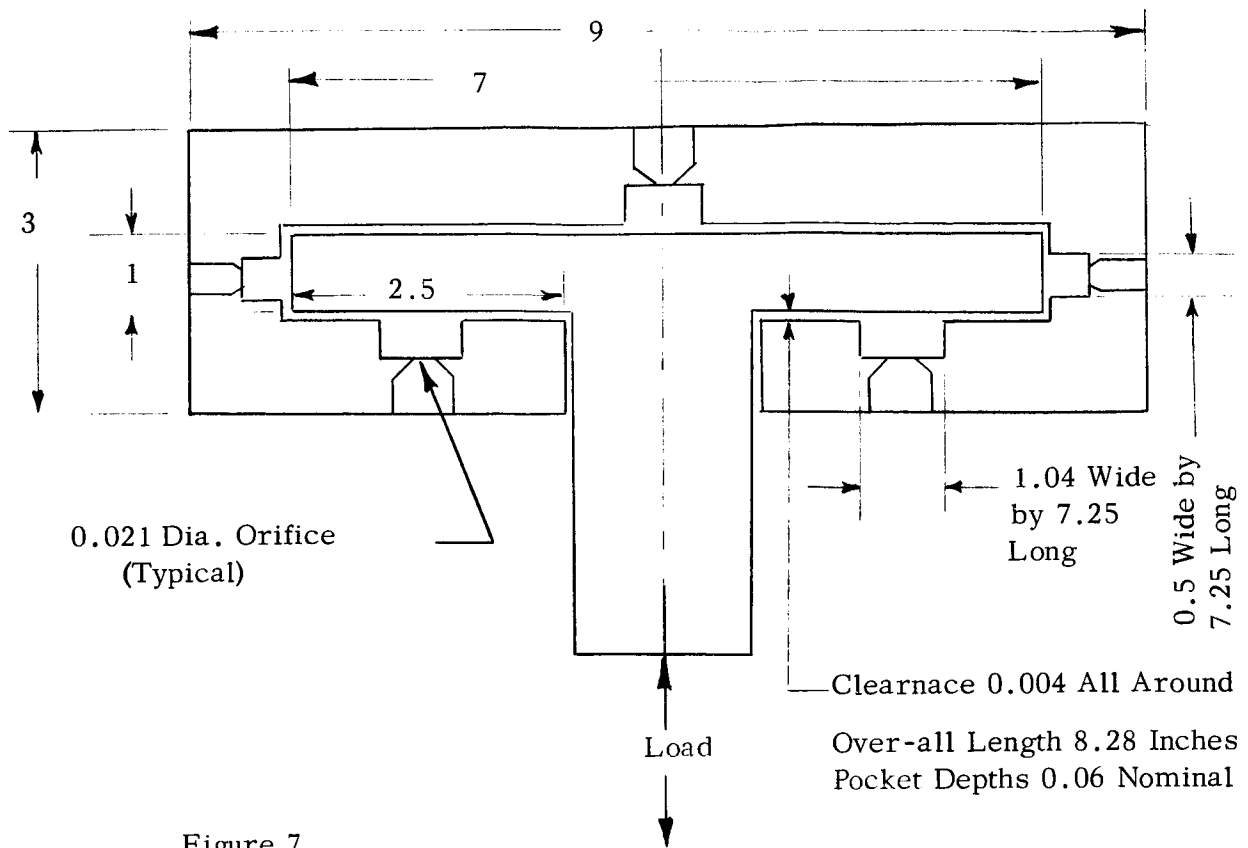


Figure 7

This sketch shows a section through one complete bearing at one-half its length. Over-all length of the bearing is 8.28 inches and the five pockets are each 7.25 inches long. Oil is admitted to the outside of each orifice at a supply pressure of 2500 psig in this design. The orifices meter the oil to reduce the pressure in the film on the unloaded side, while allowing it to rise on the loaded side.

For example, assume that a downward load of 26,000 lbs. is applied to the T-shaped runner. The runner moves down, decreasing the film thickness above the bottom bearing surfaces, thereby increasing the resistance to outflow. The pressure in this film therefore goes up.

The top film thickness, of course, increases and the pressure in that film drops because the upper orifice restricts oil flow into it.

This process continues, with the runner moving down and the pressure difference from top to bottom changing, until equilibrium is reached. The calculated performance of the design in this respect appears in the graph on the following page (Figure 8).

This load capacity curve is for a bearing with a total vertical clearance of 0.008 inch. It is not symmetrical because two bearings resist downward loads, while only one supports upward loads. In the case of the 26,000 lbs. down load, the lower film thickness will be 0.00215 inch, and the runner will therefore be 0.00185 inch below center. Note that when all load is removed from the bearing, it comes to an equilibrium position about 0.0006 inch above center.

Total flow through the bearing is also shown in this figure, as a function of load. This is for 3 vertical pockets plus 2 side pockets, although the latter do not appear in the sketch over the graphs.

These computations assumed Oronite 8515 since this was the original lubricant chosen. Later, MIL-H-5606 was selected instead because of its better chemical stability. This will not significantly alter the performance of this bearing since the viscosity and density of the two fluids are practically the same at the 0°F operating temperature. At the time a detailed design is carried out, the calculations can be done for MIL-H-5606 oil.

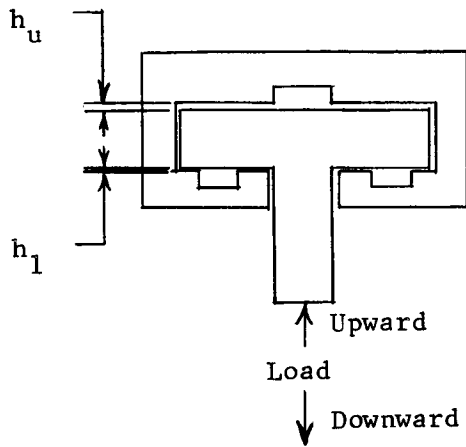
b) Second Preliminary Design

It will be observed from the foregoing load capacity curve that the first design was very conservative. This was the result of an original load estimate of 60,000 lbs. (instead of 47,000), and the use of a conservative oil supply pressure of 2500 psig.

The later load estimate, combined with a supply pressure increase to 3000 psig give an approximate scaling factor of

$$\frac{2500}{3000} \times \frac{47\,000}{60\,000} = 0.65$$

LOAD CAPACITY AND TOTAL OIL FLOW FOR PRELIMINARY BEARING DESIGN



Each Bearing Pocket:
 7.25 Long by 1.04 In. Wide
 One 0.021 Orifice
 Lubricant:
 Oronite 8515 at 0°F and 2500 psig

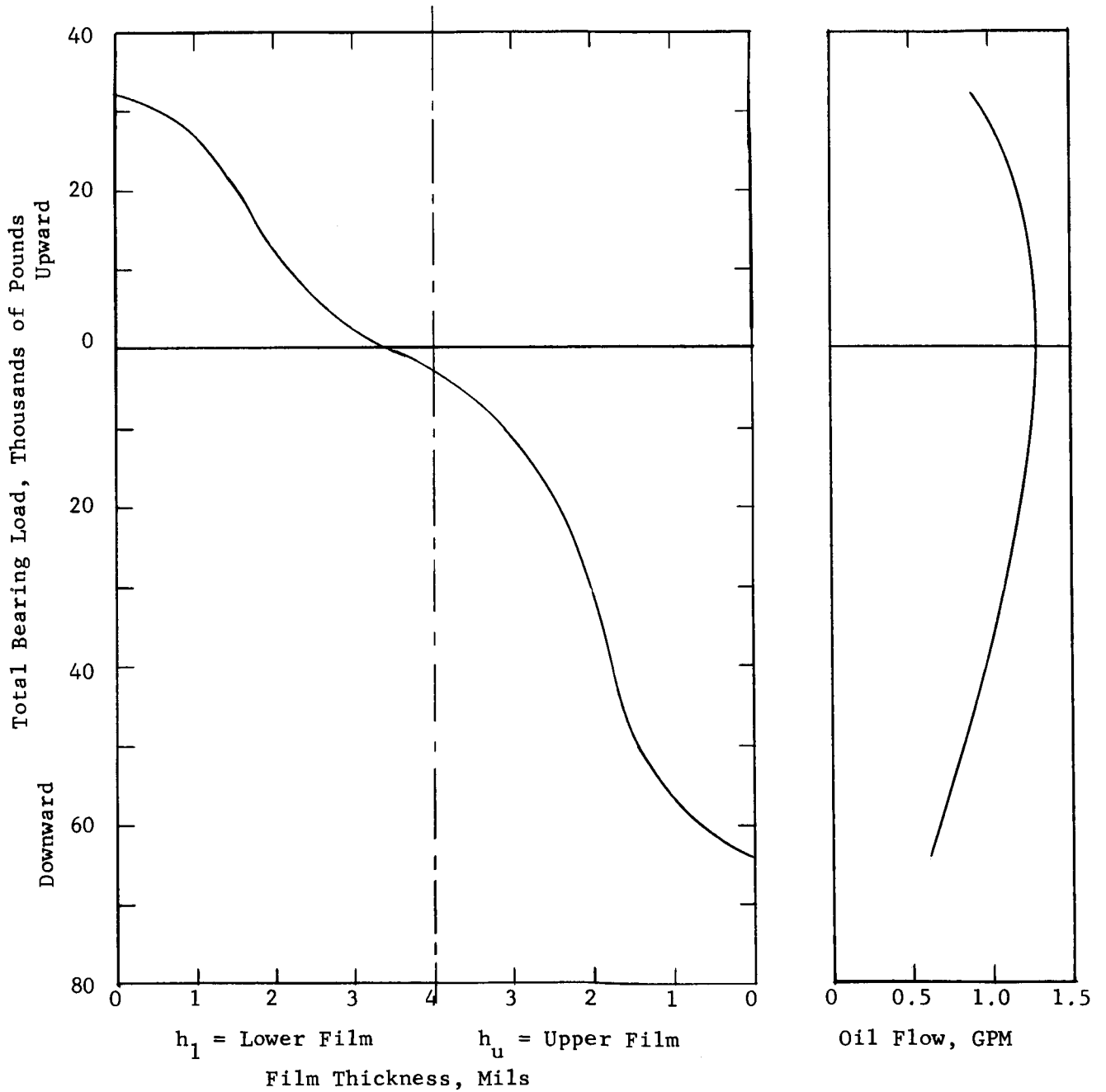


Figure 8

This means that the area of each bearing can be reduced by slightly more than one third, as a means of cutting weight and space.

Instead of lower bearing pads 2.5 wide by 8.3 long, they can be reduced to 2 inches wide by 6.63 long, as a first approximation. Detailed computations of load and flow were not repeated since this task would be done in accomplishment of a detailed design.

Besides weight and space, size reduction is important to minimize bending deflections which may interfere with satisfactory bearing performance.

c) Hydraulic Circuitry

From the flow curves in the preceding figure, it will be observed that a maximum of about 1.3 gpm per bearing, or 2.6 gpm total would be required, as a first estimate. At 2500 psig, this requires a total of about 4.0 horsepower pump input, neglecting efficiency, which appears to be a reasonable value.

In reducing the size of these bearings, the working pressure goes up, but the flow goes down because of the reduced flow area, so the total power consumption does not change greatly. It is concluded that the design is also feasible from a power standpoint.

Considering flow rate, these flows are likewise small, with modest piping and control requirements. Some thought will have to be given to collection and return of the oil by scavenge pump to the reservoir, to prevent leakage into hazardous areas and the loss of fluid from the reservoir.

With a reservoir containing about 9 gallons, continuous operation would be possible even though the actual engine testing period may be only a minute or two.

5.4.4 Conclusions

Basic feasibility of an oil lubricated hydrostatic bearing design has been shown for this application. However, the final weight

of the bearing makes it prohibitive as part of the measuring system. Initial calculations indicate a weight of 200 lbs. and the most improvement that can be expected from optimum design is a weight reduction of 125 lbs.

6.0 RESULTS OF JETTISON DYNAMIC ANALYSIS

A dynamic analysis of the ramjet jettison was made to determine the extent of ramjet guiding required to prevent the ramjet from striking the X-15 and the time required to clear the X-15. Assumptions made in this analysis were 1) lift and drag forces remain constant and their resultant point of application remains constant during jettison 2) the mass moment of inertia of the ramjet is that of a slender rod, and 3) a two dimensional mathematical model was constructed considering aft movement and rotation.

The fore-aft slider jettison system analysis, Appendix VI, also assumes that the translational and rotational modes are decoupled. It can be concluded that with a lift force of 60,000 pounds acting at fus. sta. 425 and a drag force of 6,000 pounds the ramjet will strike the ventral fin if the ramjet is not guided until the nose clears fus. sta. 565 with reasonable clearances between the ventral fin and ramjet. The time lapse from initiation of jettison to clearance of the aircraft is expected to be less than one second at Mach 8. A detailed analysis of the jettison dynamics was beyond the scope of this study program but should be conducted to 1) determine all forces acting on the guiding system and ventral, 2) the location of the ramjet with respect to the ventral fin, 3) the tendency of the ramjet to sway and wedge in the ventral fin and 4) effect of excessive warping of ramjet and/or extended ventral fin on jettison.

The analysis of the peel off jettison concept, Appendix VI, further assumed that the pivot about which the ramjet rotates at jettison was frictionless and the drag resisting the downward ejection force is a linear function of velocity - acting $2/3$ of the distance from the pivot to the ramjet nose. It is concluded from this rough analysis that an ejection impulse of 120,000 pound seconds will jettison the ramjet and clear the aircraft in approximately one second if there is no swaying of the ramjet and the ramjets structure is capable of resisting the loads.

7.0 AXISYMMETRICAL VS. TWO-DIMENSIONAL ENGINE

The axisymmetrical engine has some distinct advantages from an instrumentation design point of view over the two-dimensional engine. These advantages are:

- (1) The aerodynamic lift forces are greatly reduced, hence the over-all errors are reduced by making less error corrections.
- (2) It lends itself more readily to the direct measurement of internal nacelle net thrust.
- (3) The engine is shorter in length.
- (4) Methods of engine attachment and jettison may be designed less complex because of the reduced lift forces.

8.0 RECOMMENDATIONS FOR "FOLLOW-UP"

The following recommendations are made as a "follow-up" program:

1. Study of the dynamic compatibility of the ramjet-X-15 A-2 attachment.
2. Single prototype thrust measurement element evaluation.
3. Complete prototype thrust measurement system evaluation.
4. Design and manufacture of a flyable thrust measurement system for the ramjet engine.

8.1 Compatibility Study of Attachments

This phase of the "follow-up" program is necessary to determine a design criteria for the ventral fin structure, the ramjet attachment structure and overall dynamic characteristics of the system.

The program should consist of at least seven steps to obtain the necessary information.

1. The components of the X-15 A-2 sensitive to vibration should be determined. This information can probably be made available by NASA Edwards from their experience with the X-15 aircraft flights.
2. Measure direct and transfer impedance equal force acceleration from the ventral fin to the sensitive components as dictated by NASA Edwards flight experience.
3. Compute ventral fin characteristics from the aircraft structure manufacturing (North American) drawings.
4. Compute direct and transfer impedance (Z) for the thrust measuring devices.
5. Compute direct and transfer impedance (Z) for ramjet structure.

6. Stack up (i. e.) assemble the complete system analytically and determine the system response.
7. Finally determine transmissability of random vibration generated by the ramjet engine into the various components of the system.

Figure 9 illustrates the sequence of this study to obtain the final overall characteristics of the system.

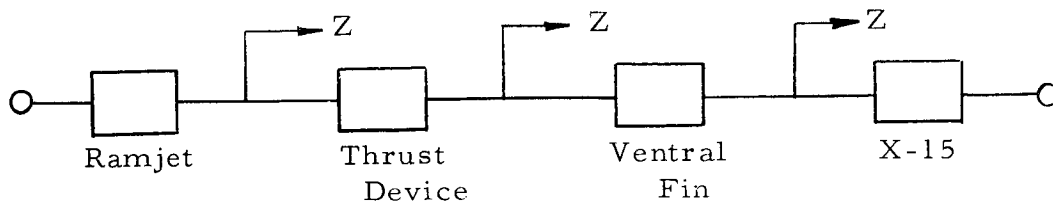


Fig. 9

It may be necessary to measure the direct and transfer impedance (item 2) by attaching a vibration shaker to the ventral fin. A force gage and a accelerometer is attached between the driven head of the shaker and the ventral fin structure. Additional accelerometers are attached to various components of the X-15 aircraft. The measurements should then include the following data, frequency (f), force (F), acceleration input (g_1) phase angle (θ) between force and acceleration and component acceleration (g_c).

This information should be taken with the present ventral fin structure and repeated on the redesigned ventral fin structure.

8.2 Single Prototype Thrust Element Evaluation

Optimizing of the thrust element is necessary to obtain maximum accuracy and performance.

The following is a suggested program:

1. Build and assemble prototype single thrust element.
2. Verify the calculations of the spring constant and stress level for given thrust loads of the flexures.

3. Evaluate the errors induced in the LVDT due to,
 - a) Large applied moments
 - b) Temperature gradients across sensor attachment points
 - c) Calibration techniques
 - d) Vibration sensitivity
4. Reduce overall weight of the element without sacrificing performance or structural integrity.
5. Optimize and check out the electronics according to performance, calibration techniques and weight.

It is believed this step is necessary before evaluating a complete system which will introduce additional variables.

8.3 Complete Prototype Thrust Measuring System Evaluation

After the single element is evaluated and optimized by necessary modifications, it is recommended that the complete thrust/drag measuring system be evaluated. The evaluation of the complete thrust/drag system would follow the sequence shown below:

1. Build and assemble complete thrust measuring system. Three elements with sensors and accelerometers, bearings, simulated ramjet, etc.
2. Evaluate the performance (frictional type of mounting) of roller or linear roller bearings at the moving measuring elements.
3. Verify results of system analysis.
4. Evaluate the overall performance of the suspension system with simulated vibrations and aerodynamic and thermal forces, for,
 - a) Frequency response

- b) Calibration stability and repeatability
- c) Thrust measurements electronics
- d) Accelerometers
- e) Temperature effects
- f) Overall system accuracy and reliability

Figure 10 illustrates a possible simplified and economical approach for laboratory testing of the complete system.

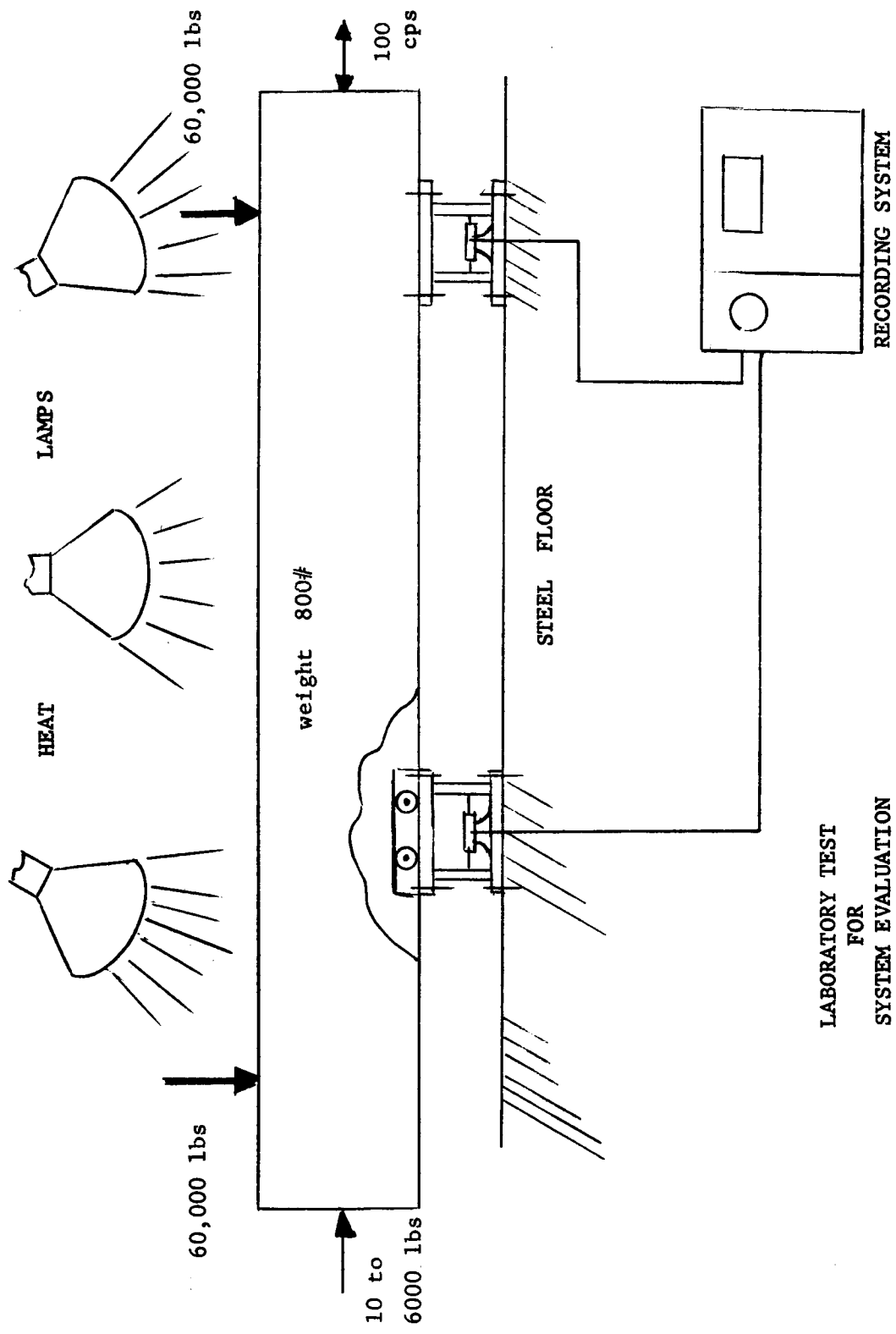
It can be noted from the sketch that the elements are attached to a heavy foundation. However, a ventral fin structure (if available) can be attached between the thrust measuring elements and the solid foundation. The steel box having the characteristics and proper weight can be used to simulate the ramjet. Aerodynamic loads and thrust loads can be applied by means of hydraulic jacks. The dynamic loading (100 cps) can be applied by attaching an electro-dynamic shaker to one end of the steel box. Heat lamps or quartz heaters can be used to apply thermal gradients across the system.

The simulated loads can be applied simultaneously or varied since this type of setup is flexible to permit this.

8.4 Design and Manufacture of Flyable Thrust/drag Measurement System

With the necessary information gathered from the first three phases of the program, a flyable system can be designed. This portion of the program would then involve:

1. Design, manufacture and calibration of a complete flyable system.
2. A laboratory calibration.



LABORATORY TEST
FOR
SYSTEM EVALUATION

Fig. 10

3. Engine ground test. The measuring system would be attached to the ramjet engine and calibrated for drag with the engine cold and the engine running. These tests would be made in a wind tunnel or engine test cell, such as at NASA Ames, or NASA Langley.
4. Field Service to assist in aircraft installation, calibration in place, and data evaluation.

The recommended program can easily be completed before the scheduled ramjet hot test run in mid 1967.

APPENDIX I

ANALYSIS OF SENSOR BLOCK

1.1 Block Concept

The function of the sensor block is to support the ramjet and house a sensor capable of detecting a 10# drag/thrust force with a frequency response of 100 cps. This sensor may measure stress in the sensor block or deflection between two points in the block. To obtain a response of 100 cps, the suspension system must have a natural frequency of 200 cps or greater. Assuming the ramjet and suspension system a single degree of freedom system, the required spring constant is

$$k_e = \omega^2 m \quad (1-1)$$

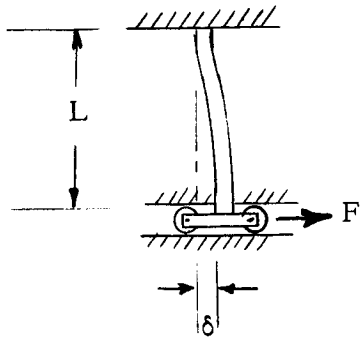
Where k_e = Equivalent spring constant of suspension system

m = Mass of ramjet (1000# weight assumed)

ω = Natural frequency

$$k_e = (200 \times 6.28)^2 \times \frac{1000}{386} = 4.1 \times 10^6 \text{ lb/in} \quad (1-2)$$

1.1.1 Strain Detection: The minimum strain that can be detected with foil strain gages is approximately 10×10^{-6} in/in. Since the threshold force is 10# and maximum force is 6000#, the range is 600 times the threshold reading or 6000×10^{-6} in/in comparable to a stress of 180,000 psi in steel. Because of this high stress level, a two range device must be designed. The problem, however, is to find a beam having $k_e = 4.1 \times 10^6$ in/in and a stress of 300 psi when under a force of 10#. A schematic of a proposed beam is shown below:



For small deflections, δ , the spring constant is

$$k = \frac{F}{\delta} = \frac{12 EI}{L^3} \quad (1-3)$$

$$k/b = E \left(\frac{h}{L} \right)^3 \quad (1-4)$$

Where b = Depth of beam
 h = Thickness of beam

The largest stress that is a function of F is the flexure stress

$$\sigma = \frac{Mc}{I} = \frac{6M}{bh^2} \quad (1-5)$$

For a rectangular cross section. The maximum moment M is $F/2$. For $F = 10\sigma$ must be at least 300 psi. Equation (1-5) becomes

$$300 = \frac{6 \times 5}{bh^2}$$

$$b = \frac{1}{10h^2} \quad (1-6)$$

Substituting (1-5) and (1-2) into (1-4) gives for $L = 2.0$

$$h = \frac{kL^3\sigma}{6EM} = \frac{4.1 \times (2)^3 \times 300}{6(30)(5)}$$

$$h = 10.9 \quad (1-7)$$

$$b = 0.00918$$

The cross section area is 0.100 in^2 . The expected axial force, σ , from the lift component of force is $120,000\#$ at front suspension point and $60,000\#$ at rear suspension point. The compressive or tension stress in the element would be

$$\sigma_{\text{front}} = \frac{120,000}{.1} = 1.2 \times 10^6 \text{ psi}$$

(1-8)

$$\sigma_{\text{rear}} = 0.6 \times 10^6 \text{ psi}$$

Both stresses are beyond the ultimate limit of existing materials. If other practical values of L are assumed ($1 < L < 12$), the same result is obtained.

Conclude that it is not practical to measure strain and maintain a frequency response of 100 cps.

1.1.2 Displacement Detection: The other method of sensing a drag/thrust force is to measure the displacement between two points in a block, the proposed block is shown below:

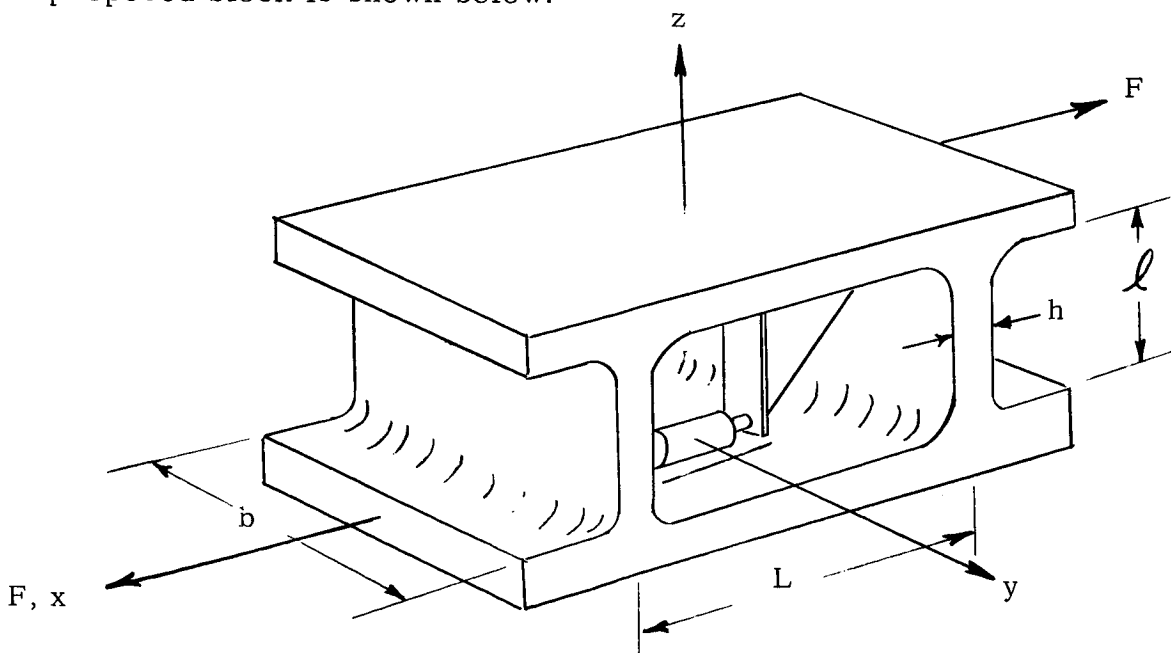


Figure 1-1

Proposed Deflection Block

The sensor has the capability of detecting a displacement of 2×10^{-6} inches. A 10# force applied to a spring with a stiffness of 5×10^6 lb/in produces a displacement of 2×10^{-6} inches.

Conclude that a displacement block approach is feasible.

The form of the block has been selected because

- 1) Two beams increases the cross sectional area to lower stress due to lift force.
- 2) Is a self-contained unit easily calibrated.
- 3) Easily mounted and disconnected for jettison.

1.2 Spring Constant of Displacement Block:

Examination of the X-15 structure and ventral fin shows that there are two convenient areas to fasten the ramjet to the X-15. These areas are designated forward suspension point between fuselage station 483 and 495 and rear point at fuselage station 565. Two types of block are to be designed 1) block rigidly attached to ramjet and 2) block to measure friction forces in rolling elements.

1.2.1 Displacement Block Fixed to Ramjet. The spring constant of this block must be at least 4.1×10^6 lb/in to insure a frequency response of 100 cps. The spring constant of the block is twice that given by equation (1-3) since the two legs work in parallel. The spring constant per unit length is

$$\frac{k}{b} = 2E \left(\frac{h}{l} \right)^3 \quad (1-9)$$

For $h = 0.5$ and $l = 2$

$$\frac{k}{b} = 2 \times 28.5 \times 10^6 \left(\frac{.5}{2} \right)^3 = 0.89 \times 10^6 \text{ lb/in} \quad (1-10)$$

The width required to obtain a spring constant equal to 4.1×10^6 lb/in is

$$b = \frac{4.1 \times 10^6}{0.89 \times 10^6} = 4.62 \text{ inches} \quad (1-11)$$

Thus it is possible to use a block 4.62 inches wide or two blocks each 2.81 inches wide. The choice depends on ease of installation and stability.

1.2.2 Displacement Block to Measure Friction Forces. Friction forces greater than 10# must be measured. In the suspension systems under study, rollers on both sides of the engine allow thermal growth without large forces induced in the structure. Only the rollers at fuselage station 495 or 565 are premitted to touch during measurements. Each block must be capable of detecting 5#. With a LVDT capable of detecting 2×10^{-6} inches, the block must have a spring constant of

$$k_e = \frac{5}{2 \times 10^{-6}} = 2.5 \times 10^6 \text{ lb/in} \quad (1-12)$$

Substituting (1-12) into (1-9) and for $b = 2$ and $L = 2$

$$h^3 = \frac{kl^3}{2Eb} = \frac{2.5 \times (2)^3}{2 \times 28.5 \times 2}$$

$$h = 0.560 \text{ in} \quad (1-13)$$

1.2.3 Effect of Axial Load on Spring Constant

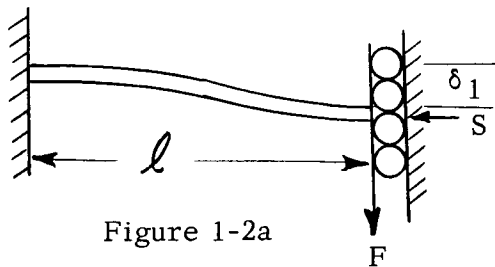


Figure 1-2a

F - Lateral load
S - Axial load

Figure 1-2a is a schematic of one leg of the displacement block whose spring constant is

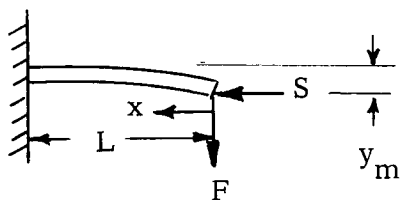


Figure 1-2b

$$k_L = \frac{F}{\delta} \quad (1-14)$$

$$k_L = \frac{F}{\delta_1} \quad (1-14)$$

This spring constant can be determined by considering half its length as a cantilever beam shown in Figure 1-2b.

In equilibrium the variation of the energy is zero

$$\Gamma \pi = \Gamma (U - W) = 0 \quad (1-15)$$

Where Γ - Variational symbol

U - Strain energy in the beam due to bending

W - Work due by external forces

Assume the deflection curve give by

$$y = y_M \left(1 - \cos \frac{\pi x}{2L} \right) \quad (1-16)$$

Strain energy due to bending is

$$U = \frac{1}{2} \int_0^L EI \left(\frac{dy^2}{dx^2} \right)^2 dx \quad (1-17)$$

Work due by lateral load

$$W_f = F y_M \quad (1-18)$$

Work done by axial force S is

$$W_s = S \lambda \quad (1-19)$$

$$\text{Where } \lambda = \frac{1}{2} \int_0^L \left(\frac{dy}{dx} \right)^2 dx \quad (1-20)$$

Substituting (1-16) into (1-20) gives

$$W_s = \frac{S y_M^2 \pi^2}{16 L} \quad (1-21)$$

Substituting (1-16) into (1-17) gives

$$U = \frac{E I y_M^2 \pi^4}{64 L^3} \quad (1-22)$$

Substituting (1-18), (1-21), and (1-22) into (1-15) gives

$$\Gamma \left(\frac{E I y_M^2 \pi^4}{64 L^3} - \frac{S y_M^2 \pi^2}{16 L} - F y_M \right) = 0$$

Taking the variation gives

$$\frac{E I y_M \pi^4}{32 L^3} = \frac{S y_M \pi^2}{8 L} + F \quad (1-23)$$

Rearranging gives the spring constant for the cantilever

$$k_c = \frac{F}{y_M} = \frac{E I \pi^4}{32 L^3} - \frac{S \pi^2}{8 L} \quad (1-24)$$

The leg of the displacement block is 2 cantilever springs in parallel or

$$k_L = \frac{k_c}{2} \quad (1-25)$$

$$k_L = \frac{EI \pi^4}{64L^3} - \frac{S \pi^2}{16L} \quad (1-26)$$

Substituting for L, $L = l/2$ gives spring constant per leg:

$$k_L = \frac{EI \pi^4}{81l^3} - \frac{S \pi^2}{8l} \quad \text{If } S \text{ is compressive} \quad (1-27)$$

$$k_L = \frac{EI \pi^4}{81l^3} + \frac{S \pi^2}{8l} \quad \text{If } S \text{ is tensile}$$

Equation (1-27) is derived using energy principle and is an approximation to the exact solution. To establish the degree of accuracy, let $S = 0$ and compare with equation (1-4)

Selecting $b = 5$, $h = 0.5$, $l = 2$, $E = 28.5 \times 10^6$, and $S = 60,000$ from (1-27)

$$k_L = \frac{28.5 \times 10^6 \times 5 \times (.5)^3 \pi^4}{12 \times 8 \times 2^3} = 2.255 \times 10^6 \text{ lb/in} \quad (1-28)$$

From (1-4)

$$k_L = \frac{28.5 \times 10^6 \times 5 \times (.5)^3}{(2)^3} = 2.225 \times 10^6 \text{ lb/in} \quad (1-29)$$

$$\text{Error is } \frac{2.255 - 2.225}{2.225} = \frac{0.030}{2.225} = 1.35\% \quad (1-30)$$

Considering an axial force of 60,000# the spring constant per leg is from equation (1-27)

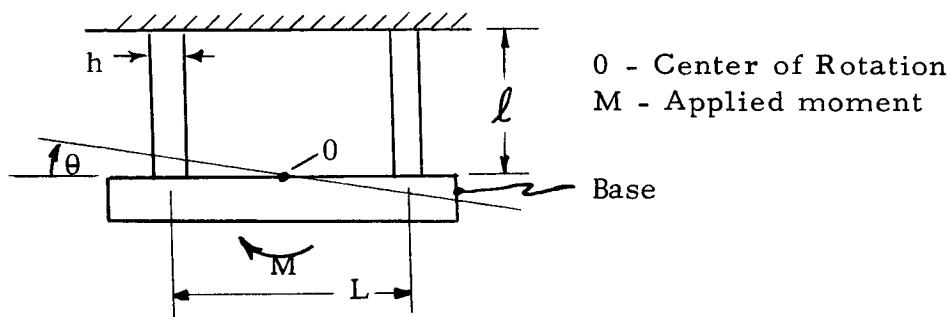
$$k_L = 2.255 \times 10^6 - \frac{(60,000)(3.14)^2}{8 \times 2} = 2.255 \times 10^6 - 37,100$$

$$k_L = 2.2179 \times 10^6 \text{ lb/in} \quad (1-31)$$

The change in spring constant is

$$\Delta = \frac{0.0371}{2.255} = 1.64\% \quad (1-32)$$

1.3 Effect of Moment Applied to Base of Block



Consider the two beams as compression or tension springs with a spring constant of

$$k = \frac{AE}{\ell} \quad (1-33)$$

For \$b = 5\$, \$h = 0.5\$, \$\ell = 2\$, and \$E = 28.5 \times 10^6\$

$$k = \frac{(5)(0.5)(28.5)(10^6)}{2} = 35.6 \times 10^6 \text{ lb/in/leg} \quad (1-34)$$

Assuming the base rigid the moment is

$$M = k \delta_2 L \quad (1-35)$$

Where δ_2 is the deflection of the end of each leg which equals

$$\delta_2 = \frac{L}{2} \theta \quad (1-36)$$

Substituting (1-36) into (1-35) gives

$$M = \frac{k L^2 \theta}{2}$$

or $\theta = \frac{2 M}{k L^2} \quad (1-37)$

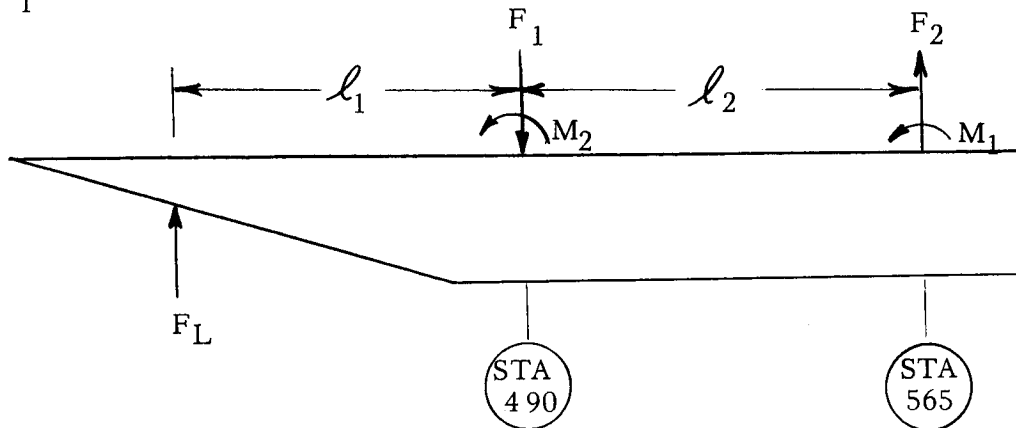
APPENDIX II
ANALYSIS OF SUSPENSION SYSTEM WITH ROLLERS AT REAR SUPPORT

2.1 Forces and Moments Applied to Ramjet - General Expressions

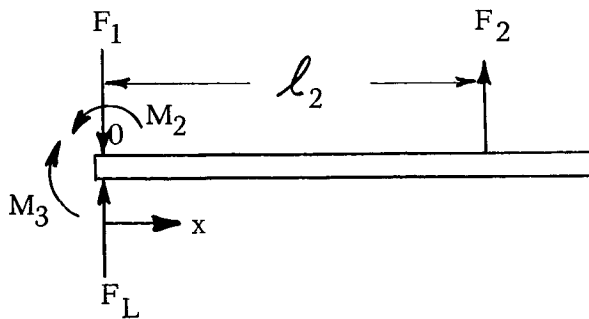
The suspension system is designed to withstand a lift force of 60,000 pounds concentrated at Fus. Sta. 425, a lateral drag force of 10,000# uniformly distributed along the side due to yaw angle, and a 6000# drag force.

Lift Force

A free body diagram of the ramjet is shown below where it is assumed that $M_1 = 0$ and EI is constant between Fus. Sta. 483 and 565.



This free body is reduced to a beam of constant EI .



$$\text{Vertical Forces: } F_1 - F_L - F_2 = 0 \quad (2-1)$$

$$\text{Moment about Sta 490: } M_3 - M_2 - l_2 F_2 = 0 \quad (2-2)$$

The Moment at a point x along the beam is

$$-EI \frac{d^2 y}{dx^2} = M_3 - M_2 - F_x \quad (2-3)$$

$$\text{Where } F = F_1 - F_L = F_2$$

Integrating EQ. (2-3) Twice Gives

$$-EI \frac{dy}{dx} = (M_3 - M_2) x - \frac{F_x^2}{2} + C_1 \quad (2-4)$$

$$-EI y = (M_3 - M_2) \frac{x^2}{2} - \frac{F_x^3}{6} + C_1 x + C_2 \quad (2-5)$$

The Boundary conditions are

$$\text{At } x = 0 \quad y = 0 \text{ (assumed)} \quad (2-6)$$

$$x = 0 \quad \frac{dy}{dx} = K_1 M_2 \quad (2-7)$$

$$x = l_2 \quad y = K_2 F_2 \quad (2-8)$$

Applying the Boundary conditions to EQ. (2-4) and (2-5) gives

$$C_2 = 0 \quad (2-9)$$

$$C_1 = -K_1 M_2 EI$$

$$M_2 = \left(\frac{\frac{EIK_2}{l_2} + \frac{l_2^2}{3}}{\frac{EIK_2}{l_2} + \frac{l_2^2}{3} + l_2 K_1 EI} \right) M_3 \quad (2-10)$$

Rewriting Equation (2-2) gives

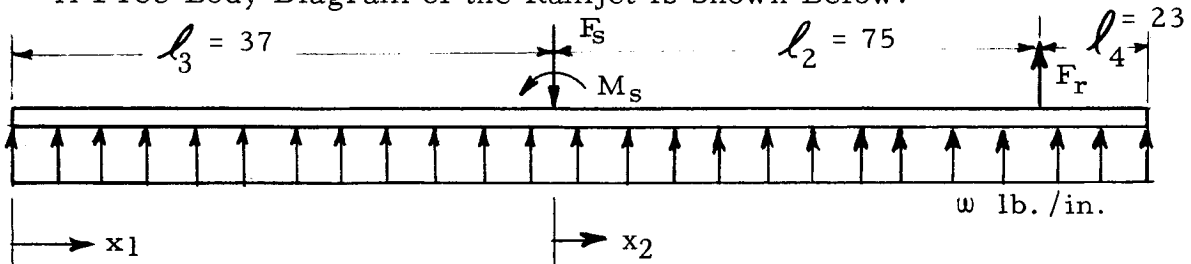
$$F_2 = \frac{M_3 - M_2}{l_2} \quad (2-11)$$

Side Loading

Assumptions:

- 1) Maximum value of side force is 10,000# acting uniformly over the 135" length
- 2) Moments applied at rear support is negligible
- 3) I of Ramjet is assumed constant
- 4) Deflection of front and rear sensor is zero

A Free Body Diagram of the Ramjet is Shown Below:



The Force per Unit length w is assumed to be

$$w = \frac{10,000}{135} = 74 \text{ \#/in.} \quad (2-12)$$

The Moment at any point x_1 where x_1 is less than l_3 is

$$M = -EI \frac{d^2 y_1}{dx^2} = \frac{w x_1^2}{2}$$

$$-EI \frac{dy_1}{dx} = \frac{w x_1^3}{6} + C_1 \quad (2-13)$$

$$-EI y_1 = w x_1^4 + C_1 x_1 + C_2 \quad (2-14)$$

The Moment at any point x_2 where x_2 is less than l_2

$$M = -EI \frac{d^2 y_2}{dx_2^2} = \frac{w x_2^2}{2} - M_S - F_S x_2 + \frac{w (95)^2}{2} \quad (2-15)$$

$$-EI \frac{dy_2}{dx} = \frac{w x_2^3}{6} - M_S x_2 - \frac{F_S x_2^2}{2} + \frac{w l_3^2 x_2}{2} + C_3 \quad (2-16)$$

$$-EI y_2 = \frac{w x_2^4}{24} - \frac{M_S x_2^2}{2} - \frac{F_S x_2^3}{6} + \frac{w l_3^2 x_2^2}{4} + C_3 x_2 + C_4 \quad (2-17)$$

Boundary Conditions:

$$\text{At } x_1 = 95 \quad y_1 = 0 = y_2 \quad x_2 = 0 \quad (2-18)$$

$$\text{At } x_1 = 95 \quad y_1^1 = y_2^1 = K_3 M_S \quad x_2 = 0 \quad (2-19)$$

$$\text{At } x_2 = 70 \quad y_2 = 0 \quad (2-20)$$

Applying Boundary Condition (2-19) by equating (2-13) and 2-16)

$$\frac{w l_3^3}{6} + C_1 = C_3 = K_3 M_S \quad (2-21)$$

Applying Boundary Condition (2-18) by Equating (2-17) and (2-14)

$$\frac{w l_3^4}{24} + C_1 l_3 + C_4 = 0 \quad (2-22)$$

Substituting (2-21) and (2-22) into (2-17) and applying Boundary Condition (2-20) gives

$$\frac{w l_2^4}{24} - \frac{M_S l_2^2}{2} - \frac{F_S l_2^3}{6} + \frac{w l_3^2 l_2^2}{4} + K_3 M_S l_2 = 0$$

Rearranging gives

$$M_S = \frac{\frac{w l_2^4}{24} + \frac{w l_3 l_2^2}{4} - \frac{F_S l_2^3}{6}}{\frac{l_2^2}{2} - K_3 l_2} \quad (2-23)$$

Summation of moments about front suspension point gives

$$\begin{aligned} \Sigma M: \quad 0 &= M_S + F_R l_2 + w (l_2 + l_3 + l_4) \left[\frac{l_2 + l_3 + l_4}{2} - l_3 \right] = 0 \\ F_R &= \frac{w}{l_2} (l_2 + l_3 + l_4) \left(\frac{l_3}{2} - \frac{l_2 + l_4}{2} \right) - \frac{M_S}{l_2} \end{aligned} \quad (2-24)$$

Summation of forces gives

$$F_S = F_R + w(l_2 + l_3 + l_4) \quad (2-25)$$

Substituting (2-24) into (2-25) and the results into (2-25) gives:

$$M_S = \frac{\frac{w l_2^2}{24} (l_2^2 + 6 l_3^2) - \frac{w l_2^3 (l_2 + l_3 + l_4)}{6} \left(\frac{l_3}{2 l_2} + \frac{1}{2} - \frac{l_4}{2 l_2} \right)}{\left(\frac{l_2^2}{2} - K_3 l_2 \right) \left(1 - \frac{l_2^2}{6 (l_2^2/2 - K_3 l_2)} \right)} \quad (2-26)$$

Equations (2-24), (2-25) and (2-26) will give the forces applied to ramjet for a given load and flexibility of support.

2.2 Forces and Moments Applied to Sensor - Specific Case

The deflection block shown in Figure 1-1 is rigidly attached with dimensions -

$$b = 5, \quad h = 0.5, \quad \ell = 2, \quad L = 4 \quad (2-27)$$

To obtain applied forces to the sensor, the moment of inertia of the ramjet must be known. Assume that 1/2 of the weight of the ramjet is concentrated at the maximum distance from the ramjet's center to give maximum I. The width of the two dimensional ramjet is taken as 24" with a length at the center line of 135". The thickness of the two plates is

$$t = \frac{W t}{b h} \quad \rho\text{-density (titanium)} \quad (2-28)$$

$$t = \frac{500}{(24)(135)(.163)} = 0.945 \text{ inches} \quad (2-29)$$

The moment of inertia of a section is assumed

$$I = \frac{b h^3}{12} = \frac{24 (20^3 - 19^3)}{12} = 2280 \text{ in.}^4 \quad (2-30)$$

To apply equation (2-10) to find M_2 , K_1 must be computed. Comparing equations (2-7) and (1-37) shows

$$K_1 = \frac{2}{k L^2} \quad (2-31)$$

Substituting (2-27) and (1-34) into (2-31) gives

$$K_1 = \frac{2 \times 10^{-6}}{35.6 \times 16} = \frac{10^{-6}}{285} \quad (2-32)$$

Lift Force

If $\ell_2 = 75''$ and $K_2 = 0$, M_2 is computed from Eq.(2-10) as

$$M_2 = \frac{\frac{(75)^2}{3}}{\frac{(75)^2}{3} + \frac{(75)(10^{-6})(28.5)(10^6)(2280)}{285}} M_3$$

$$M_2 = .1230 M_3 \quad (2-33)$$

M_3 is from the free body diagram equal to

$$M_3 = F_L \ell_1 \quad (2-34)$$

$$M_3 = (60,000)(64.625) = 3.86 \times 10^6 \text{ lb/in.} \quad (2-35)$$

Substituting (2-35) into (2-33)

$$M_2 = 0.123 \times 3.86 \times 10^6 = 475,000 \text{ in. lbs} \quad (2-36)$$

From Eq. (2-11)

$$F_2 = \frac{(3.86 - .475) \times 10^6}{75} = 45,1000 \text{ lbs.} \quad (2-37)$$

$$F_1 = 60,000 + 45,100 = 105,100 \text{ lbs.} \quad (2-38)$$

Side Loading

The moment and forces applied to the deflection block is computed using equations (2-26) and (2-25). Assuming $K_3 = 0$ and letting $\ell_2 = 75$, $\ell_3 = 37$, $\ell_4 = 23$, and $w = 74$ from Eq. (2-12).

$$M_S = \frac{\frac{(74)(75)^2}{24} \left[(75)^2 + 6(37)^2 - \frac{(74)(135)(75)^3}{6} \right] \left[\frac{37}{150} + \frac{1}{2} - \frac{23}{150} \right]}{(75)^2/2}$$
$$M_S = - 31,100 \text{ in. lbs.} \quad (2-39)$$

From Eq. (2-24)

$$F_R = 74 (135) \left(\frac{37}{150} - \frac{1}{2} - \frac{23}{150} \right) + \frac{31,100}{75}$$

$$F_R = -3,650 \quad (2-40)$$

From Eq. (2-25)

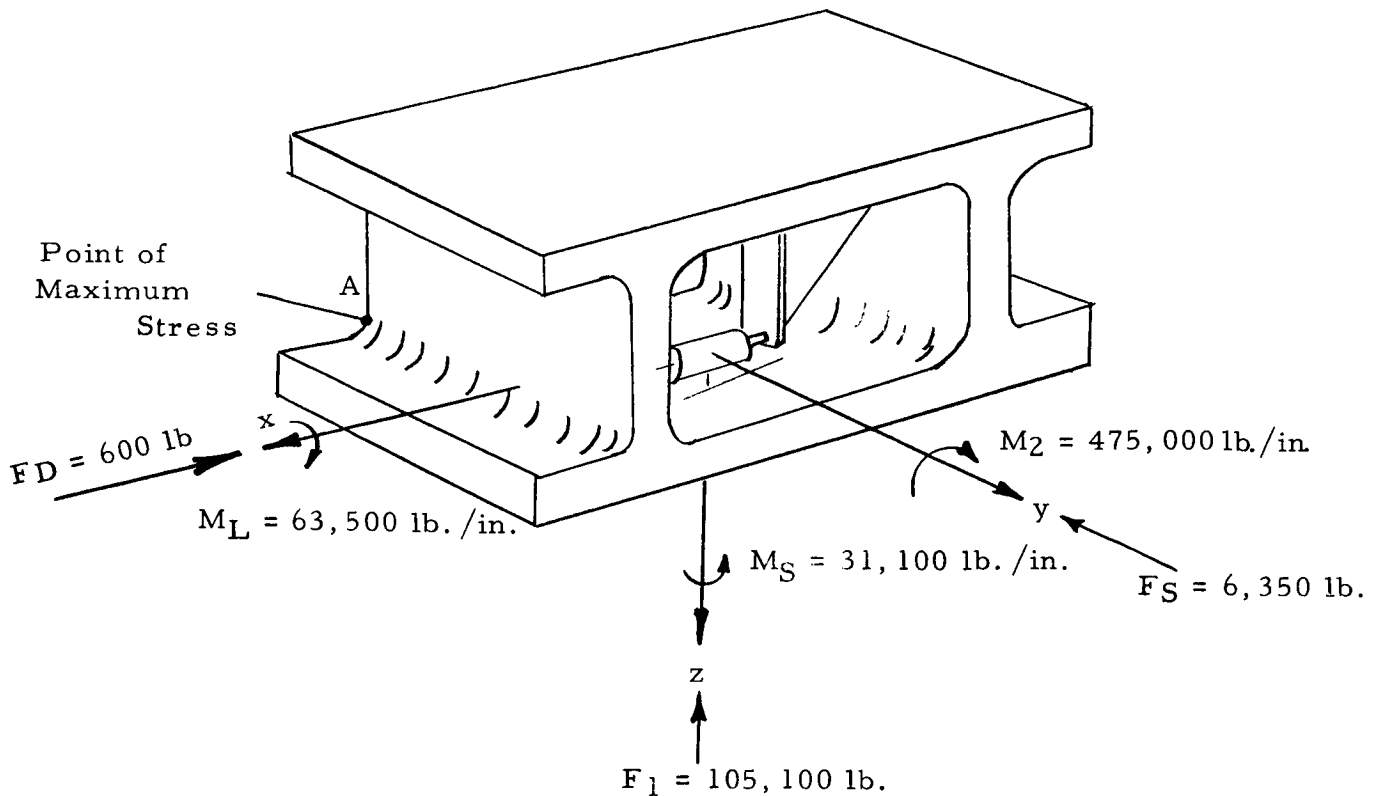
$$F_S = -3,650 + 10,000 = 6,350 \text{ lbs.} \quad (2-41)$$

The side loading is uniformly distributed with a mean 10" below the base of the deflection block producing an additional moment equal to

$$M_L = 6,350 \times 10 = 63,500 \text{ lb. in.} \quad (2-42)$$

The figure below shows the forces acting on the deflection block rigidly attached to the ramjet front support.

Figure 2-1



The stress at point A of Figure 2-1 is:

From $F_D = 6000 \text{ lbs.}$

$$\sigma_D = \frac{6M}{bh^2} = \frac{6 \times 3000 \times 1}{5 \times .5^2} = -14,400 \text{ psi} \quad (2-43a)$$

From $F_L = 105,000 \text{ lbs.}$

$$\sigma_L = \frac{P}{bh} = \frac{105,100}{5 \times .5 \times 2} = -21,000 \text{ psi} \quad (2-43b)$$

From $M_L = 63,500$

$$\sigma_L = \frac{6M}{hb^2} = \frac{6 \times \frac{63,500}{2}}{.5 \times 5^2} = -15,250 \text{ psi} \quad (2-43c)$$

From $M_S = 31,100$

$$\sigma_S = \frac{6 \times M}{hb^2} = \frac{6 \times 15,550}{.5 \times 5^2} = +7,480 \text{ psi} \quad (2-43d)$$

From $M_e = 475,000 \text{ lb. in.}$

$$\sigma_e = \frac{P}{bh} = \frac{118,750}{5 \times .5} = -47,500 \text{ psi} \quad (2-43e)$$

From $F_S = 6,350 \text{ lbs.}$

$$\sigma_S = \frac{6 \times M}{hb^2} = \frac{6 \times 3,117}{.5 \times 5^2} = -1,495 \text{ psi} \quad (2-43f)$$

The stress at Point "A" is the sum of equations (2-43)

$$\sigma_A = \underbrace{14,400}_{\text{Drag}} + \underbrace{21,000 + 47,500}_{\text{Lift Force}} + \underbrace{1,495 - 7,480 + 15,250}_{\text{Side Force}} = 99,645 \text{ psi} \quad (2-44)$$

Applying a safety factor of 1.5, the ultimate strength of the material must be

$$\sigma_U = 1.5 \times 99,645 = 149,500 \text{ psi} \quad (2-45)$$

The base of the deflection block will rotate per analysis section 1-3. This rotation will have a maximum of (from 2-19 and 2-32)

$$\theta = K_1 M_2 = \frac{10^{-6} \times 0.475 \times 10^6}{285} = 0.0066 \text{ radians} \quad (2-46)$$

If the LVDT sensor is not located at the exact center of rotation of the base, a deflection error will be induced in the sensor equal to

$$\delta = \xi \theta \quad (2-47)$$

Where ξ is the distance between the center of sensor and center of rotation. For the accuracy specified, δ must be less than 2×10^{-6} inches which requires ξ to be

$$\xi = \frac{\delta}{\theta} \leq \frac{2 \times 10^{-6}}{6600 \times 10^{-6}} = 0.00030 \text{ inches} \quad (2-48)$$

This figure indicates that the sensor location has an extremely tight tolerance. Assumptions were made to arrive at this figure which were highly conservative. These assumptions were

- 1) Legs of displacement block resist rotation by compression only. These legs do absorb energy in bending which was neglected.
- 2) Moment of inertia of the ramjet was assumed constant.

Two deflection blocks are located at fuselage station 565, 20 inches apart. Attached to the base of the block is a rail on which a rolling element rests. Friction in the roller is measured by the deflection block. The forces and moments acting on the blocks are shown schematically below:

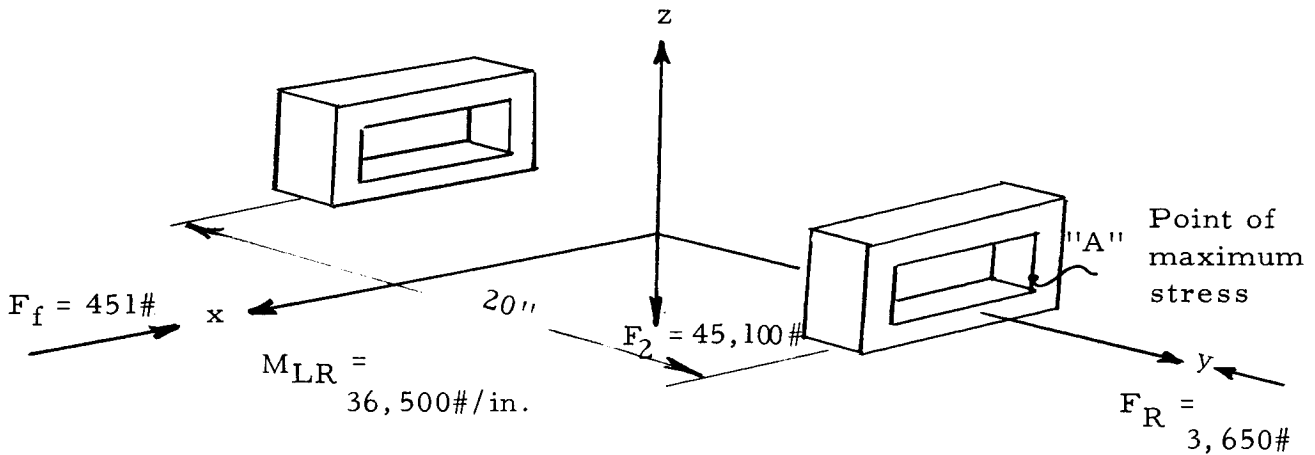


Figure 2-2

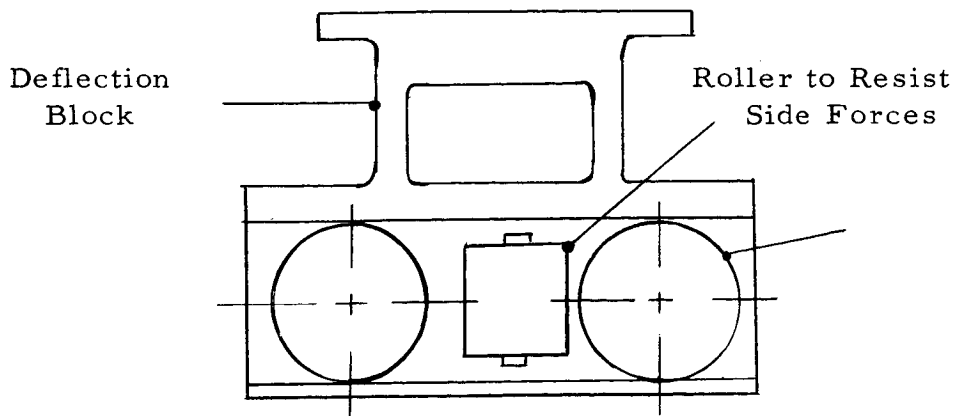
M_{LR} is the moment produced by the side loading whose line of action is 10" from the base of the block.

$$M_{LR} = F_R \times 10 = 3650 \times 10 = 36,500 \text{ lb. in.} \quad (2-49)$$

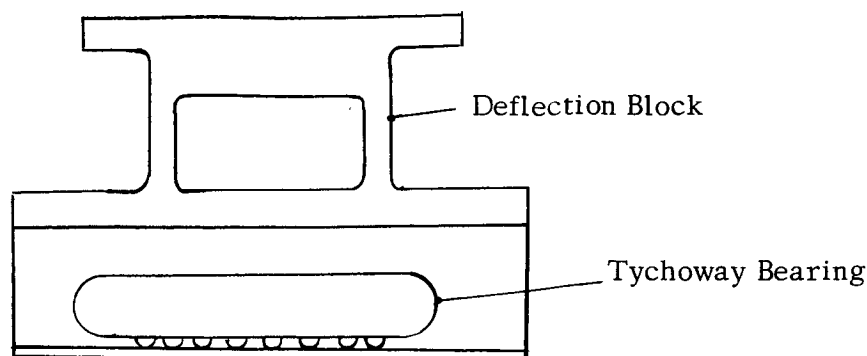
F_f is the horizontal force created due to friction in the rollers. A friction coefficient of 0.01 is assumed.

$$F_f = \mu N = 0.01 \times 45,100 = 451 \text{ lbs.} \quad (2-50)$$

A side view sketch of a deflection block using rollers or Tychoway* bearings is shown below



*Trade name - Scully Jones



The arrangement using rollers may induce the larger stresses in the deflection block. Both rollers ideally should carry the same load but practically one will carry 2/3 the load. This unbalance, not present in the Tychoway bearing arrangement, results in an applied moment to the deflection block equal to

$$M_U = \frac{1}{3} \times \frac{45,100}{2} \times 3 = 22,550 \text{ lb. in.} \quad (2-51)$$

where the distance from center of the deflection block to roller center is 3".

The stress at point "A" (Figure 2-2) in a deflection block having dimensions $b = 2$, $h = 0.5$, $\ell = 2$, and $L = 4$ is computed below:

From $F_2 = 45,100$ lbs.

$$\sigma_2 = \frac{F_2 / 2}{bh} = \frac{22550}{2 \times .5 \times 2} = 11,275 \text{ psi} \quad (2-52a)$$

From $M_{LR} = 36,500$

$$\sigma_2 = \frac{M_{LR} / 20}{bh} = \frac{36,500}{2 \times .5 \times 2} = 910 \text{ psi} \quad (2-52b)$$

From $F_f = 451$ lbs.

$$\sigma = \frac{6M}{bh^2} = \frac{6 \times 113}{2 \times (.5)^2} = 1,356 \text{ psi} \quad (2-52c)$$

From $M_U = 36,500$

$$\sigma = \frac{M_U/L}{bh} = \frac{36,500/4}{2 \times .5} = 9,150 \text{ psi} \quad (2-52d)$$

From $F_R = 3,650$

$$\sigma = \frac{6M}{hb^2} = \frac{6 \times F_R/4}{hb^2} = \frac{6 \times 912}{.5 \times 4} = 2,710 \text{ psi} \quad (2-52e)$$

The total stress is the sum of (2-52)

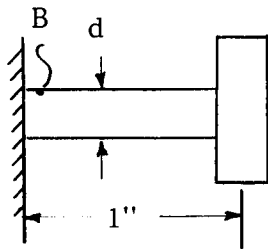
$$\sigma_T = \underbrace{1,356 + 11,275}_{\text{Lift Force}} + \underbrace{9,150 + 2710 + 910}_{\text{Side Force}} = 25,391 \text{ psi} \quad (2-53)$$

The deflection block has sufficient strength.

The weak points in the rear suspension point are:

- 1) Shaft supporting roller
- 2) Channel or rail on which the roller rolls
- 3) Contact stresses between the roller and rail

- 1) A sketch showing the roller shaft is shown below:



F = 30,000 lbs.

Bending stress at B

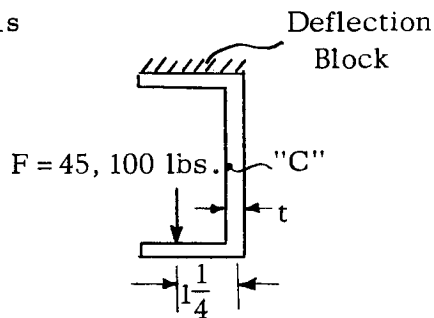
$$\sigma = \frac{32 M}{\pi d^3}$$

$$d^3 = \frac{32 M}{\sigma \pi} = \frac{32 \times 30,000}{80,000 \times 3.14}$$

$$d = 1.565 \text{ inches} \quad (2-54)$$

Where the ultimate stress is $1.5 \times 80,000 = 120,000$ psi

- 2) A sketch of a section view of the channel is shown below. The channel attached to the deflection block is about 6 inches long. Stress at "C" is



$$\sigma = \frac{6 M}{6 t^2} + \frac{F}{6 t} = \frac{6 \times \frac{45,100}{6} \times 1 \frac{1}{4}}{6 \times t^2} + \frac{45,000}{6 \times t} = 30,000 \text{ psi}$$

$$t \approx 0.70 \text{ inches} \quad (2-55)$$

The thickness can be decreased if webs are used to maintain the moment of inertia

- 3) The maximum octahedral shearing stress for a cylindrical roller on a surface are given by Seely and Smith "Advanced Mechanics of Materials" Page 366 as:

$$T_{G \max} = 0.27 \frac{b}{\Delta} \quad (2-56)$$

$$\text{Where: } \Delta = \frac{1}{(1/2 R_1) + (1/2 R_2)} \left\{ \frac{1 - \mu_1^2}{E} + \frac{1 - \mu_2^2}{E} \right\}$$

$$b = \sqrt{\frac{2q\Delta}{\pi}}$$

q = Load per unit length

R₁ = Radius of roller

R₂ = Radius of surface

μ = Poisson's ratio

E = Modulus of elasticity

For a roller on a flat surface R₂ = ∞. Assuming the roller carries 2/3 the load or approximately 30,000# and the roller and surface are made of the same material, the octahedral stress for R₁ = 1 and the roller 1 1/2" wide is:

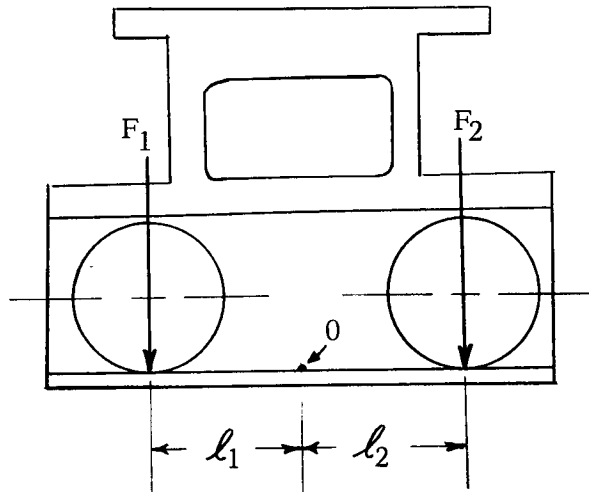
$$q = \frac{30,000}{1.5} = 20,000 \text{ lb/in}$$

$$\Delta = (2) (1) \left[\frac{2 (1 - .09)}{30 \times 10^6} \right] = 0.1212 \times 10^{-6}$$

$$b = \sqrt{\frac{(2) (20,000) (.1212) 10^{-6}}{3.14}} = 0.0391$$

$$T_{G \max} = 0.27 \left(\frac{.0391}{.1212} \times 10^6 \right) = 87,000 \text{ psi} \quad (2-57)$$

In this rear suspension arrangement, the rollers are connected to the ramjet to eliminate the moments induced when rollers are attached to the deflection block. The rollers move relative to the deflection block causing the load to shift. The effect of this shifting of load is analyzed below. The error introduced will be a rotation of the base or the deflection block.



The rotation of the deflection block base is

$$\theta = K_1 M \quad (2-52)$$

Where

$$K_1 = \frac{2}{k L^2} \quad (2-31)$$

$$k = \frac{A E}{l} \quad (1-33)$$

Substituting the dimensions of the deflection block into (1-33) and (2-31) gives

$$k = \frac{(2) (.5) (28.5 \times 10^6)}{2} = 14.25 \times 10^6 \text{ lb/in}$$

$$K_1 = \frac{2}{14.25 \times 10^6 \times (4)^2} = \frac{10^{-6}}{114} \quad (2-53)$$

Taking moments about o

$$\Sigma M_o: M_o = F_1 \ell_1 - F_2 \lambda_2 \quad (2-54)$$

$$\text{Let } F_1 + F_2 = P \text{ and } \ell_1 + \lambda_2 = \lambda$$

Substituting into (2-54) gives

$$M_o = P \lambda - P \lambda_2 - F_2 \lambda \quad (2-55)$$

Three cases will be considered:

Case I: Symmetrically loaded $F_2 = P/2$; $\lambda_2 = \lambda/2$

Substituting (2-55) into (2-52)

$$\theta = K (P\lambda - P \lambda/2 - P/2 \lambda) = 0$$

Case II: Load equally distributed between rollers, rollers not symmetrical with center line of block

$$F_2 = P/2; \lambda_2 = \lambda/4 \text{ (equal to a movement of } 1 \frac{1}{4} \text{")}$$

$$\theta = K_1 (P\lambda - \frac{P \lambda}{4} - P/2 \lambda) = \frac{K_1 P \lambda}{4}$$

For $\lambda = 5$

$$\theta = \frac{10^{-6}}{114} \times 30,000 \times \frac{5}{4} = 329 \times 10^{-6}$$

To obtain the accuracy specified, the center of the L.V.D.T. must be

less than ϵ from the center of rotation of the block's base. From (2-47)

$$\epsilon = \frac{\delta}{\theta} \leq \frac{2. \times 10^{-6}}{329 \times 10^{-6}} = 0.00609 \text{ inches} \quad (2-56)$$

Case III: Load is carried by one roller only.

$$F_2 = 0 ; \ell_2 = \lambda / 2$$

$$\theta = K_1 (P\lambda - P \lambda / 2)$$

$$\theta = 658 \times 10^{-6}$$

$$\epsilon \leq 0.003045 \text{ inches} \quad (2-57)$$

It is concluded that the center of the LVDT must also be positioned close to the center of rotation of the deflection block's base.

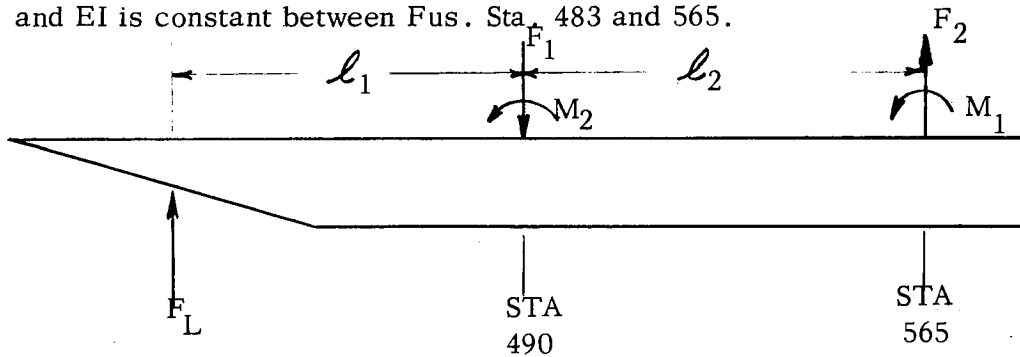
APPENDIX III
ANALYSIS OF SUSPENSION SYSTEM WITH ROLLERS AT FRONT SUPPORT

3.1 Forces and Moments Applied to Ramjet - General Expression

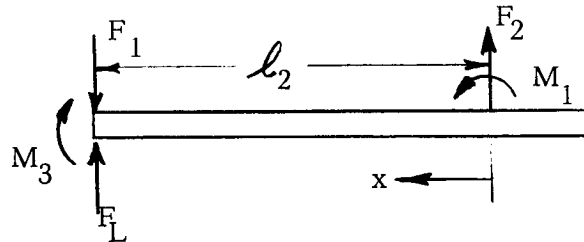
The suspension system is designed to withstand a lift force of 60,000 lbs. concentrated at Fus. Sta. 425, a lateral drag force of 10,000 lbs. uniformly distributed along the side due to yaw angle, and a 6000 lb. drag force.

Lift Force

A free body diagram of the ramjet is shown below where it is assumed that $M_p=0$ and EI is constant between Fus. Sta. 483 and 565.



This free body is reduced to a beam of constant EI.



$$\Sigma \text{ Vertical Forces: } F_L + F_2 = F_1 \quad (3-1)$$

$$\Sigma \text{ Moments about Sta. 490 } + \curvearrowright M_3 - F_2 l_2 - M_1 = 0 \quad (3-2)$$

The moment at any point x along the beam is

$$-EI \frac{d^2 y}{dx^2} = F_2 x + M_1 \quad (3-3)$$

$$-EI \frac{dy}{dx} = \frac{F_2 x^2}{2} + M_1 x + C_1 \quad (3-4)$$

$$-EI y = \frac{F_2 x^3}{6} + \frac{M_1 x^2}{2} + C_1 x + C_2 \quad (3-5)$$

The boundary conditions are:

$$\text{at } x = 0 \quad y = 0 \quad (3-6a)$$

$$x = 0 \quad y' = K_1 M_1 \quad (3-6b)$$

$$x = l_2 \quad y = 0 \quad (3-6c)$$

Applying boundary conditions to Eq. (3-4) and (3-5) gives:

$$C_2 = 0 \quad (3-7)$$

$$C_1 = -EI K_1 M_1$$

$$M_1 = \frac{F_2 l_2^2 / 6}{EI K_1 - l_2 / 2} \quad (3-8)$$

Substituting (3-8) into (3-2) gives:

$$F_2 = \frac{M_3}{l_2 + \frac{1}{\frac{6EI K_1}{l_2^2} + \frac{3}{l_2}}} \quad (3-9)$$

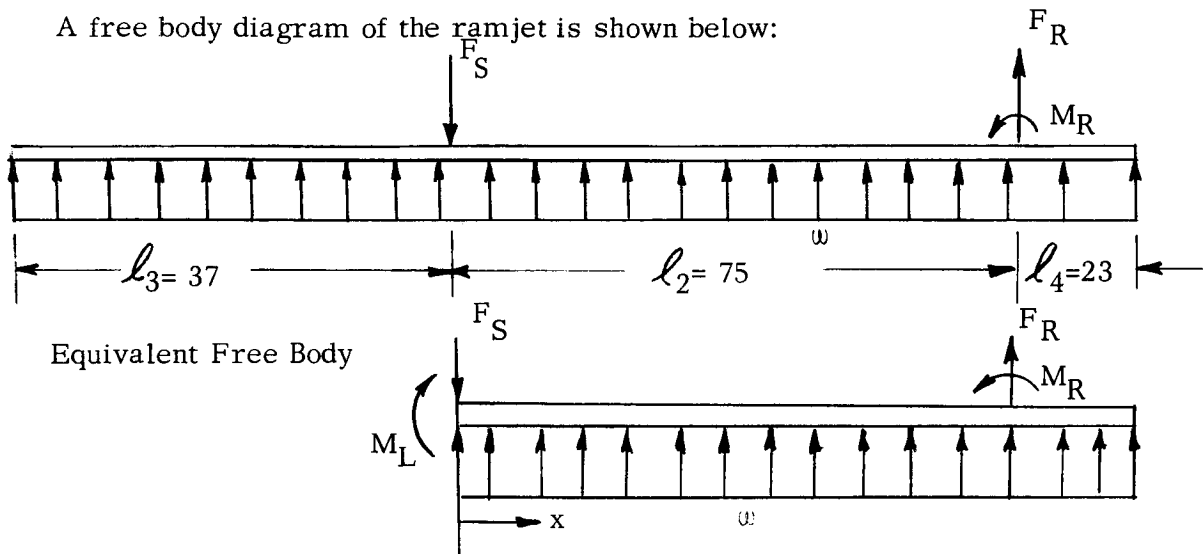
With equations (3-9), (3-8) and (3-1), the unknown forces F_1 , F_2 , and M_1 are determined.

Side Loading

Assumptions:

- 1) Maximum value of side force is 10,000 # acting uniformly over 135" length.
- 2) Moment applied at front support is negligible
- 3) I of Ramjet is assumed constant
- 4) Deflection at front and rear sensor is zero

A free body diagram of the ramjet is shown below:



$$M_L = \frac{\omega l_3^2}{2} \quad ; \quad F_L = \omega l_3 \quad (3-10)$$

The force per unit length ω is assumed to be

$$\omega = \frac{10,000}{135} = 74\#/in \quad (3-11)$$

The moment at any point x where x is less than l_2 is

$$-EI \frac{d^2 y}{dx^2} = M_L + (F_L - F_S) x + \frac{\omega x^2}{2} \quad (3-12)$$

$$-EI \frac{dy}{dx} = M_L x + (F_L - F_S) \frac{x^2}{2} + \frac{\omega x^3}{6} + C_1 \quad (3-13)$$

$$-EI y = \frac{M_L x^2}{2} + (F_L - F_S) \frac{x^3}{6} + \frac{\omega x^4}{24} + C_1 x + C_2 \quad (3-14)$$

Boundary conditions:

$$\text{at } x = l_2 \quad y = 0 \quad (3-15a)$$

$$x = l_2 \quad y' = 0 \quad (3-15b)$$

$$x = 0 \quad y = 0 \quad (3-15c)$$

Applying boundary conditions to Eq. (3-14) and (3-15)

$$C_2 = 0$$

$$C_1 = (F_S - F_L) \frac{l_2^2}{2} - M_L l_2 - \frac{\omega l_2^3}{6}$$

$$M_L = \frac{\omega l_2^2}{4} + \frac{2(F_S - F_L) l_2}{3} = \frac{\omega l_3^2}{2}$$

$$F_S - F_L = \frac{3}{8} \omega l_2 - \frac{3}{4} \omega \frac{l_3^2}{l_2} \quad (3-16)$$

$$\Sigma \text{ Forces: } F_S - F_L - \omega (l_2 + l_4) - F_R = 0$$

$$F_R = -\omega \left(\frac{5l_2}{8} + l_4 + \frac{3l_3^2}{4l_2} \right) \quad (3-17)$$

Σ Moments about rear support

$$\Sigma M_{565} : M_L + (F_L - F_S) l_2 + \frac{\omega l_2^2}{2} - \frac{\omega l_4^2}{2} - M_R = 0$$

$$M = \omega \left(\frac{l_2^2}{8} - \frac{l_3^2}{4} - \frac{l_4^2}{2} \right) \quad (3-18)$$

With equations (3-18), (3-17) + (3-16), the unknown forces F_S , F_R and M_R are determined.

3.2 Forces and Moments Applied to Sensor - Specific Case

Two deflection blocks similar to the one shown in Figure 1-1 are rigidly attached to the ramjet with dimensions

$$b = 2.5, h = 0.5, \ell = 2, L = 4 \quad (3-19)$$

The moment of inertia of the ramjet is assumed to be that given by equation (2-30)

$$I = 2280 \text{ in.}^4 \quad (2-30)$$

To compute the forces and moments, K_1 in equations (3-9) and (3-8) must be known. Since the total width of the deflection blocks is the same as the block considered in Section 2.2.

$$K_1 = \frac{10^{-6}}{285} \quad (2-32)$$

If $\ell_2 = 75''$, F_2 is computed from Eq. (3-9)

$$F_2 = \frac{M_3}{75 + \frac{1}{\frac{6 \times 28.5 \times 10 \times 10^{-6} \times 2280}{285 \times (75)^2} + \frac{3}{75}}}$$

$$F_2 = 0.0127 M_3 \quad (3-20)$$

M_3 is (from the free body diagram) equal to

$$M_3 = F_L \ell_1 = (60,000) (64.625)$$

$$M_3 = 3.86 \times 10^6 \text{ lb. in.} \quad (3-21)$$

$$F_2 = 49,000 \text{ lbs.} \quad (3-22)$$

Substituting (3-22) into (3-8) gives

$$M_1 = \frac{(49,000) (75)^2 / 6}{\frac{28.5 \times 10^6 \times 2280 \times 10^{-6}}{285} - \frac{75}{2}}$$

$$M_1 = 241,500 \quad (3-23)$$

Substituting (3-22) into (3-1) gives

$$F_1 = 60,000 + 49,000 = 109,000 \text{ lbs.} \quad (3-24)$$

The moment and forces applied to the deflection block by the side loading is completed using equations (3-17), (3-18), and (3-16). Let $l_2 = 75$, $l_3 = 37$, $l_4 = 23$ and $\omega = 74$

$$F_R = -74 \left(\frac{5 \times 75}{8} + 23 + \frac{3(37)^2}{4(75)} \right) = -6,200 \text{ lbs.} \quad (3-25)$$

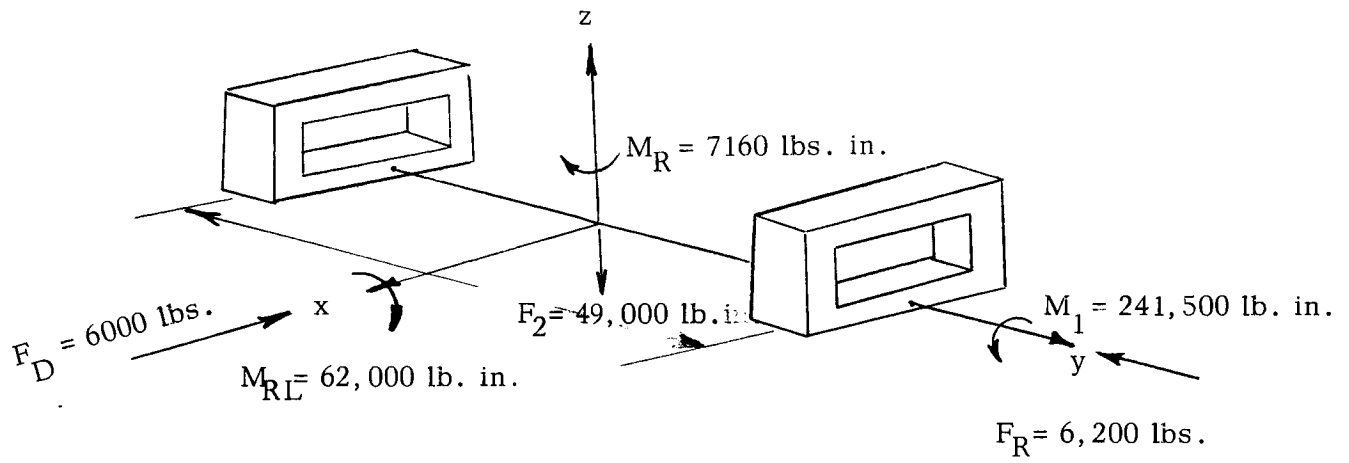
$$F_S = 74 \left(\frac{3 \times 75}{8} - \frac{3(37)^2}{4(75)} \right) + 74(37) = 3,800 \text{ lbs.} \quad (3-26)$$

$$M_R = 74 \left(-\frac{(37)^2}{4} + \frac{(75)^2}{8} - \frac{(23)^2}{2} \right) = -7,160 \text{ lb. in.} \quad (3-27)$$

Since the resultant side load acts at the mid-section of the ramjet, an additional moment is induced equal to

$$M_{R_L} = F_R (10) = 62,000 \text{ lb. in.} \quad (3-28)$$

The forces acting on the deflection blocks located 12 inches apart are shown in the sketch below.



The forces on each deflection block are shown below.

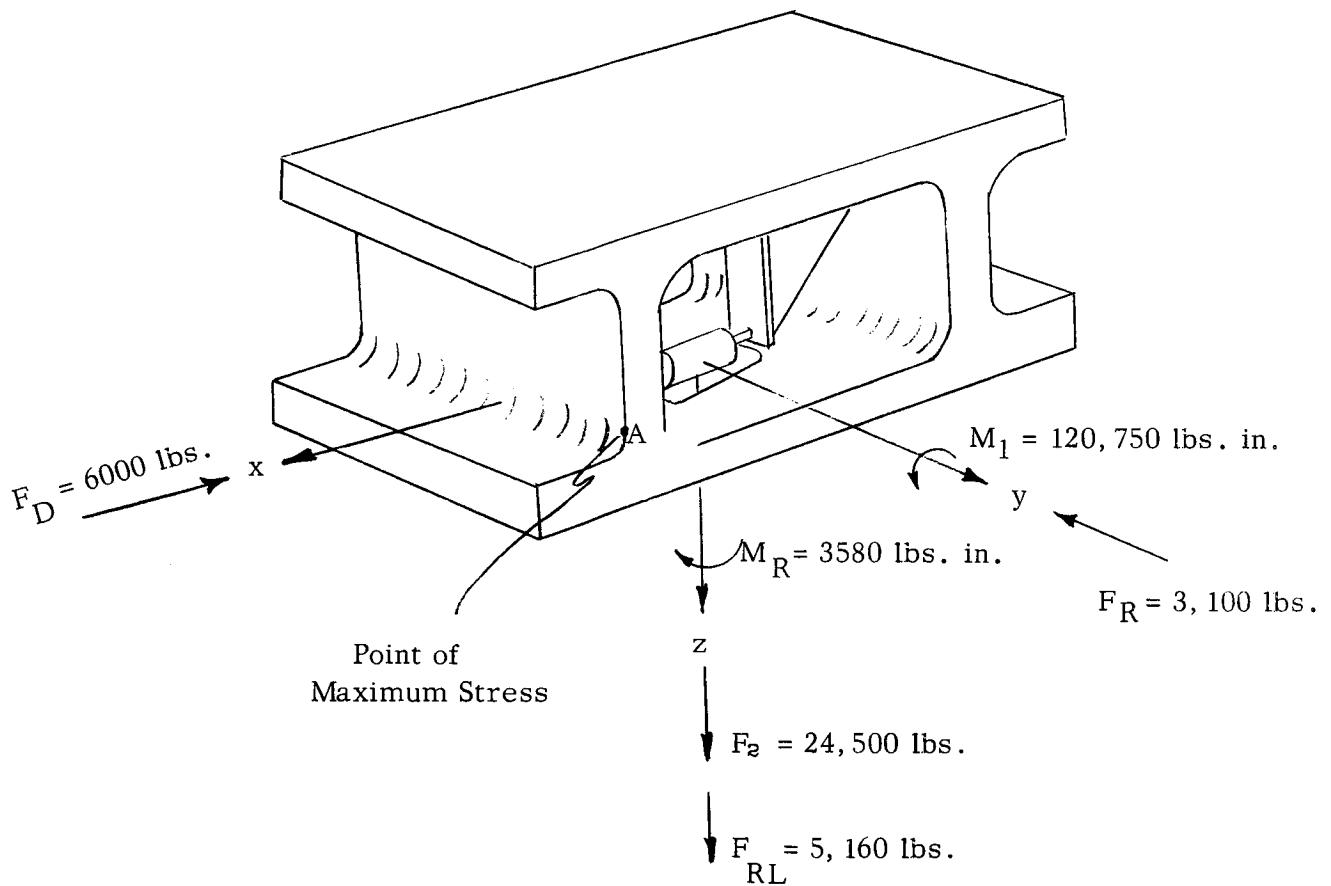


Figure 3-1

The stress at point A of Figure 3-1 is:

$$\text{from } F_D = 6000$$

$$\sigma = \frac{6M}{bh^2} = \frac{6 \times 3,000 \times 1}{2.5 \times (.5)^2} = 28,800 \text{ psi} \quad (3-29a)$$

$$\text{from } F_2 \text{ and } F_{RL} = 29,660$$

$$\sigma_2 = \frac{P}{bh} = \frac{29,660}{(2.5)(.5)} = 23,650 \text{ psi} \quad (3-29b)$$

$$\text{from } M_1 = 120,750 \text{ lb. in.}$$

$$\sigma = \frac{120,750/4}{1.25} = 24,100 \text{ psi} \quad (3-29c)$$

$$\text{from } F_R = 3,100 \text{ lbs.}$$

$$\sigma = \frac{6M}{hb^2} = \frac{6 \times 1,550}{.5 \times (2.5)^2} = 300 \text{ psi} \quad (3-29d)$$

$$\text{from } M_R = 3580 \text{ lb. in.}$$

$$\sigma = \frac{6M}{hb^2} = \frac{6 \times \frac{3580}{4}}{.5 \times (2.5)^2} = 1,720 \text{ psi} \quad (3-29e)$$

The total stress is the sum of equations (3-29)

$$\sigma_{\text{total}} = 28,800 + 23,650 + 24,100 + 300 + 1,720 = 78,570 \quad (3-30)$$

Applying a safety factor of 1.5, the ultimate strength of the material must be

$$\sigma_u = 1.5 \times 78,570 = 118,000 \text{ psi} \quad (3-31)$$

The base of the deflection block will rotate per analysis section 1-3. This rotation will have a maximum of (from 2-32 and 3-23)

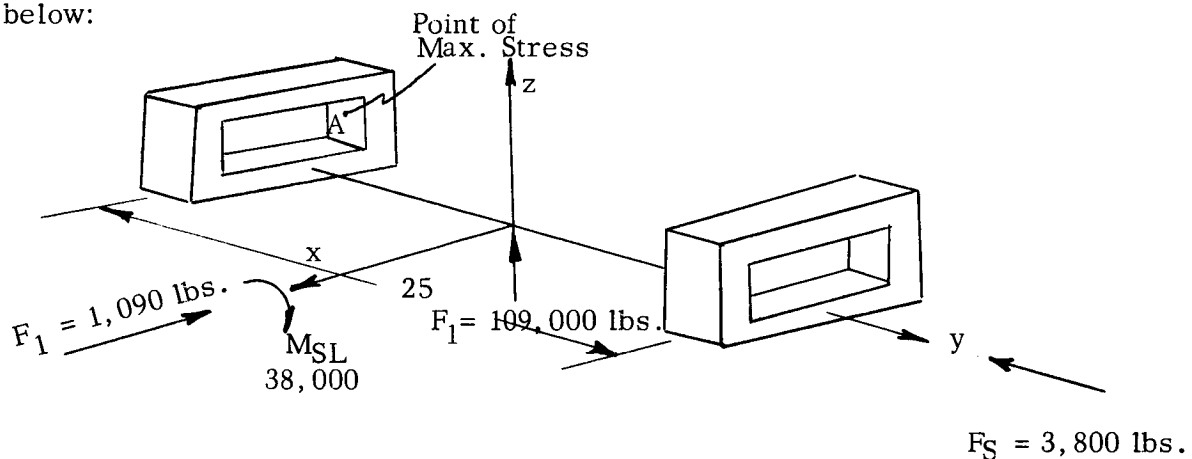
$$\theta = K_1 M_1 = \frac{10^{-6} \times .241 \times 10^{-6}}{285}$$

$$\theta = 0.000846 \text{ Radians}$$

Following the analysis in Appendix II, the tolerance in locating the LVDT is:

$$\Sigma = \frac{\delta}{\theta} < \frac{2 \times 10^{-6}}{845 \times 10^{-6}} = 0.00236 \quad (3-32)$$

Two deflection blocks are located in the extended ventral fin at fuselage station 490 about 25 inches opposite one another. Attached to the base of the block is a rail on which a rolling element rests. Friction in the roller assembly is measured by the deflection block. The forces and moments acting on the blocks are shown schematically below:



M_{RL} is the moment produced by side loading whose line of action is 10" from the base of the block.

$$M_{SL} = F_S \times 10 = 38,000 \text{ lb. in.} \quad (3-33)$$

F_f is the horizontal force created due to friction in the rollers. A friction coefficient of 0.01 is assumed

$$F_f = \mu N = 0.01 \times 109,000 = 1090 \text{ lbs.} \quad (3-34)$$

The discussion in Appendix II on the rollers in the rear deflection block applies here.

The stress at Point "A" (Figure 3-2) in a deflection block having dimensions $b = 2$, $H = 0.5$, $\ell = 2$ and $L = 4$ is computed below

$$\text{From } F_1 = 109,000$$

$$\sigma_2 = \frac{F_1/4}{b h} = \frac{27,250}{2 \times .5} = 21,800 \text{ psi} \quad (3-35a)$$

$$\text{From } M_{SL} = 38,000$$

$$\sigma = \frac{M_{SL}/20}{2 b h} = \frac{1600}{2 \times 2 \times .5} = 800 \text{ psi} \quad (3-35b)$$

$$\text{From } F_f = 1090 \text{ lbs.}$$

$$\sigma = \frac{6 M}{b h^2} = \frac{6 \times \frac{1090}{4} \times 1}{2 \times (.5)^2} = 3,270 \text{ psi} \quad (3-35c)$$

$$\text{From } F_S = 3800 \text{ lbs.}$$

$$\sigma = \frac{6 M}{h b^2} = \frac{6 \times \frac{3800}{2} \times 1}{2 (.5) (2)^2}$$

$$\sigma = 3,620 \text{ psi} \quad (3-35d)$$

$$\text{From } Mu = \frac{1}{3} \times \frac{109,000}{2} \times 3 = 54,500 \text{ lb. in.}$$

$$\sigma = \frac{Mu/L}{b h} = \frac{54,500/4}{2 \times .5} = 13,625 \text{ psi} \quad (3-35e)$$

The total stress is the sum of equation (3-35)

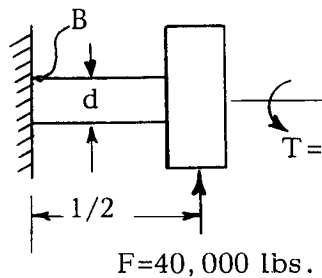
$$\sigma_T = 21,800 + 800 + 3,270 + 3,620 + 13,625 = 43,115 \text{ psi} \quad (3-36)$$

Conclude that the front deflection blocks have sufficient strength when made of the same material as the rear deflection block.

The weak points in the rear suspension point are:

- 1) Shaft supporting roller
- 2) Channel or rail on which the roller rolls
- 3) Contact stresses between the roller and rail

1) A sketch showing the roller shaft is shown below:



Bending Stress at B

$$\sigma = \frac{32 \times M}{\pi d^3}$$

if $d = 1.75$

$$\sigma = \frac{32 \times 40,000 \times 1/2}{(3.14) (1.75)^3} = 38,000 \text{ psi}$$

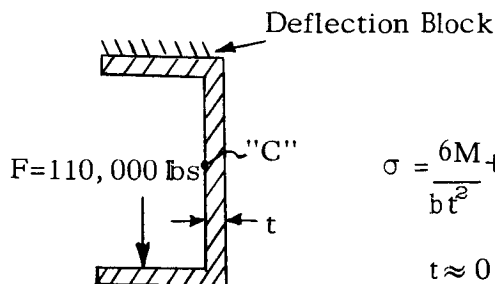
(3-37)

Shear stress due to torque $T = 730 \text{ lb. in.}$

$$S_s = \frac{Tr}{J} = \frac{730 \times 32 \times 0.875}{3.14 \times (1.75)^3} = 1215 \text{ psi} \quad (3-38)$$

A shaft of 1.75 inch diameter has sufficient strength. It is made large to accommodate the bearing required to take the load.

2) A sketch of a section view of the channel is shown below. The channel attached to the deflection block is about 6 inches long. Stress at "C" is



$$\sigma = \frac{6M}{bt^2} + \frac{F}{bt} = \frac{6 \times \frac{110,000}{6} \times 1 \frac{1}{4}}{6 \times t^2} + \frac{110,000}{6 \times t} = 50,000$$

$$t \approx 0.89 \text{ inches}$$

(3-39)

The thickness and, therefore, the weight can be decreased if webs are used to maintain the moment of inertia.

- 3) The contact stress is computed using the method used in Appendix II. For a roller 1 1/2" wide and 4 inches in diameter supporting a load of 40,000#, the maximum octahedral shearing stress is

$$\tau_{G_{\max.}} = 0.27 b/\Delta = 0.27 \frac{0.0481}{.182 \times 10^{-6}} = 79,100 \text{ psi} \quad (3-40)$$

Conclude that a 4" roller will not produce an excessive stress and the friction coefficient, therefore, should be low.

The front deflection blocks are loaded in the same manner as the rear deflection block discussed in Appendix II. Therefore an error arises due to the shifting of load due to thermoexpansion. Considering only case III where the load is carried by one roller only, the rotation of the deflection block base is (see Appendix II).

$$\theta = K_1 (\tau \lambda - \tau \lambda/2) = \frac{10^{-6}}{114} \times \frac{54,500 \times 5}{2}$$

$$\theta = 0.001195 \text{ Radians} \quad (3-41)$$

Tolerance on positioning of the LVDT is

$$\Sigma = \frac{\delta}{\theta} < \frac{2 \times 10^{-6}}{1195 \times 10^{-6}} = 0.00167 \text{ inches} \quad (3-42)$$

APPENDIX IV FLUID BEARING ANALYSIS

4.1 Gas Lubricated Configuration

The first type of bearing examined was a gas supported type, using high pressure (3000 psi) air or nitrogen. This would require a reservoir of 655 cubic inches to supply the bearings for a total operating time of 2 minutes. The system would be attractive because there would be no fire hazard, and it would be very simple because the gas would exhaust to atmosphere after passing through the bearing. By contrast, a recirculating oil system would require collection of the lubricant and scavenge pumping to return it to the reservoir.

Gas flow rates were calculated on the basis of experiments conducted in the Advanced Technology Laboratory in 1960 (see Ref. 42) on a large bearing of the type appropriate to this application. The test bearing was 25 inches long. The runner was T-shaped as in this application, with bearing surfaces 2.5 inches wide on top and 1.25 inches wide underneath.

This slider was tested up to 20,000 lbs. at a supply pressure of 760 psig. Total gas flow was 0.8 lb/sec at this condition.

Based upon an early load estimate of 60,000 lb. for this application, 3 of these sliders would, therefore, be required with a total flow rate of 2.4 lb/sec. The use of pressure loaded seals around the periphery of the bearing pockets was considered in an attempt to reduce gas consumption. The static axial sliding friction from this combination was computed to be 2200 pounds, which is not tolerable.

Therefore, despite the fact that a gas bearing would be feasible from a load capacity standpoint and desirable for its simplicity, it was concluded that a workable design could not be made within the limits of weight and space in this application.

One further aspect of these bearings also contributed to the decision to eliminate them from contention. Very often bearings of this type are statically unstable because of resonance between the bearing structural elements and the high pressure gas in the supply lines. It is not possible within the state-of-the-art to predict this analytically with high enough accuracy, so that a stable design can be reliably accomplished. This potential problem, therefore, reinforced the conclusion that the gas lubricated bearing was not suitable for this application.

4.2 Oil Lubricated Configuration

The use of a recirculating oil hydrostatic bearing system has significant advantages in this application, the most important being:

- the bearing system can be operated continuously, for periods of hours, if desired instead of minutes or seconds as in the case of gas bearings.
- the bearing area can be made much smaller, and therefore lighter, since it can be designed for a supply pressure of 3000 psig. A stored gas system would have to be designed for the minimum pressure available (750 psig) after the system was bled down during operation.
- design, construction, testing and installation can be carried out with a higher probability of success because analytical tools for design are more highly developed and reliable than for gas bearings. This will obviously save time and expense.

For the present study, in which the purpose was to examine feasibility only and not to carry out a detailed design, approximate analytical techniques were used (Ref. 43). The design curves from this reference were obtained with an electric analog field plotter, which results in some inaccuracies when compared to pure mathematical solutions for the same flow problems.

The resulting bearing design is, therefore, only approximate and certainly not optimum. Feasibility is shown, however, because these analytical inaccuracies are at worst on the order of 20 percent, and further computations would be expected to optimize the load capacity with respect to oil flow rate. The design which was presented earlier in this report should, therefore, be regarded as a worst case.

The first assumption made in the design was that the bearing configuration would be rectangular because of the engine jettison requirement. Two T-shaped runners would be attached to the engine and the mating bearings would be mounted side by side in the lower ventral fin of the aircraft.

Two identical bearings, each capable of supporting 30,000 lbs. in a downward direction, would be used. Each bearing would have one oil pocket on top facing the top of the T. Two pockets, one underneath each side of the crossbar of the T would take the main load. The purpose of the top pocket is to stiffen the fluid film and prevent bottoming in the event of an unforeseen load in the upward direction.

For simplicity in calculation, all three pockets were assumed identical. Small side pockets to resist minor side loads would also be required. These were not analyzed.

Equal lengths of the sills on all sides of the pockets were assumed, and a pocket length to width ratio of 4 was used. Width of the pocket was assumed to one-half the width of the bearing pad.

Oronite 8515 at 0°F was initially chosen as the working fluid and all calculations were made on this basis. The later change to MIL-H-5606 does not affect these results to any extent because its viscosity and density are quite close to the Oronite fluid.

Supply pressure was set at 2500 psig to stay within the state-of-the-art of aircraft hydraulic systems.

For the geometry as above, load, flow and pump power coefficients are obtained from Ref. 43 as follows:

$$\text{Load: } a_f = 0.7$$

$$\text{Flow: } q_f = 4.1$$

$$\text{Power: } H_f = 6.0$$

Actual values of load, flow and power are obtained from the relations:

$$\text{Load: } W = a_f A_p p_r$$

$$\text{Flow: } Q = q_f (W/A_p) h^3 / \mu$$

$$\text{Power: } H_B = P_r Q$$

The recess, or pocket pressure, P_r , is related to the film thickness h , by the flow characteristics of the metering orifice. Capillary tubes or constant flow valves were not regarded as useful in this application from a standpoint of mechanical complexity.

An orifice diameter of 0.021 inch was settled upon after flow calculations for both larger and smaller diameters were made. The factor k_o was computed as follows:

$$k_o = \frac{C_d \pi d_o^2}{4 \sqrt{\rho}} = \frac{0.6 (\pi) (0.021)^2}{4 \sqrt{90 \times 10^{-6}}} = 0.022$$

Film thickness versus load, and flow versus film thickness are now computed from the design curves for a single bearing pad. The following results were obtained:

<u>Load-Thousands of lbs.</u>	<u>Film Thickness, Mils</u>	<u>Flow GPM</u>	<u>Pump Power, HP</u>
3.0	3.70	0.38	0.62
6.0	2.95	0.36	0.58
9.0	2.56	0.34	0.54
12.0	2.30	0.31	0.51
18.0	1.89	0.26	0.42
20.0	1.74	0.23	0.37

Assuming a total vertical clearance of 0.008 inches as a practical value, combined performance curves can be computed for the complete bearing with one of these pads on top and two on the bottom. Some extrapolation is required for film thicknesses greater than 3.7 mils and less than 1.74.

The extrapolated values used were as follows:

<u>Load-Thousands of lbs.</u>	<u>Film Thickness, Mils</u>	<u>Flow GPM</u>	<u>Pump Power, HP</u>
0	8.0	0.40	0.62
1.2	7.0	0.40	0.62
1.5	6.0	0.39	0.62
1.9	5.0	0.38	0.62
2.5	4.0	0.38	0.62
29.0	1.0	0.12	0.21
32.0	0.0	0.0	0.0

The combined performance curves for load capacity and flow, given earlier in this report, were produced by assuming the T-shaped runner to be displaced within the vertical clearance of 0.008 in. For a given displacement, the upper and lower film thicknesses are known, and therefore, the force being exerted by a given bearing pad (either up or down), and its oil flow can be obtained from the above table.

Adding the force vectors from the three pads and the flow from each gives the over-all performance of the complete bearing.

4.3 Oil Lubricant

The preceding computations were based upon the following properties of Oronite 8515:

<u>Temperature °F</u>	<u>Specific Gravity</u>	<u>Viscosity, Centistokes</u>
-65	0.982	2357
0	.955	210
100	.915	24.3
210	.870	8.1

An operating temperature of 0°F was selected to minimize hydraulic circuit difficulties. This may require heating the oil system and bearings when the aircraft structure is soaked at -65°F.

Because of various possible chemical instabilities which could occur when this fluid is exposed to air, a change was made to MIL-H-5606, a red hydraulic oil which is also used on the aircraft.

Properties of this fluid are as follows:

<u>Temperature °F</u>	<u>Specific Gravity</u>	<u>Viscosity, Centistokes</u>
-65	.916	2500
0	.893	170
100	.860	19
210	.818	5.5

Its similarity to Oronite 8515 is evident. Its high temperature capabilities are very limited, however, so a careful design will be required to prevent exposure of this lubricant to hot surfaces.

APPENDIX V
JETTISON ANALYSIS

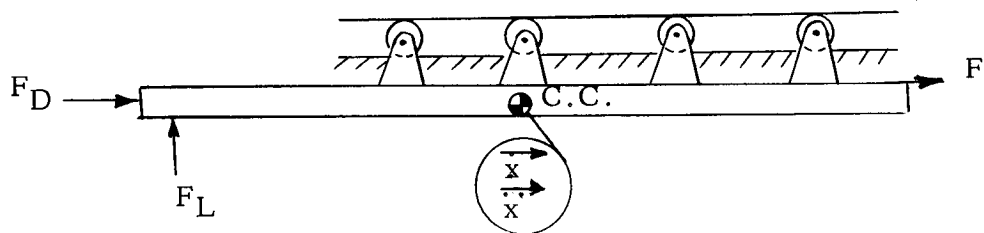
5.1 Dynamics of Guide System - General Expressions

In the system to be analyzed, the rollers are attached to the ramjet and the guide channel built into the ventral fin. Four modes exist during jettison: 1) jettison force is applied, 2) no jettison force is applied with at least two rollers in contact, 3) same as two but only one roller in contact, and 4) no rollers in contact.

The assumptions made to form a model are:

- 1) Lift and drag forces remain constant and their point of application remains constant during jettison.
- 2) Two-dimensional model is used, x coordinate and θ coordinate.
- 3) The translational motion is not affected by rotation.
- 4) Negligible roller friction force

Mode I - Initiation of Jettison



F_j - Jettison force assumed to be constant

F_L - Lift force

F_D - Drag

There will not be any rotation of the ramjet during this mode because of roller guiding.

The equation of motion for translation is

$$F_D + F_J = m \ddot{x}$$

$$x_1 = -\frac{F_D + F_J}{2m} t_1^2 \quad \dot{x}_1 = \frac{F_D + F_J}{m} t_1 \quad (5-1)$$

Where : m is mass of ramjet

t_1 is time

x_1 distance measured from attachment state

Mode II: At least two rollers in contact and no jettison force

$$x_2 = \frac{F_D}{2m} t_2^2 + \dot{x}_{1F} t_2 \quad (5-2)$$

$$\dot{x}_2 = \frac{F_D}{m} t_2 + \dot{x}_{1F} \quad (5-3)$$

Where : t_2 - Time since release of jettison force

\dot{x}_{1F} - Velocity of ramjet at release of jettison force

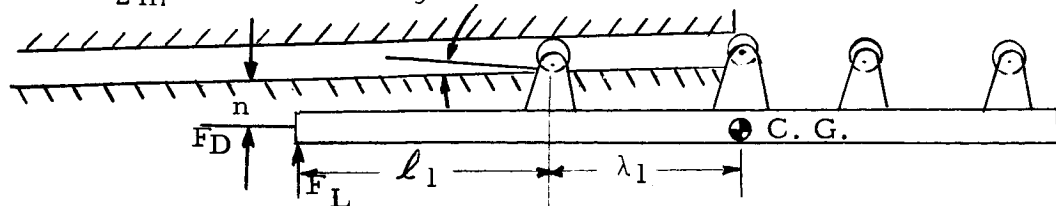
x_2 - Distance measured from release of jettison force

Mode III: One roller in contact

Translation:

$$\dot{x}_3 = \frac{F_D}{m} t_3 + \dot{x}_{2F} \quad (5-4)$$

$$x_3 = \frac{F_D}{2m} t_3^2 + \dot{x}_{2F} t_3 \quad (5-5)$$



Rotation :

$$T = I \ddot{\theta}_1$$

$$F_L \ell_1 - F_{Dn} = (I_{CG} + m \lambda_1^2) \ddot{\theta}_1$$

$$\dot{\theta}_1 = \frac{F_L \ell_1 - F_{Dn}}{I_{CG} + m \lambda_1^2} t_3 \quad (5-6)$$

$$\theta = \frac{F_L \ell_1 - F_{Dn}}{I_{CG} + m \lambda_1^2} \frac{t_3^2}{2} \quad (5-7)$$

Where : x_3 - Distance measured from beginning of Mode III.

θ_3 - Rotation of ramjet

t_3 - Time from start of Mode III

Mode IV : No rollers in contact:

Rotation:

$$F_L(\ell_1 + \lambda_1) = I_{CG} \ddot{\theta}_2$$

$$\dot{\theta}_2 = \frac{F_L(\ell_1 + \lambda_1)}{I_{CG}} t_4 + \dot{\theta}_1 F \quad (5-8)$$

$$\theta_2 = \frac{F_L(\ell_1 + \lambda_1) t_4^2}{I_{CG}} + \dot{\theta}_1 F t_4 \quad (5-9)$$

Translation:

$$x_4 = \frac{F_D}{2m} t_4^2 + \dot{x}_3 F t_4 \quad (5-10)$$

5.2 Specific Case Where The Front Roller Is At Station 465

Assume : 1) F_J is applied over a distance $L_1 = 4$ inches

2) F_D adjusted to account for roller friction

$$F_D = 5,000 \text{ lbs.}$$

3) $F_J = 10,000$ lbs.

Mode I : Equation (5-1)

$$t_1^2 = \frac{2m \times 1}{F_D + F_J} = \frac{2 \times 1000 \times 4}{386 (15,000)}$$

$$t_1 = 0.037 \text{ sec.} \quad (5-11)$$

$$\dot{x}_{1F} = \frac{(15,000)(386)}{1000} (.037) = 214 \text{ in/sec} \quad (5-12)$$

Mode II : Equations (5-2) and (5-3)

The front roller is at fuselage station 465 and the second roller at 495. Ventral fin ends at fuselage station 565.

$$x_2 = 565 - 495 - 4 = 66 \text{ inches.}$$

$$\frac{F_D}{2m} t_2^2 + \dot{x}_{1F} t_2 - x_2 = \frac{5000 \times 386}{2 \times 1000} t_2^2 + 214 t_2 - 66 = 0$$

$$t_2^2 + 0.33 t_2 - 0.102 = 0$$

$$t_2 = 0.1945 \quad (5-13)$$

$$\dot{x}_{2F} = \frac{F_D}{m} t_2 + x_{1F} = \frac{5000 \times 386}{1000} \times 0.1945 + 214$$

$$\dot{x}_{2F} = 589 \text{ in/sec} \quad (5-14)$$

Mode III : Equations (5-4) thru (5-7)

$$\lambda_1 \text{ is } 495 - 465 = 30 \text{ inches} = x_3$$

From equation (5-5)

$$\frac{F_D}{2m} t_3^2 + \dot{x}_{2F} t_3 - x_3 = \frac{5000 \times 386}{2 \times 1000} t_3^2 + 589 t_3 - 30 = 0$$

$$t_3 = 0.0479 \text{ sec} \quad (5-15)$$

Substituting into equation (5-7) gives

$$\theta = \frac{(60,000)(40) - (5000)(10)}{7000 + \frac{1000}{386}(-75)^2} \times \frac{(0.479)^2}{2}$$

$$\theta = 0.1245 \text{ radians.} \quad (5-16)$$

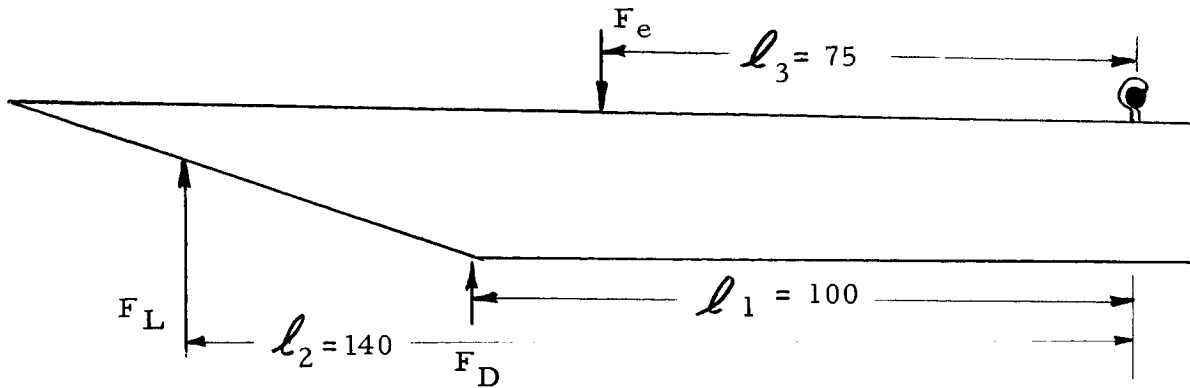
As the last roller leaves the channel guide track, the nose of the engine some 65 inches in front of the roller has raised.

$$\delta = 65\theta = 7.3 \text{ inches} \quad (5-17)$$

If the ramjet nose undergoes a rotation of this magnitude, it will strike the ventral fin of the X-15.

Other cases were considered and the conclusion was reached that rollers or other means of guiding must be provided right up to the nose of the ramjet.

5.3 Peel Off Jettison Study



F_L - Lift force = 60,000 lbs.

F_D - Drag force resisting jettison

F_e - Ejection force

The fluid resisting force due to the movement of ramjet through a fluid is

$$F_D = -C_D \frac{\rho AV^2}{2g} \quad (5-18)$$

C_D - Drag Coefficient = Assumed to be 2

ρ - Density of fluid = Assumed to be 0.001 lb/in³

V - Velocity of ramjet

A - Cross sectional area

It is assumed that the resultant drag force acts at 100 inches from the pivot

$$F_D = -C_D \frac{(.001)(188)(24)V^2}{2(386)} = 0.00585 C_D V^2$$

Taking moments about the pivot gives

$$M_D = 100F_D = 0.585 (2) (100)^2 \theta^2 = 1.17 \times 10^4 \theta^2 \quad (5-19)$$

As a first approximation

$$M_D = 0.585 \times 10^4 \theta \quad (5-20)$$

At jettison, the rigid connection is completely severed and the rear connection severed forming a pivot.

Taking moments about this pivot assuming it to be frictionless and the drag-thrust force to be negligible compared to lift force .

$$\Sigma M_R = 75 F_e - 140 F_L - M_D - I_o \ddot{\theta} = 0 \quad (5-21)$$

Where I_o - Mass moment of inertia about rear support

$$I_o = \frac{W}{g} d^2 + I_{CG} = m d^2 + \frac{1}{2} m l^2 \quad (5-22)$$

$$I_o = \frac{900}{386} \times (70)^2 + \frac{1}{12} \left(\frac{900}{386} \right) (188)^2 = 11,400 + 6860$$

$$I_o = 18,260 \text{ in. lb. sec.}^2$$

Substituting (5-20) and (5-23) into (5-21) gives

$$18,260 \ddot{\theta} + 0.585 \times 10^4 \theta = 75 F_e - 8.4 \times 10^6$$

$$\ddot{\theta} + 0.320 = 0.0041 F_e - 460 \quad (5-24)$$

The general solution is

$$\theta = A_1 \sin \sqrt{.32t} + B \cos \sqrt{.32t} + 0.0128 F_C - 1435 \quad (5-25)$$

Applying boundary conditions

$$\text{At } t = 0 \quad \theta = 0$$

$$t = 0 \quad \theta = 0$$

$$\theta = (.0128 F_e - 1435) (1 - \cos. 568t) \quad (5-26)$$

(Must be positive)

To jettison F_e must be greater than

$$F_e \geq \frac{1435}{.0128} = 112,000 \text{ lbs.} \quad (5-27)$$

If $F_e = 120,000 \text{ lbs.}$, the time for the ramjet to rotate 7° is

$$t = 1.76 \cos.^{-1} \left(1 - \frac{.1221}{100} \right)$$

$$t = (1.76) (.0510) = 0.0897 \text{ sec.} \quad (5-28)$$

APPENDIX VI MATHEMATICAL MODEL DYNAMIC ANALYSIS OF SUSPENSION SYSTEM

6.1 Fuel-Line Stiffness

It was assumed that fuel to the ramjet would be fed from the X-15 through a flexible tube of 1.5 to 2.0 in I. D. A check with various manufacturers of cryogenic equipment showed that the beam stiffness of their flexible tubing was unknown to them. In our cryogenics laboratory we examined such flexible tubing and found that its beam stiffness was nearly zero. The application of internal pressure did not materially stiffen the tubing. The quick-disconnect joints used with such tubing introduce additional flexibility because of the manner in which the joint has been arranged to minimize heat input.

In this light, we could not see how the fuel-line stiffness would need to be a source of error in the thrust measurements. Ordinary attention in design to avoid too short a length of flexible tubing across the ramjet - X-15 interface should be adequate.

6.2 Electrical-Line Stiffness

It was assumed that the number of electrical leads to cross the ramjet - X-15 interface might be as great as several hundreds. This would produce a single bundle 2 or 3 inches in diameter, which when served, coated and taped would be too stiff and be a source of error. Since there is no overriding reason why all wires would have to be in one stiff cable, it was concluded that when the electrical harness is designed, the wire bundles must be kept small and flexible. The total fore-and-aft stiffness of the wires across the interface must be less than 2000 lb/in at the temperatures at which measurements are to be made.

6.3 Static Load Stresses

In order to evaluate stresses and deformations in the sensor equipment, analyses were set up for machine computation. These computations followed the sequence:

1. Devise a mathematical model of the X-15, sensors and ramjet which will provide the desired motion and stress data
2. Calculate by hand the elementary beam stiffnesses and geometry for input to the programs.
3. Compile the stiffness matrix for the model.
4. Reduce the size of the stiffness matrix to eliminate coordinates not essential to the problem.
5. Invert the stiffness matrix to a flexibility matrix.
6. Multiply the flexibility matrix by a static load matrix to get the deformations.
7. Apply these deformations to the elementary beam stiffness to get shears and moments.
8. Convert the shears and moments to stresses.

For additional information in the aft-jettison design a further step was added:

9. Calculate the normal frequencies and mode shapes.

6.4 Method of Stiffness Compilation

The method of compiling stiffness matrices discussed in Reference 44 was the method used for this problem. This method considers the structure to have its masses concentrated at specific points, called "mass points", while the structure between the mass points is considered to consist of simple beams. For the mathematical model shown in Figure 6-1, for example, it is natural to locate mass points at the numbered circles, and observe that the elements between are flexure members.

We take each flexure member as shown in Figure 6-2, as a simple cantilever beam with its centroidal axis along the Z-axis, and usually with its principal axes of bending parallel to the X and Y axes. In this condition, the flexibilities of the cantilever are computed by the usual strength of materials relationships, except that shear deformation is included since the members are often short compared to their transverse dimensions. For Figure 6-2, the formulas would be:

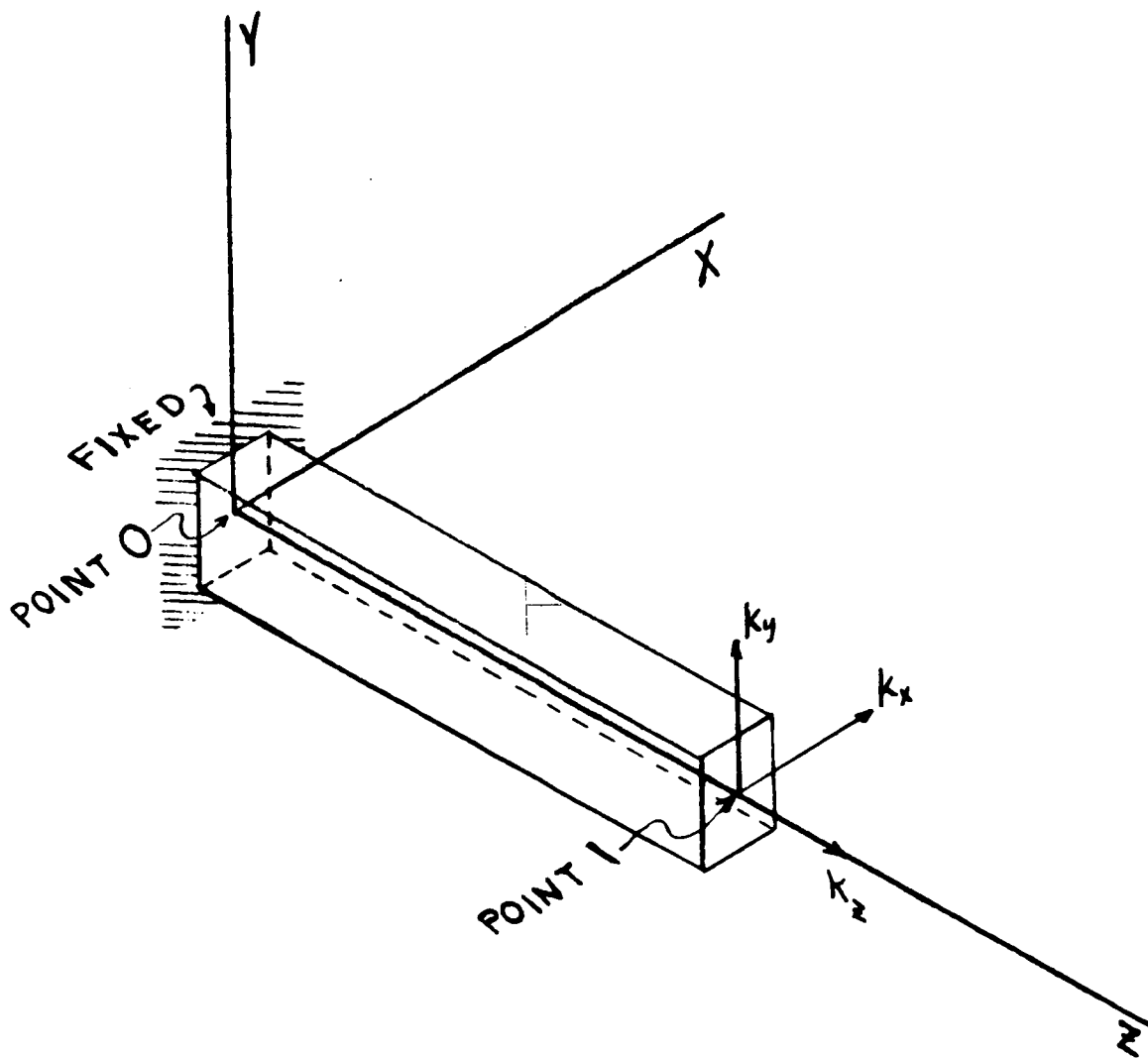


Figure 6-2 Cantilever Beam Element

$$f_{xx} = \frac{l^3}{3E I_y} + \frac{F_x l}{G A_{wx}} \quad x - \text{direction flexibility}$$

$$f_{yy} = \frac{l^3}{3E I_x} + \frac{F_y l}{G A_{wy}} \quad y - \text{direction}$$

$$f_{zz} = \frac{l}{EA} \quad z - \text{direction}$$

$$f_{\theta\theta} = \frac{l}{E I_x} \quad \theta - \text{rotation}$$

$$f_{\phi\phi} = \frac{l}{E I_y} \quad \phi - \text{rotation}$$

$$f_{\psi\psi} = \frac{l}{GJ} \quad \psi - \text{rotation}$$

$$f_{\theta y} = \frac{l^2}{2E I_x} \quad \theta y - \text{cross flexibility}$$

$$f_{x\phi} = \frac{l^2}{2E I_y} \quad x\phi - \text{cross flexibility}$$

in which E = Young's modulus - psi

I = Moment of inertia - in⁴

F = Shear deflection form factor - dimensionless

A_w = Area of web in shear - in²

A = Total area of cross section - in²

J = Torsional moment of inertia - in⁴

l = Length - in

d = Depth of section - in

G = Shear modulus of elasticity - psi

Once the flexibilities of the cantilever element have been calculated, they are arranged into a 6 x 6 flexibility matrix, K^{-1} , which is inverted to give the basic stiffness matrix K_b . This basic stiffness matrix is the building block from which the matrix is compiled.

$$K_b = \begin{bmatrix} k_{xx} & 0 & 0 & 0 & k_{x\phi} & 0 \\ 0 & k_{yy} & 0 & k_{y\theta} & 0 & 0 \\ 0 & 0 & k_{\theta\theta} & 0 & 0 & 0 \\ 0 & k_{y\theta} & 0 & k_{\theta\theta} & 0 & 0 \\ k_{x\phi} & 0 & 0 & 0 & k_{\phi\phi} & 0 \\ 0 & 0 & 0 & 0 & 0 & k_{\psi\psi} \end{bmatrix} \quad (6-1)$$

In order to rotate the beam element in Figure 6-3 from position 0-1 to its final orientation in space, 0-2, we multiply K_b by the rotation matrix, R ,

$$K_r = R^T K_b R \quad (6-2)$$

Since it often happens that the end of the beam element, (2), and the mass point, (3), do not coincide, we can also translate the stiffness from (2) to (3) by a translation matrix, T ,

$$K_{rT} = T^T K_r T = K_{33} \quad (6-3)$$

The stiffness matrix at point 0 can now be obtained by the application of equilibrium and geometry, which reduce to a carry-over matrix, B . If the root of the cantilever element, 0, does not coincide with the near-end mass point, 4, then the carry-over matrix accounts for this and B is

$$B = \begin{bmatrix} -1 & 0 & 0 & 0 & -(z_3 - z_4) & + (y_3 - y_4) \\ 0 & -1 & 0 & +(z_3 - z_4) & 0 & - (x_3 - x_4) \\ 0 & 0 & -1 & -(y_3 - y_4) + (x_3 - x_4) & 0 & 0 \\ 0 & 0 & 0 & -1 & 0 & 0 \\ 0 & 0 & 0 & 0 & -1 & 0 \\ 0 & 0 & 0 & 0 & 0 & -1 \end{bmatrix} \quad (6-4)$$

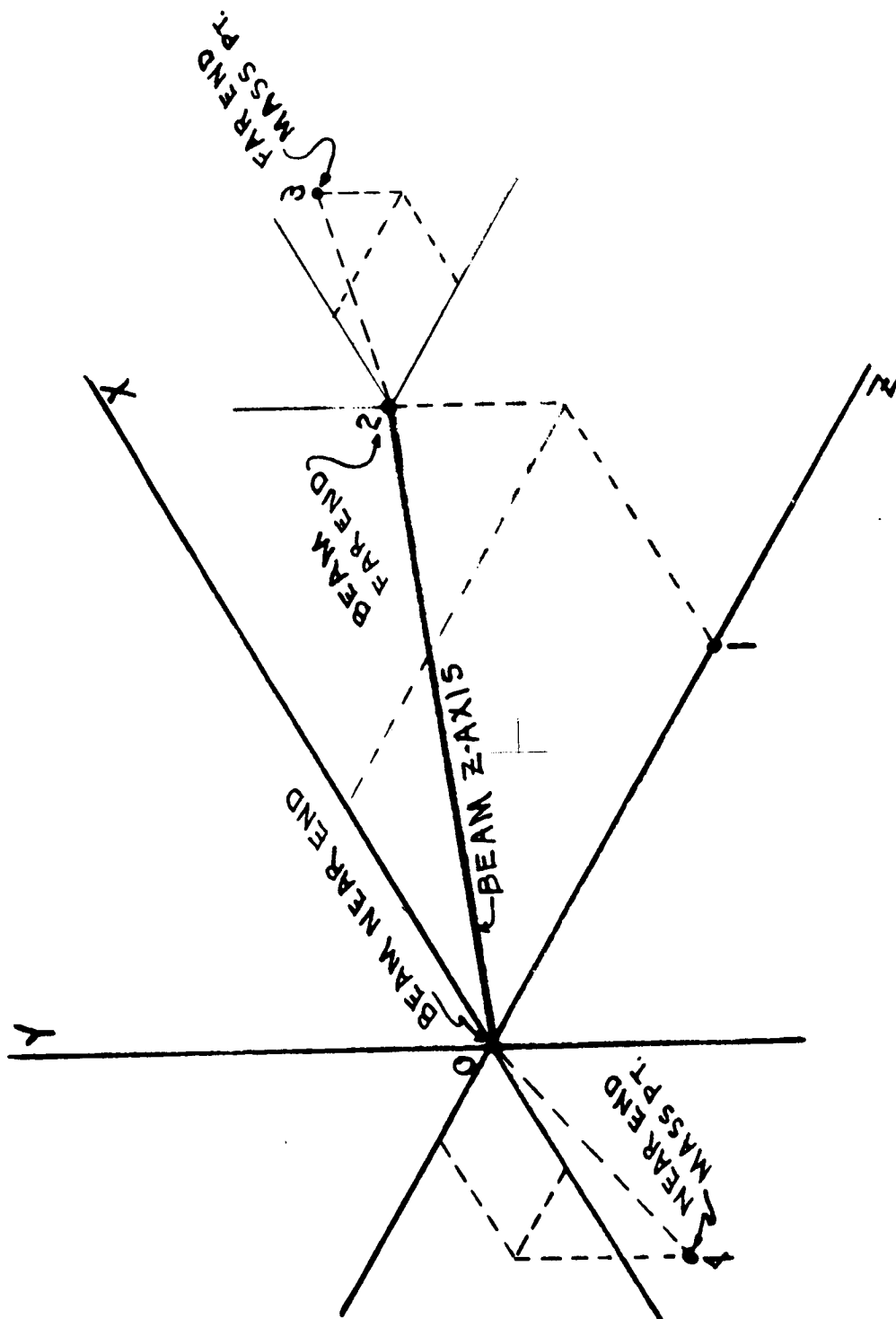


Figure 6-3 Rotation & Translation of Beam

Whence

$$K_{34} = K_{33} B \quad (6-5)$$

Now we have all of the information necessary to compile the stiffness matrix. Consider Figure 6-4 and realize that each elementary spring has two ends, each associated with a particular mass point. Consequently each spring needs to have 4 submatrix slots allocated to it in the structure matrix. In terms of Figure 6-3, one slot, 33, is needed when displacements are applied to point 3; and a second slot, 34, for the carry-over to point 4. Another slot, 44, is needed when displacements are applied to point 4; and a fourth slot, 43, for the carry-over to point 3. The matrix for slot 33 is different from the matrix for slot 44 (in all but special cases), and the matrix for 34 is the transposed of the matrix for 43 in every case by the reciprocity theorem. Since the displacement of point 4 in Figure 6-3 still requires equilibrium of the forces and moments on the spring, we can get the 44 matrix by operating on the 43 matrix with the B matrix:

$$K_{43} = K_{34}^T \quad (6-6)$$

$$K_{44} = K_{43} B \quad (6-7)$$

This is shown diagrammatically in Figure 6-4. Every slot for a submatrix which is on the main diagonal, 44, 33, and so on, will stack up as many submatrices as there are springs framing into the mass point, but the off-diagonal slots, 34, 43, and so on, will only have one submatrix.

To summarize the process of generating a stiffness matrix, we use these steps:

1. Study the structure to see where mass points need to be and what coordinates should be applied to these mass points.
2. Cut out individual spring elements from the structure and compute their basic matrices, K_b .
3. Calculate the rotation matrix, R, to get the member oriented as it is to be in the structure.
4. Calculate the translation matrix, T, to get the effect of the far end of the spring moved to the mass point.
5. Calculate the carry-over matrix, B, from the far-end mass point to the near-end mass point.

6. Allocate four submatrix slots in the structure matrix.
7. Perform the multiplications and drop the matrices in their slots according to Figure 6-4.
8. Check for symmetry and to insure that each row does in fact represent an equilibrium condition.
9. Continue with each spring element like stacking dominoes until the matrix is complete.

Reduction of Matrix Size

There is usually one or more of these reasons for reducing the size of a matrix:

10. It was convenient to compile more coordinates than are finally needed in a problem, and now it is to be reduced in size to run at lower cost.
11. It is desirable to constrain some coordinates to zero to provide a ground to an otherwise floating system.
12. It is desirable to constrain some coordinate to zero to divide the problem into symmetric and anti-symmetric parts.

Crossing out rows and columns in a stiffness matrix constrains those coordinates to zero motion. Crossing out rows and columns in a flexibility matrix requires the forces or moments on those coordinates to be zero. If we consider the following two matrix equations:

force	stiffness	displacement	
$\begin{bmatrix} P_1 \\ P_2 \\ P_3 \end{bmatrix}$	$\begin{bmatrix} K_{11} & K_{12} & K_{13} \\ K_{21} & K_{22} & K_{23} \\ K_{31} & K_{32} & K_{33} \end{bmatrix}$	$\begin{bmatrix} X_1 \\ X_2 \\ X_3 \end{bmatrix}$	(6-8)

$$\begin{array}{ccc}
 \text{force} & \text{flexibility} & \text{displacement} \\
 \left[\begin{array}{c} X_1 \\ X_2 \\ X_3 \end{array} \right] & \left[\begin{array}{ccc} f_{11} & f_{12} & f_{13} \\ f_{21} & f_{22} & f_{23} \\ f_{31} & f_{32} & f_{33} \end{array} \right] & \left[\begin{array}{c} P_1 \\ P_2 \\ P_3 \end{array} \right]
 \end{array} \quad (6-9)$$

We see that eliminating row 3 and column 3 in (6-8) has the same effect as making $X_3 = 0$. On the other hand, eliminating row 3 and column 3 from (6-9) has the same effect as making $P_3 = 0$. To comply with reason 10 above then requires a cross-out operation on a flexibility matrix (or the equivalent on a stiffness matrix by making $P_3 = 0$). To comply with reasons 11 or 12 above requires a cross-out operation on a stiffness matrix (or the equivalent on a flexibility matrix by making $X_3 = 0$).

Inversion of Stiffness to Flexibility

Inversion of a matrix is a standard operation which usually goes through with no trouble. Sometimes, for reasons which would be too expensive to track down, the direct inversion will not run properly. When this happens, it sometimes is necessary only to rearrange rows and columns, and other times it is necessary to partition into smaller matrices. Both of these devices are standard and unremarkable.

Flexibility Times Load Equals Deformation

This operation is standard matrix multiplication and requires no discussion.

Conversion of Deformations to Shears and Moments

At this stage of the calculation, we have the following items available:

X = Matrix array of displacements caused by various loads.

K_b = The basic stiffness of each beam element.

The geometry illustrated in Figure 6-3 results from the application of calculated displacements to the elementary beam of Figure 6-2.

To do this we can form,

- T_{32} the 6 x 6 matrix to translate distortions from a mass point to a beam end as in Figure 6-3.
- R_{21} the 6 x 6 matrix to rotate distortions into beam axes as from 02 to 01 in Figure 6-3.
- T_{42} the 6 x 6 matrix which projects the 4-end distortions to the 2-end of the beam.
- T_{24} the 6 x 6 matrix which translates forces and moments at the 2-end to the equilibrating forces and moments at the 4-end.

With this information, we then calculate

$$P_1 = K_b (R_{21} T_{32} X_3 - T_{42} R_{21} X_4) \quad (6-10)$$

in which P_1 is the 6 x 1 vector of forces and moments

X_3 is the 6 x 1 vector of displacements at mass point 3

X_4 is the 6 x 1 vector of displacements at mass point 4.

Conversion of Shears and Moments to Stresses

According to the way in which each beam element was set up in the beginning, it is now possible to apply the load vector, P_1 , to the 1 end of the beam in Figure 6-2. Stresses can then be calculated at any location in the beam by the usual means. Where many load vectors or many beams are involved, it is better to mechanize this operation also. We form a stress-conversion matrix, S , and let it operate on P_1 to give the stress, σ , thus:

$$\sigma = SP_1 \quad (6-11)$$

The stresses coming out of equation (6-11) often contain combinations of shear and direct stress that can be significantly more severe than the uniaxial stress would imply. Consequently, we combine these stresses into an "equivalent tensile stress", taken as

$$2\gamma_{\max} = \left[\sigma_z^2 + 4\gamma_{xz}^2 \right]^{\frac{1}{2}} = \left\{ \begin{array}{l} \text{Equivalent} \\ \text{Tensile} \\ \text{Stress} \end{array} \right\} = \text{SE} \quad (6-12)$$

Figure 6-5 illustrates a beam element and the stress situation at four locations involved in this particular operation.

6.5 Results for Peel-Off Design

The mathematical model used in the peel-off design is shown in Figure 6-1. A machine print-out has been prepared and includes the following:

- a) stiffness compilation input
- b) compiled stiffness matrix
- c) reduced stiffness matrix
- d) inverse of the reduced matrix
- e) load matrix
- f) beam shears, moments and stresses
- g) tensile stress.

Table 6-2 is a log of these data sheets for convenient reference. Table 6-3 lists the relative motions between mass points 13 and 14 in the Z direction as the sensor would see them. The maximum stresses in the three important springs are listed in Table 6-4, and it is clear that some stresses are too high and will require some design changes if this design is to be used. The loads applied are listed in Table 6-1.

6.6 Results for Fore-and-Aft Design

The mathematical model for the fore-and-aft jettison design is shown in Figure 6-6. This model was used as a symmetric model, so only the front half of the mass points are numbered and used. The data sheet log is given in Table 6-5. The loads applied are listed in Table 6-6, the relative motions across the measurement points in Table 6-7, and the significant

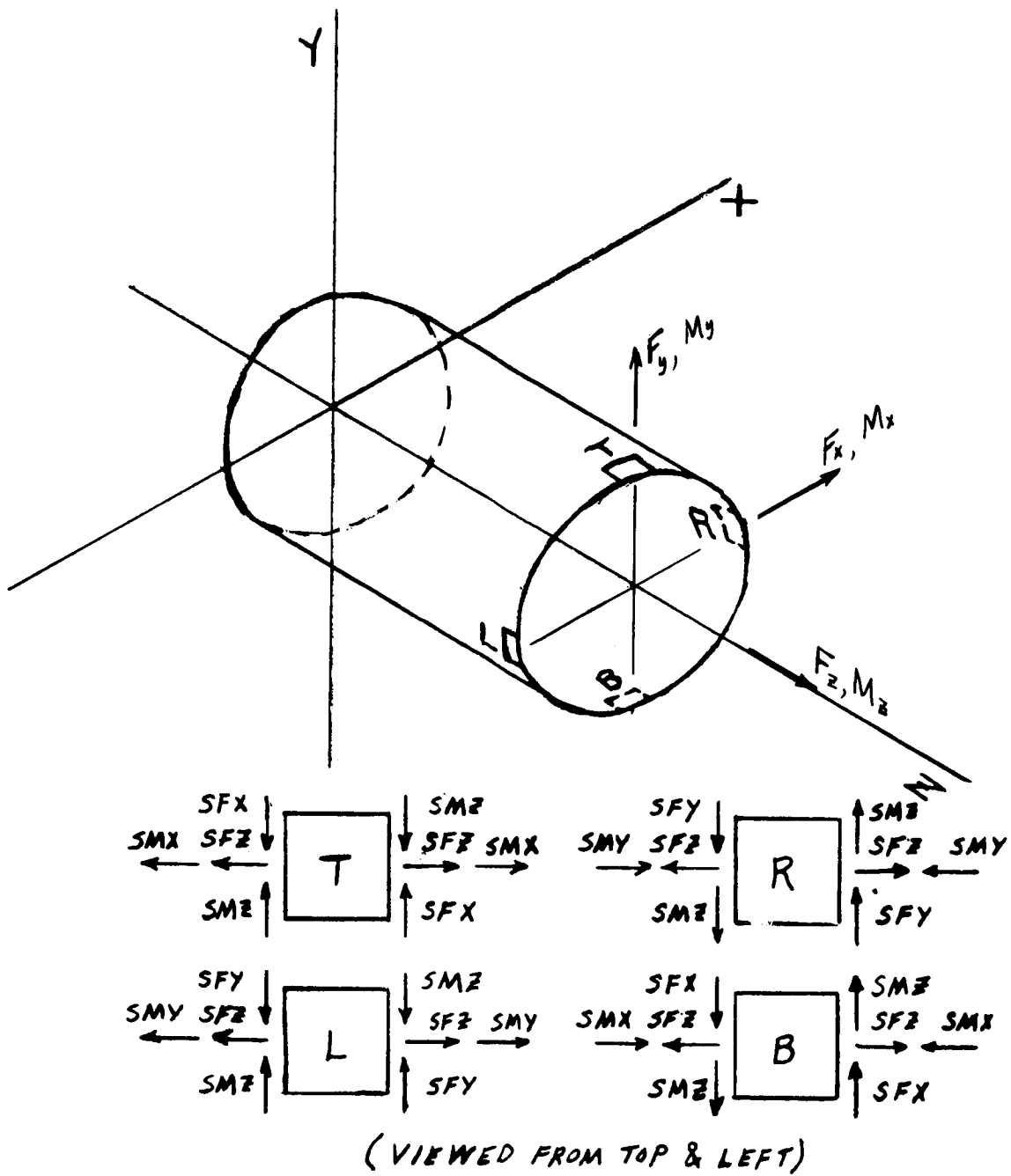


Figure 6-5 Stresses for Combination into "Equivalent Stress Intensity"

TABLE 6 -1

Load Vectors - Case 1

Coord. No.	Mass No.	Vector No.								
		1	2	3	4	5	6	7	8	9
65	19Z	+6000	0	0	0	0	0	0	0	0
63	19Y	0	+60000	0	0	0	0	0	0	0
61	19X	0	0	+10000	0	0	0	0	0	0
53	17Z	0	0	0	+10	0	0	0	0	0
51	17Y	0	0	0	0	+10000	0	0	0	0
49	17X	0	0	0	0	0	+10000	0	0	0
59	18Z	0	0	0	0	0	0	+500	0	0
57	18Y	0	0	0	0	0	0	0	-10000	0
55	18X	0	0	0	0	0	0	0	0	+10000

TABLE 6 -2

Data Sheet Log - Case 1

From Sheet No.	To Sheet No.	
001	024	Input to Stiffness Compilation
025	099	Stiffness Matrix as Compiled, K
100	118	K Reduced in Size to K_R
119	138	K Reduced and Inverted to K_R^{-1}
139	143	Load Matrix, L
143	147	Deformation Matrix, R
148	156	Shears, Moments, and Stresses
157	165	Equivalent Tensile Stress

TABLE 6-3

Relative Z-Motion of Masses 13 & 14
Case 1

Vector No.	Load Lbs.	At.	Relative Motion-In.
1	+6000	19Z	+.00498
2	+60000	19Y	-.00080
3	+10000	19X	-.00415
4	+ 10	17Z	+.00001
5	+10000	17Y	-.00002
6	+10000	17X	+.00115
7	+ 500	18Z	+.00041
8	-10000	18Y	-.00005
9	+10000	18X	+.00595

TABLE 6-4

Summary of Stresses - Case 1

Vector No.	Lbs.	Load At.	Stress - Psi		
			1-3	2-4	9-10
1	+6000	19Z	55580	58850	9576
2	+60000	19Y	243000	190800	158500
3	+10000	19X	131000	89390	47970
4	+ 10	17Z	92	98	16
5	+10000	17Y	18610	17700	120
6	+10000	17X	63090	66470	19740
7	+ 500	18Z	4630	4903	806
8	-10000	18Y	1470	1619	26620
9	+10000	18X	94280	150400	61270

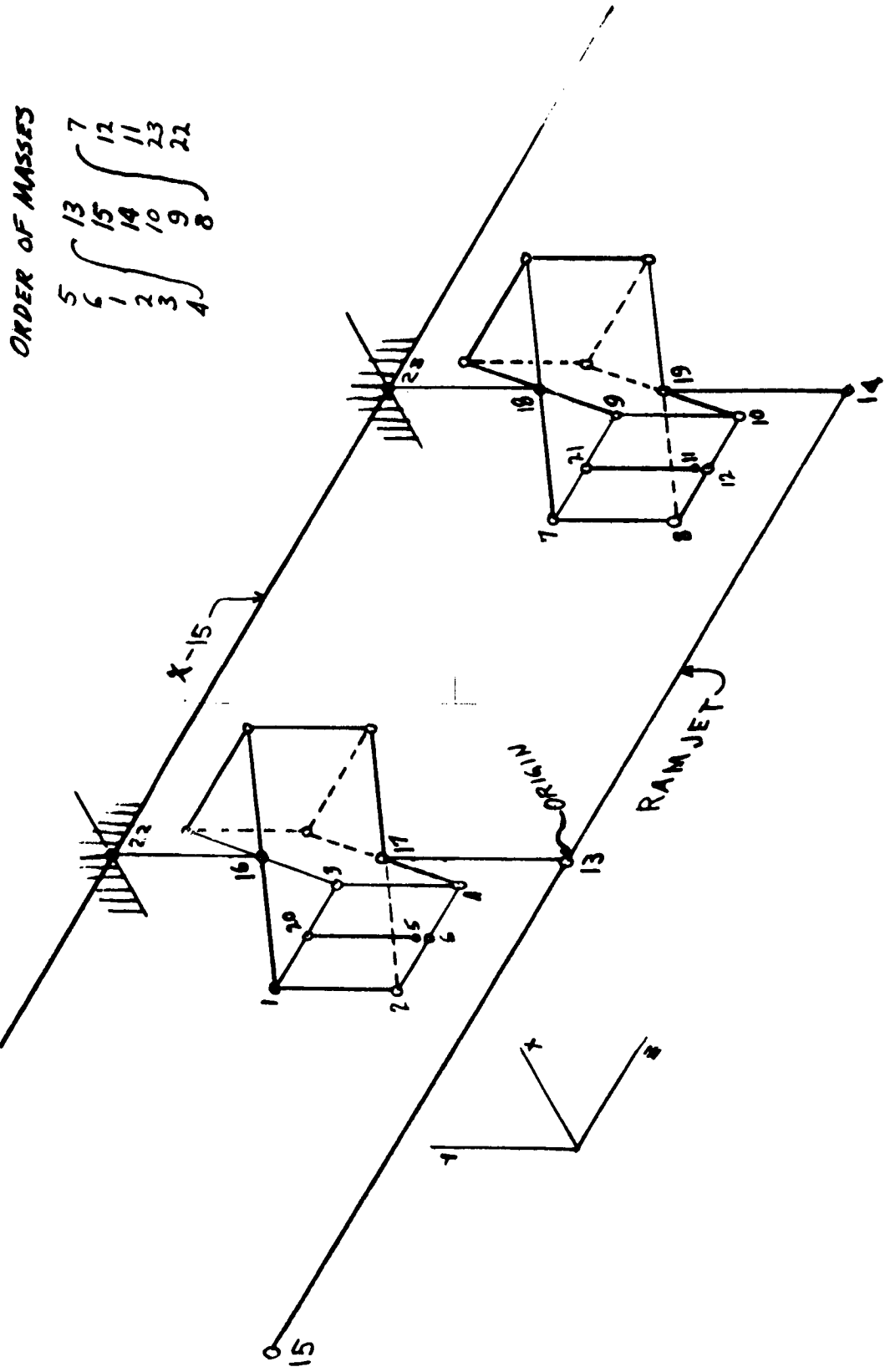


Figure 6-6 Mathematical Model for Fore & Aft Jettison

TABLE 6 - 5

Data Sheet Log - Case 2

From Sheet No.	To Sheet No.	
001	019	Input to Stiffness Compilation
020	088	Stiffness Matrix as Compiled, K
089	129	K Reduced in Size to K_R
130	159	K Reduced and Inverted to K_R^{-1}
160	162	Load Matrix, L
162	165	Deformation Matrix, R
166	189	Shears, Moments, and Stresses
190	213	Equivalent Tensile Stress
214	246	Eigenvalues and Eigenvectors

TABLE 6-6

Load Vectors - Case 2

Coord. No.	Mass No.	Vector No.								
		1	2	3	4	5	6	7	8	9
42	15Z	+6000	0	0	0	0	0			
41	15Y	0	+60000	0	0	0	0			
39	13Z	0	0	+10	0	0	0			
38	13Y	0	0	0	+10000	0	0			
45	14Z	0	0	0	0	+ 500	0			
44	14Y	0	0	0	0	0	-10000			
40	15X							+10000	0	0
37	13X							0	+10000	0
43	14X							0	0	+10000

TABLE 6-7

Relative Z-Motion of Masses
Case 2

Vector No.	Load Lbs.	At.	Relative Mass 5-6	Motion -In Mass 11-12
1	+6000	15Z	$.5 \times 10^{-11}$	$.72 \times 10^{-4}$
2	+60000	15Y	$.9 \times 10^{-9}$	$.25 \times 10^{-3}$
3	+ 10	13Z	$.9 \times 10^{-14}$	$.12 \times 10^{-6}$
4	+10000	13Y	$.7 \times 10^{-10}$	$.25 \times 10^{-6}$
5	+ 500	14Z	$.4 \times 10^{-12}$	$.68 \times 10^{-5}$
6	-10000	14Y	$.2 \times 10^{-12}$	$.11 \times 10^{-4}$

stresses in Table 6-8. The stresses reported in this last table are those associated with the bending of the sensor elements about the system X axis. In the machine print-out higher stresses are shown which are associated with bending about the system Z axis. These stresses can be reduced by a factor of 10 or more by the appropriate stiffening of beams 1-16, 3-16, 2-17, 4-17 and so on. To demonstrate this design refinement would require another full cycle of computation. The relative motions across 11-12 Z for Y-direction loads would be very much reduced by this stiffening process, also,

For the fore-and-aft design, a mass matrix was put together and the normal modes and frequencies were run. The resulting normal frequencies are listed in Table 6-9. The lowest 2 or 3 of these frequencies would be raised by the stiffening of the transverse members referred to above.

TABLE 6 -8

Summary of Stresses - Case 2

Vector No.	Load Lbs.	At	Fwd. Sensor	Aft Sensor	Fwd. Sens. Frame	Aft Sens. Frame
1	+6000	15Z	228	5710	0	4672
2	+60000	15Y	18700	58700	0	12490
3	+ 10	13Z	0	10	0	10
4	+10000	13Y	1593	52	0	36
5	+ 500	14Z	20	518	0	443
6	-10000	14Y	5	8839	0	1571

TABLE 6 -9

Normal Mode Frequencies - Case 2

Mode No.	$\frac{1}{W^2}$ (rad/sec) ⁻²	W^2 (rad/sec) ²	f cps
1	.9878-5	1.012+5	50.7
2	.2484-5	4.03+5	101.0
3	.1663-5	6.02+5	123.5
4	.9930-6	1.008+6	160.
5	.2301-6	4.38+6	333.
6	.2028-6	4.93+6	353.
7	.1836-6	5.45+6	372.
8	.1749-6	5.72+6	381.
9	.1014-6	9.85+6	500.
10	.8645-7	1.157+7	540.

6.7 Study of the Flexure as a Flexible Support

The flexure design problem reduces to one of finding the load capacity of a member carrying axial load, shear, and flexure simultaneously. The sketch in Figure

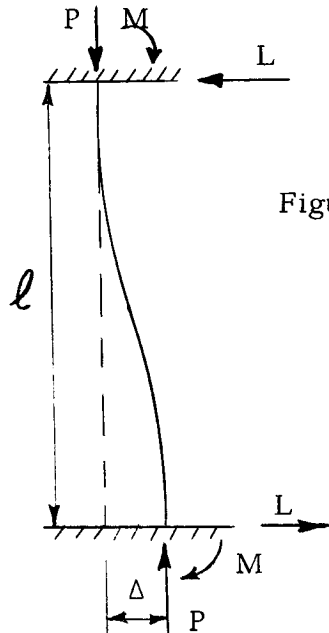


Figure 6-7

shows such a member, with P the axial load, L the shear, and M the bending moment. The direct stress is,

$$\sigma_a = \frac{P}{bt} \quad (6-13)$$

in which b is the width and t the thickness of the member. The bending stress is

$$\sigma_b = M \frac{t}{2I} = \frac{6M}{bt^2} \quad (6-14)$$

The lateral force, or shear is

$$L = \frac{12EI\Delta}{l^3} = Ebt \left(\frac{t}{l} \right)^2 \frac{\Delta}{l} \quad (6-15)$$

when the axial load is zero. For axial compression, this value of L is reduced by a factor which may be approximated by

$$1 - \alpha = 1 - \frac{P}{P_{cr}} \quad (6-16)$$

in which

$$P_{cr} = \frac{\pi^2 EI}{l^2} = \frac{\pi^2}{12} Ebt \left(\frac{t}{l} \right)^2 \quad (6-17)$$

Now let us define

$$\frac{t}{l} = \gamma, \frac{\Delta}{l} = \delta, \quad bt = A \quad (6-18)$$

and write

$$L(1 - \alpha) = EA\gamma^2\delta - \frac{12}{\pi^2} P\delta \quad (6-19)$$

By statics

$$2M = L\ell + P\Delta \quad (6-20)$$

and

$$M = EA\tau^2\delta\frac{l}{2} + P\delta\frac{l}{2}\left(1 - \frac{12}{\pi^2}\right) \quad (6-21)$$

$$\sigma_b = 3\delta\left(E\tau - 0.216\frac{P}{A}\frac{1}{\tau}\right) \quad (6-22)$$

The total stress is then

$$\sigma_t = \frac{P}{A} + 3\delta\left(E\tau - 0.216\frac{P}{A}\frac{1}{\tau}\right) \quad (6-23)$$

and from equation (d7)

$$L_c = EA\tau^2\delta - 1.218 P\delta$$

and the parameters τ , δ , and A can be varied to see if practical arrangements can be made which produce.

$$\sigma_t < \frac{2}{3} \sigma_{\text{yield}} \quad \left. \vphantom{\sigma_t} \right\} \quad (6-24)$$

and

$$0 < L < 100 \text{ Lbs.} \quad \left. \vphantom{L} \right\}$$

when

$$P = 60,000 \text{ Lbs.} \quad \left. \vphantom{P} \right\} \quad (6-25)$$

$$\Delta = 1''$$

$$E = 28 \times 10^6 \text{ psi} \quad \left. \vphantom{E} \right\}$$

For a tensile load on the member, equation (6-16) becomes

$$1 + \alpha = 1 + \frac{P}{P_{\text{cr}}} \quad (6-26)$$

which leads to

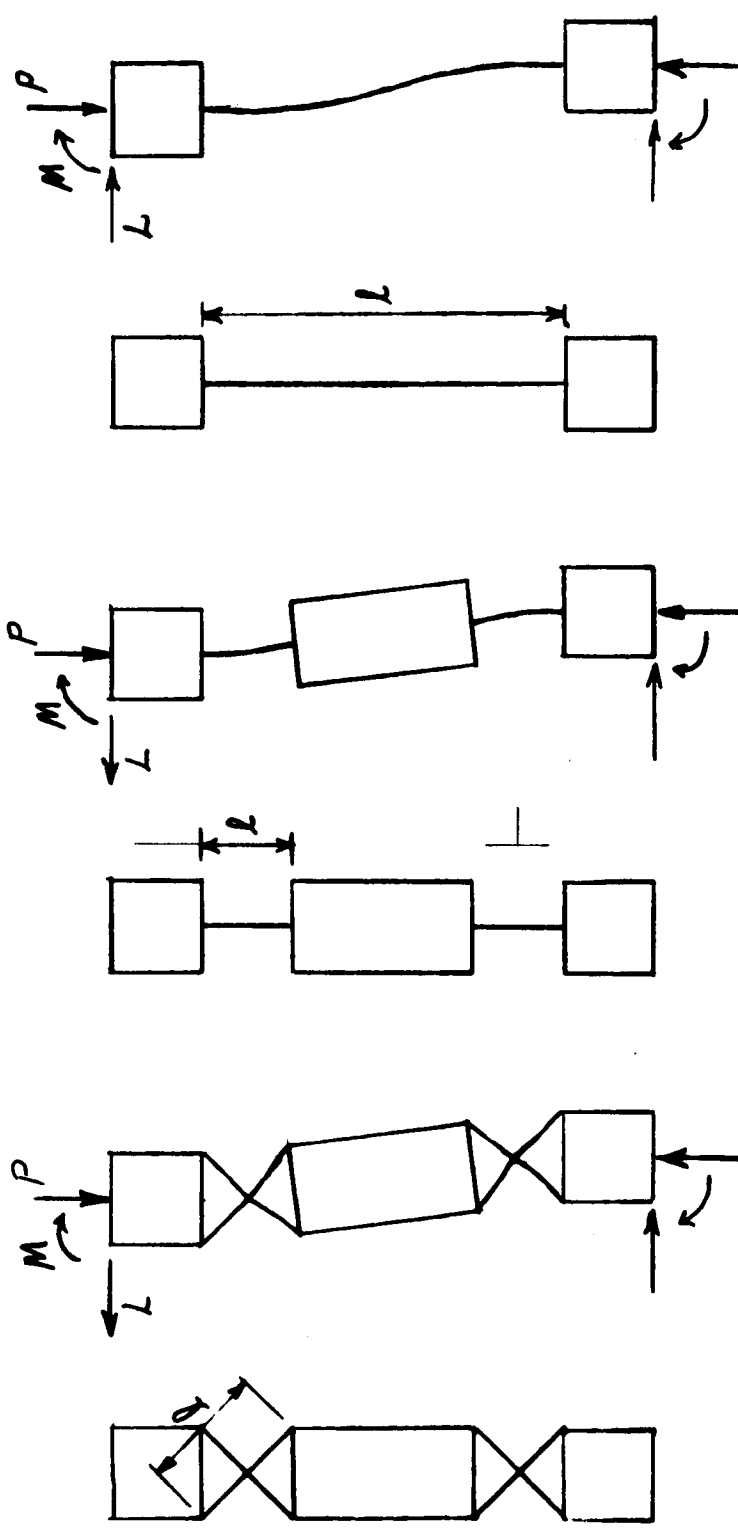
$$\sigma_b = 3\delta\left(E\tau + 2.216\frac{P}{A}\frac{1}{\tau}\right) \quad (6-27)$$

and

$$L_T = EA\tau\delta + 1.218 P\delta \quad (6-28)$$

and again the parameters can be varied to see if conditions (6-24) and (6-25) can be satisfied.

The first configuration to which the above criteria were applied was Figure 6-8a.



(a) Cross-Flexure Hinges, Double

(b) Straight Flexure Hinges, Double

(c) Straight Flexure Hinge, Single

Figure 6-8 Flexure Configurations

With

$$b = 5''$$

$$\Delta = 1''$$

$$l = 2.2''$$

$$\sigma_{\text{allow}} = 30,000 \text{ psi}$$

$$E = 28 \times 10^6 \text{ psi}$$

$$P = 60,000 \text{ Lb.}$$

the thickness, t , needs to be $> 0.30''$ to satisfy stress requirements with $\Delta = 0$, but with $\Delta = 1.0$ and $P = 0$, then $< 13000\#$. These results are not compatible, and we were unable to find a combination of dimensions which would work with both P and Δ so large and yet not have L too large.

The second configuration to be tried was that of Figure 6-8b. A similar set of assumptions to those for the previous try were made, and they led to results which were again incompatible. For a $0.1''$ thick flexure, the working stress would be at the buckling limit of $170,000 \text{ psi}$, and this was not acceptable. Alternatively, for

$$t = 0.10''$$

$$W = 10.0''$$

$$\Delta = 1.0'',$$

the buckling load worked out to be $34,000 \text{ lb.}$ with $L = 210 \text{ lbs.}$ at that load, and this was also unacceptable. Again the $60,000 \text{ lb.}$ load and the 1-in. deflection were too severe for this configuration.

The third configuration to be tried was that shown in Figure 6-8c. For this case, A needs to be greater than 2.0 in.^2 for $P = 60,000 \text{ lbs.}$ and $\Delta = 0$. With $P = 0$ and $\Delta = 1.0''$, $L = 1000 \text{ lb.}$ for $t = .035 \text{ in.}$, but then buckling occurs long before $P = 60,000 \text{ lb.}$ is reached and b would have to be about 60 in. In this case again, the flexibility needed to keep L small requires dimensions that buckle under the application of P .

Numerous different combinations of parameters were tried on each of these configurations, each combination leading to some anomaly. After several tries, it was concluded that it was necessary to arrange the design such that the flexibility to accommodate Δ and the stiffness to carry P would not simultaneously be required.

6.8 X-15 Ramjet Lift Forces

An estimate of the lift force on the X-15 ramjet was made for the conditions of flight at Mach 7.8.

Ambient pressure = $0.37\#/in.^2$ (approx. 82,000 ft.)

Velocity = 7540 ft./sec.

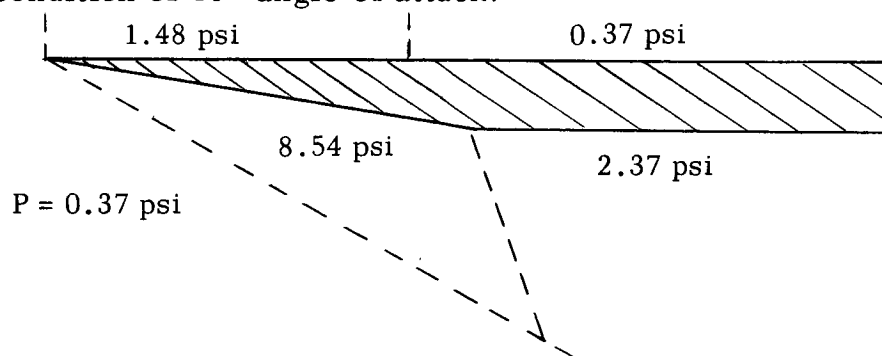
Dynamic Pressure = $2270\#/ft.^2$

Three conditions were considered:

- A. Ramp door closed at a 10° positive flight angle of attack.
- B. Ramp door closed at 0° flight angle of attack.
- C. Ramp door open with a normal shock at the wedge leading edge at 0° angle of attack.

The calculations are based on an attached oblique shock at the leading edge of the wedge followed by an isentropic expansion to the aft body of the ramjet. Two dimensional flow is assumed throughout.

The pressures acting in the various flow regions are illustrated below for the condition of 10° angle of attack.



The lift forces for the three cases are calculated:

$$A = 18,000\#$$

$$B = 4100\#$$

$$C = 257,900\#$$

The force magnitude in the event of shock regurgitation depends on the extent of forward travel of the shock along the ramp. A maximum force was calculated based on a two dimensional normal shock moving to the leading edge. The actual movement may not be this extreme and since this represents the most severe load condition values would best be based on wind tunnel tests. In addition some reduction in pressure from the two dimension assumption would be expected due to flow spillage over the sideplates. Thus, the calculation "C" is an outside rather than a most probable or design value.

APPENDIX VII RAMJET THERMAL ANALYSIS

7.1 Ramjet Support Temperature Rise

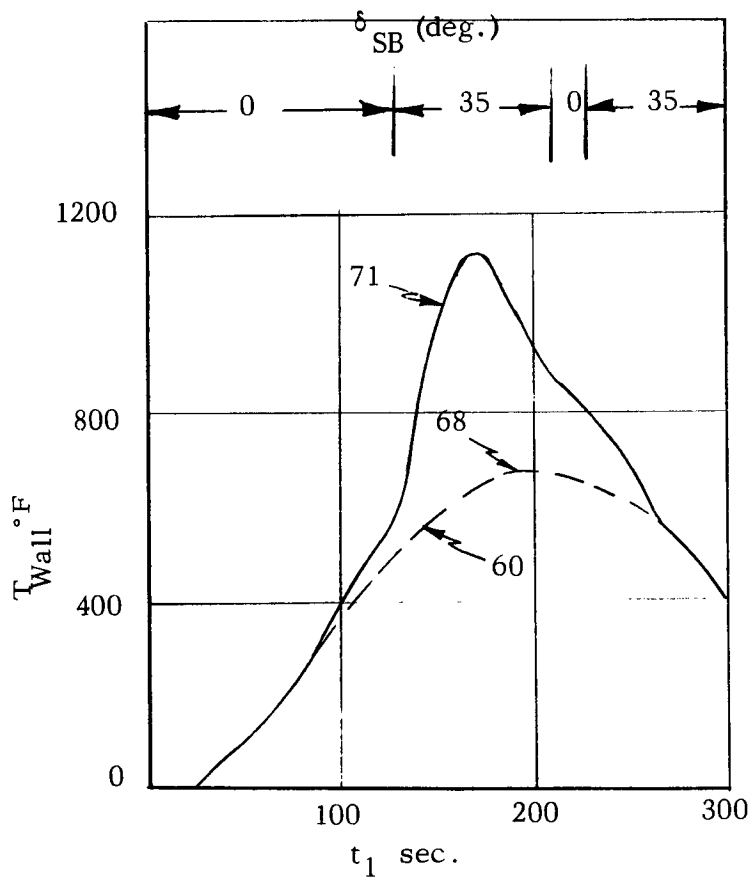
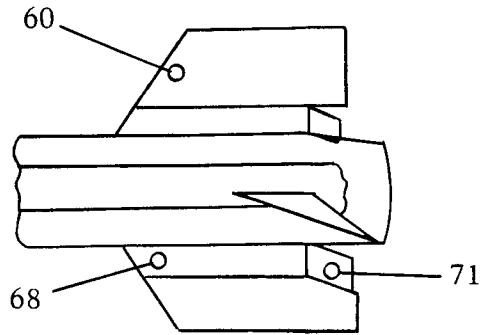
In the absence of shock impingement, a conservative estimate of the skin temperature surrounding the support results in values of 1600°R and 2000°R upon reaching $M = 8$ and after 20 seconds at $M = 8$ respectively. The aerodynamic heating was calculated using similar relations to those referred to in NASA report TMX-883. Figure 7-1 shows a plot of in flight temperature measurements taken by NASA Flight Research Center at Mach 6 in the ventral fin area. Extrapolations were made from this data to determine the temperatures at Mach 8. It is assumed that thermocouples 60 and 68 were probably located on the inner surface of the ventral fin skin. A skin emissivity of 0.75 was also taken from this reference.

Even if some allowance is made for convective heating, the maximum temperature rise for a 1" by 1/2" Inconel X support, due to radiant heating from the surrounding skin, is less than 100°F in the 170 second time period from the initial condition. An emissivity of 0.75 was taken for this calculation, and it is assumed that no direct impingement of shock heated air takes place on any portion of the support for the thrust measuring system.

Heat conduction is not expected to be a serious problem in the relatively short time period of the proposed X-15 flights. As an example, if one assumes that, for structural reasons, one end of the support for the thrust measuring system is fastened to a section on the X-15 structure which undergoes a linear temperature rise of, say 1000°F in 100 seconds, then the local temperature rise of the support at a point 6" away from this hot end is in the order of 100°F . Hence, a total temperature rise of less than 200°F , from the initial temperature, is expected at the end of the 170 second test period. It was assumed that for the last 20 seconds of this period the aircraft is at $M = 8$.

7.2 Thermodynamic Protection Considerations

It is assumed that protection for the X-15 structure from the thermal environment will be provided for the high design speeds of 8000 f. p. s., and also for lower speed flights which have relatively long mission times at high heating rate conditions. For example to maintain the skin temperature at approximately 600°F using ablation material such as ESM-1004 of 70# density, a thickness of .74" may be required at the leading edge and .075" at the sides of the lower ventral fin.



Temperature vs. Time Ventral Fin X-15
Mach 6 - Max. Altitude 102,000 ft.

Figure 7-1

Ref. - NASA-TMX883

7.3 Thermal Protection of the Deflection Block

Further protection of the deflection block from conductive and radiated heat can be made to reduce temperature rise during the test mission.

Conduction: A spacer may be inserted between the deflection block supports made of a low thermal conduction material such as asbestos mill board. (Thermal conductivity $K = 1.07 \text{ BTU/hr. /sq. ft/}^\circ\text{F/in}$) can be inserted.)

Radiation: A thermal shield constructed to protect the deflection block from radiated heat emitted by the surrounding hot structure and any hot gas leakage can easily be applied to this design.

APPENDIX VIII

SENSOR EVALUATION

8.1 Strain Measurements

Strain measurements by mounting wire or foil strain gages on a deflection block were eliminated as a result of sensitivity requirements for the two ranges of thrust force and resolution. A two range mechanical system was considered but it was found impractical. For example, calculation showed that a 10 lb. force would produce approximately a strain of 1.2 micro-strain. If four active gages were used a total strain of 4.8 micro strain would be required to be measured. The problem areas were then obvious, such as requiring higher gain amplifiers, drift due to temperature and also other problems associated with strain gages under extreme environments.

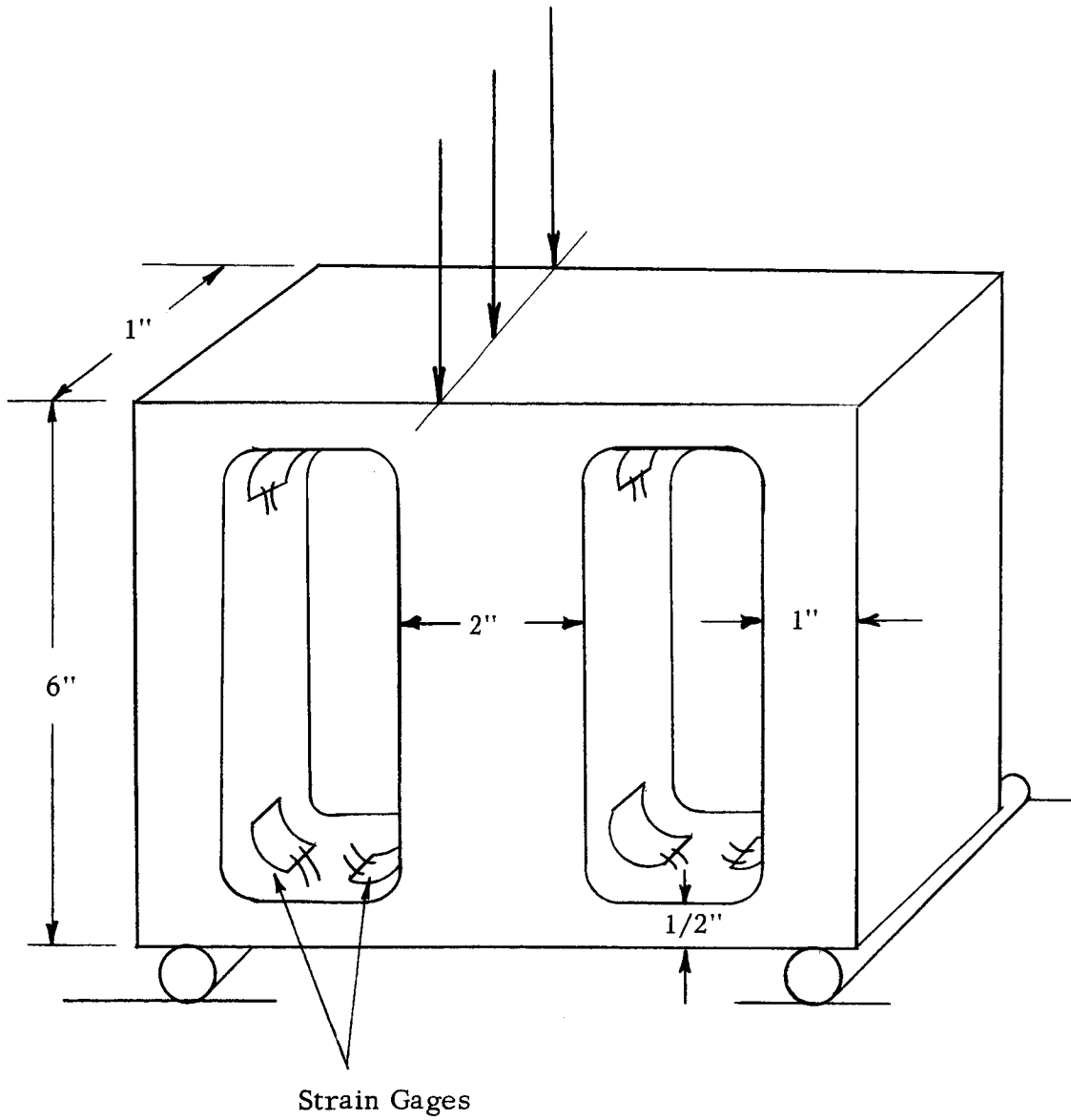
A deflection block was built as shown in Figure 8-1 to verify our calculations. Strain gages were mounted in the fillets as shown in Figure 8-1. The strain gages were connected in a 4 arm Wheatstone bridge circuit, all being active. The results are plotted on Figure 8-2. It can be noted that the magnitude of the strain in the lower load range makes it impractical to record with any accuracy. Semi-conductor strain gages were also considered. The state of the art to date is such that a large amount of development work would be necessary to fulfill the specification requirements.

8.2 Force Measurement

The direct measurement of force was also considered, but it was felt that the mechanical and electrical system would be complex.

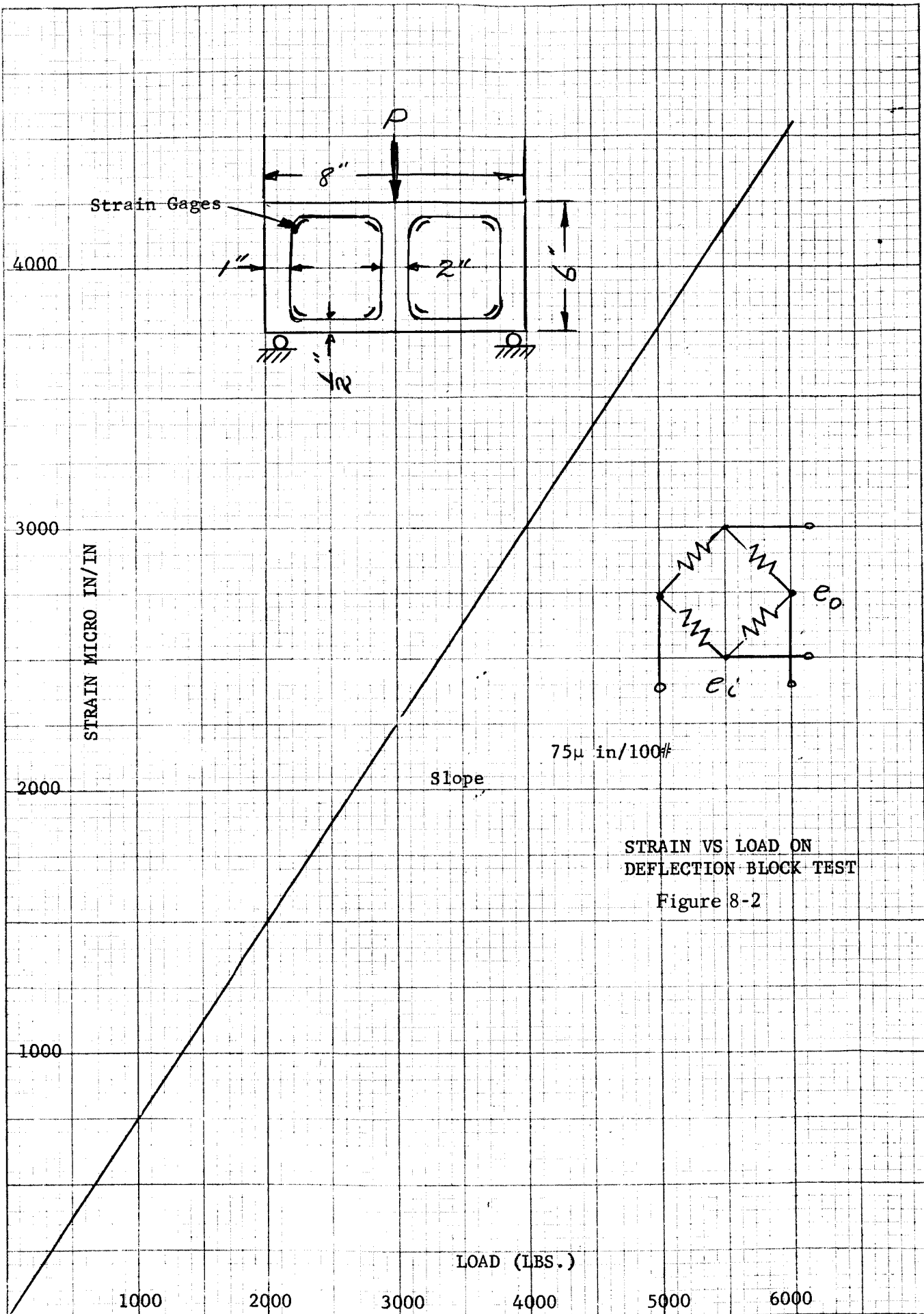
A load cell, known as a Pressductor manufactured by ASEA Electric Company, Sweden, was found to be very interesting. If some time in the future, development funds were available, some consideration should be given in this type of load cell.

The basic design of the pressductor is shown in Figure 8-3.



Deflection Block
Built for Test Purposes

Figure 8-1



STRAIN VS LOAD ON
DEFLECTION BLOCK TEST
Figure 8-2

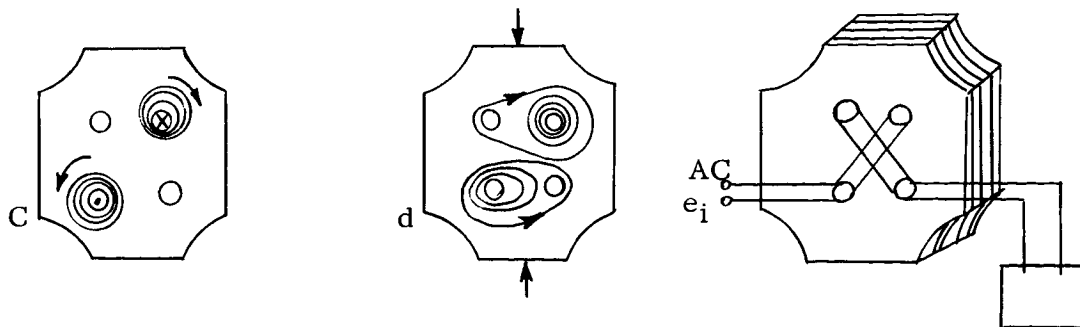


Figure 8-3

It comprises a number of similar stampings of transformer sheets glued together to form a block. The primary and secondary windings are led through four holes in the block and are so arranged that they cross one another at right angles. The primary winding is supplied with alternating current, which gives rise to a flux that does not influence the secondary winding when the pressductor is unstressed (c). If on the other hand, the pressductor is subjected to a load, the permeability is reduced in the direction of the pressure. This brings about an alteration in the field pattern (d); the flux will pass partly through the secondary winding and induce a voltage in this. The induced voltage is directly proportional to the load.

The primary windings of the pressductor are supplied with alternating current from a power supply unit. This unit comprises, in principle, a current limiting reactor and a capacitor for power factor correction. The magnitude of the current is adapted to the size and type of pressductor used.

Since for practical reasons, the pressductor is wound with a few turns of heavy wire, the impedance level will be low. In order to achieve a better matching between the low-ohmic pressductors and the rectifier unit, which has a considerably higher impedance level, a matching device is inserted in the circuit.

The secondary voltages of the pressductor is rectified. The magnitude of the direct voltage obtained is directly proportional to the mechanical load on the pressductor.

The problem areas of this application are:

- (1) Lamination cement to withstand high temperature.
- (2) Lamination material to withstand high temperature.
- (3) Design the pressductor for high frequency carrier for high frequency response.

- (4) Redesign of associated electronic equipment for airborne use. The present equipment is large and heavy.
- (5) Engineering talent for consulting located in Sweden, hence communications are time consuming.

8.3 Deflection Measurements

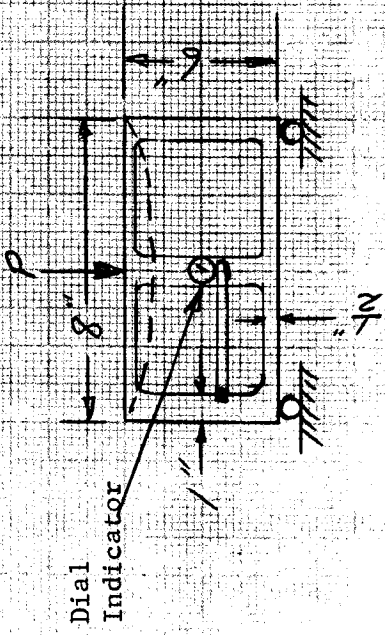
After careful considerations of all possible approaches, the measurement of the flexure movement with applied force was chosen. Calculation of the movement of the flexure members of the deflection block revealed that a 6000 lb. force would result in a movement of approximately .0012 inches. The deflection block shown in Figure 8-1 was used to verify our calculation. Load was applied to the deflection block and the flexure member motion was measured with dial displacement indicators.

Figure 8-4 shows a plot of deflection vs load. It can be noted that the deflection was in general agreement with the deflection expected.

The Linear Variable Differential Transformer (L.V.D.T.) was selected as the sensor because of its stepless resolution, sensitivity and other qualities, which are conducive to this application.

8.4 Linear Variable Differential Transformer (L.V.D.T.)

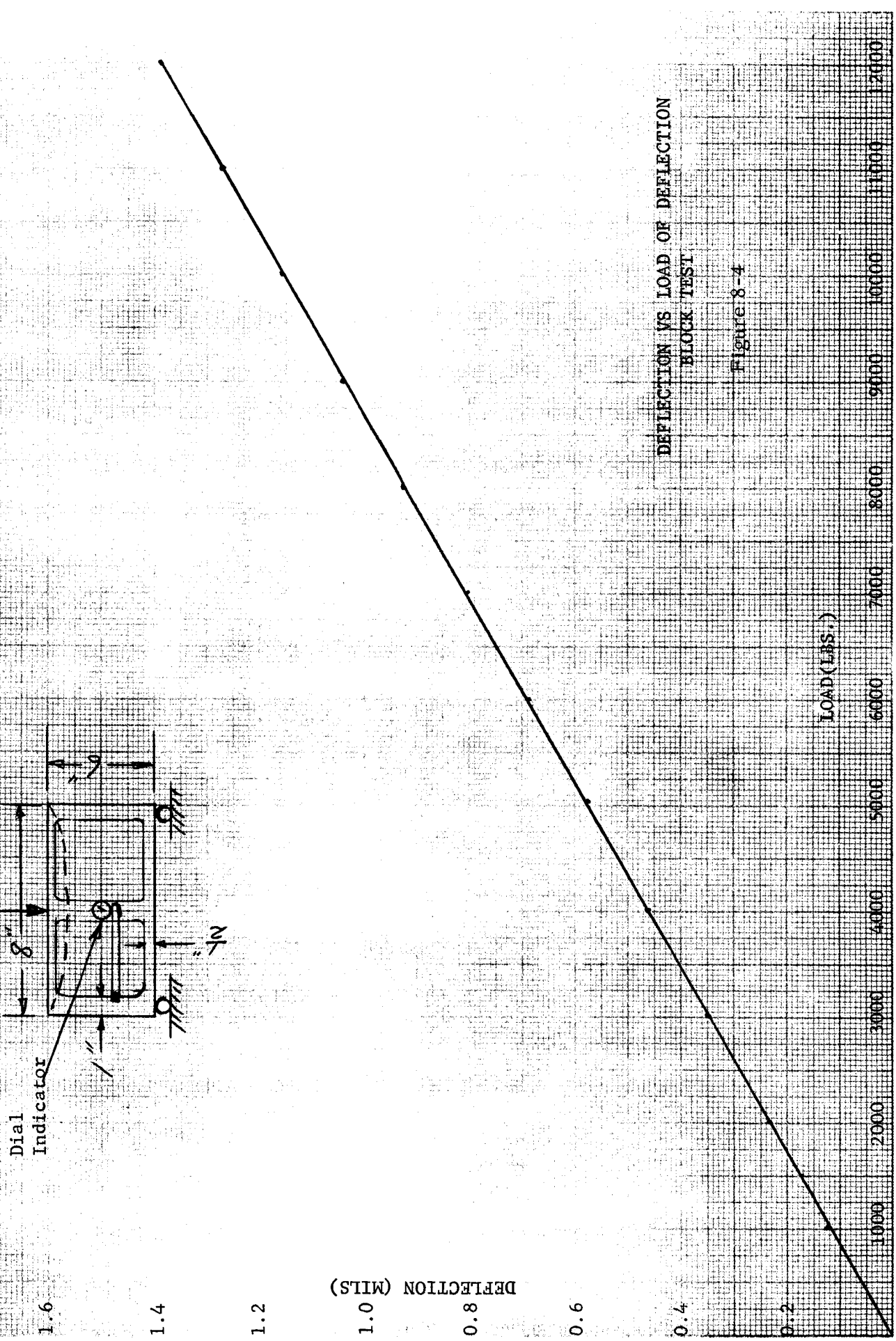
8.4.1 Principles of Operation. The Linear Variable Differential Transformer (L.V.D.T.) is an inductive device. Its ferro-magnetic core develops a variable magnetic coupling between the primary and two secondary windings. When the primary winding is excited by a suitable (preferably regulated) source of alternating current, (2000 cps) a voltage is induced in each of the secondary windings. The movement of the core changes the number of turns encircled by the magnetic flux, which causes an increase in the output of one of the secondary windings and a decrease in the output of the other. The core and winding schematic is shown in Figure 8-5.



Dial
Indicator

DEFLECTION VS LOAD OR DEFLECTION
BLOCK TEST

Figure 8-4



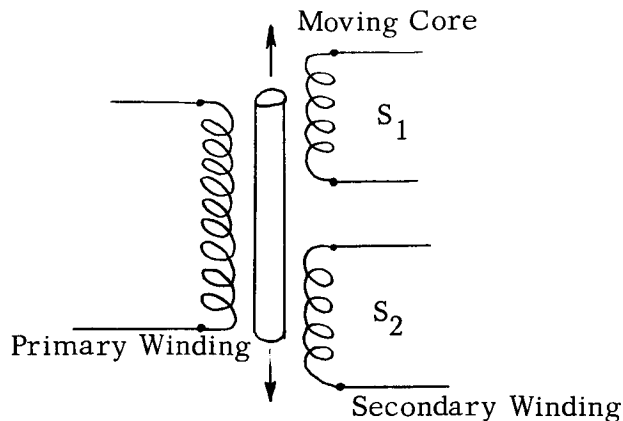


Figure 8-5

There are several arrangements to connect the secondary windings. The most common is the series-opposed, so that when the output voltages of the secondary windings are equal, the net output will be nearly zero. Figure 8-5 shows the voltage curve of the secondary windings as the core is moved through the linear range of displacement. There is one position of the core at which the voltages of both secondary windings are equal but of opposite phase. This is the null position, Point A, Figure 8-6.

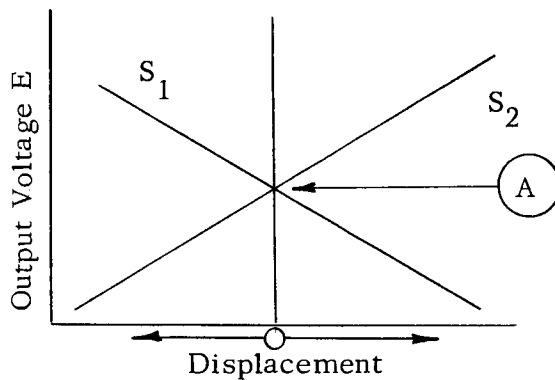


Figure 8-6

When the secondary windings are connected series opposed the net output curve appears as shown in Figure 8-7. The output at the null position is not exactly zero.

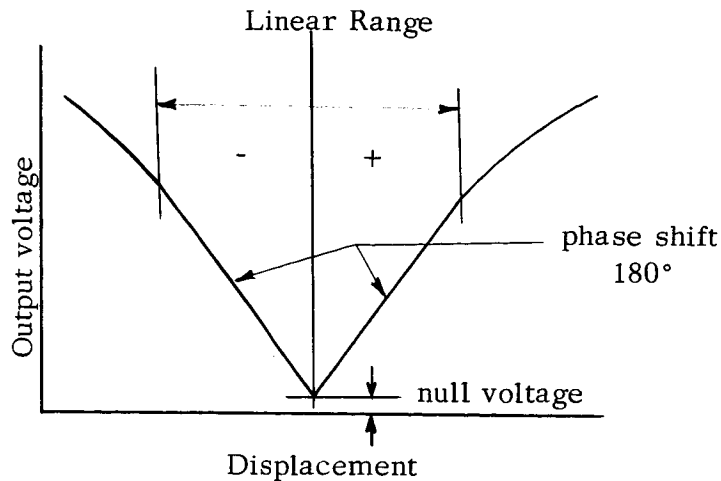


Figure 8-7

The residual voltage which exists at null consists mostly of the third harmonic of the primary input voltage and by design, is limited to no more than 0.25% of the full range output of the transformer at the standard frequency. As the core passes thru the null position, the phase of the output voltage shifts 180 degrees. By comparing the output phase with the input phase, the location of the core with respect to null can be determined.

In addition to this change of phase angle at null position, there is a shift of phase angle between the primary input voltage and the net secondary output voltage. This phase angle has a static component and a dynamic component. The static component is dependent upon transformer size, design, operating frequency, ambient temperature and load. The dynamic phase shift is dependent upon the core position within the range of core travel and load. Its magnitude is, in most cases, a fraction of one degree but in long range units it may be two or three degrees.

Several manufacturers of L. V. D. T. are listed below.

Automatic Timing and Controls, Inc.
King of Prussia, Pennsylvania.

Minatron Comporation
Belle Mead, New Jersey.

Pacific Electrokinetics
329 South Vermont Avenue
Glendora, California.

Shaevitz Engineering
P. O. Box 505
Camden, New Jersey.

Sanborn Company
175 Wayman Street
Watham 54, Massachusetts.

Vinson Manufacturing Company
8044 Woodley Avenue
Van Nuys, California.

G. L. Collins Corporation
2820 East Hullett Street
Long Beach 5, California

I. R. C. Instrumentation and Systems Division

International Resistance Company
401 N. Broad Street
Philadelphia, Pennsylvania.

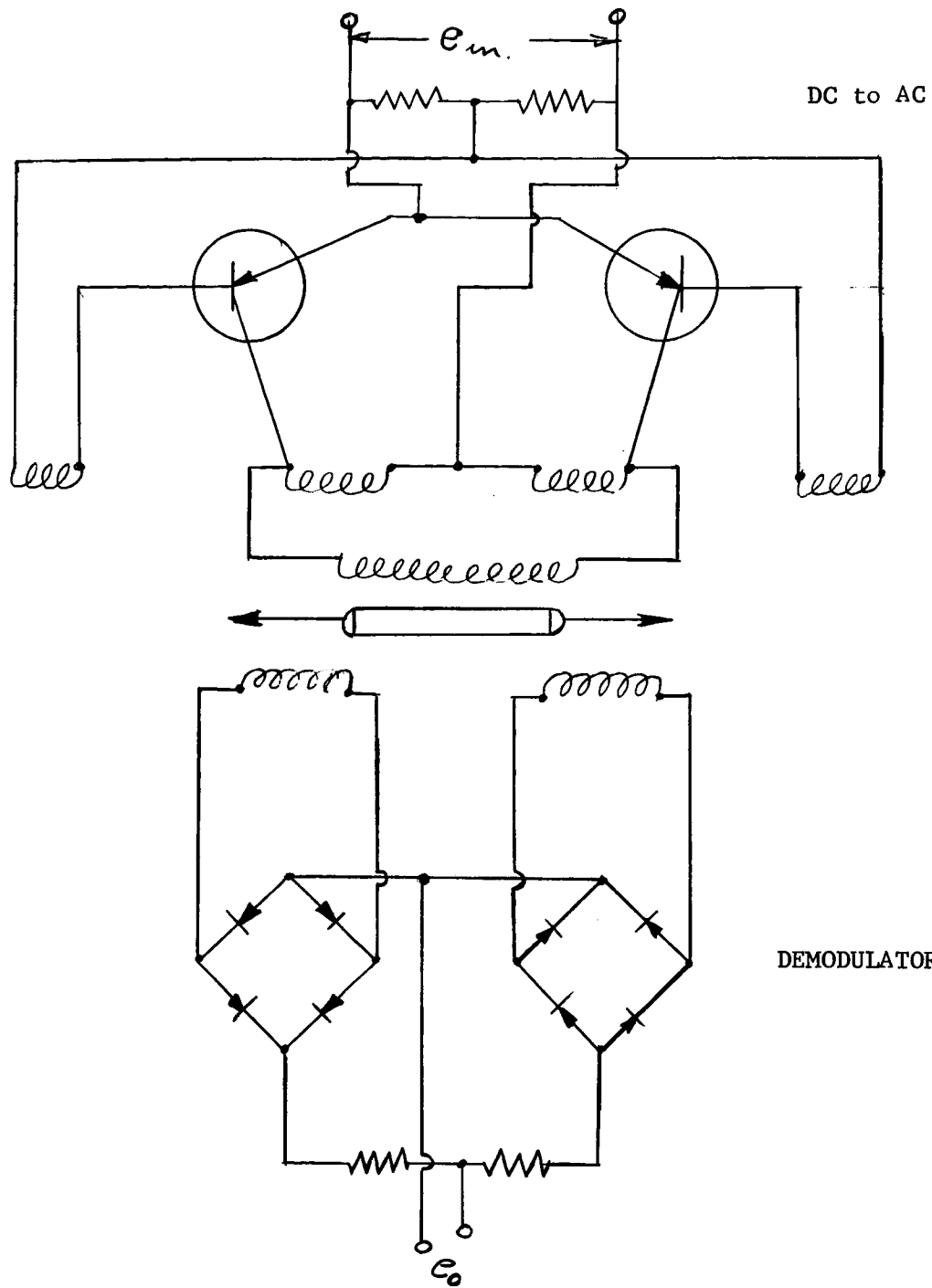
A d. c. signal suitable for telemetry purposes may be obtained by use of a demodulator and low pass filter. In transducer applications, the AC input power is often obtained from a transistorized inverter to allow operation from a d. c. bus. The inverter, differential transformer, demodulator and filter are usually contained in one package along with the sensing element. Manufacturers will also supply the units in separate packages. The inverter or modulator (often called by manufacturers) generates a square wave carrier which permits simple capacitors filtering to achieve low ripple output. The electro-mechanical response is determined by the degree of filtering required and may be related to ripple approximately as follows.

$$\% \text{ ripple (rms)} = \frac{10 \times \text{desired response}}{\text{carrier frequency.}}$$

Figure 8-8 shows a schematic wiring diagram of the modulator or inverter, sensor, and demodulator circuit.

8.4.2 Linearity and Linear Range. The output voltage of an air core differential transformer is a linear function of core displacement within a certain range of motion, beyond this range the linearity deviates from a straight line.

The differential transformer may be connected to a wide variety of load impedances from infinity to approximately the impedance of the secondary coil of the transformer. The load impedance can be given in any value in this range with only a small effect on linearity and linear range.



SCHMATIC CIRCUIT OF LVDT INVERTER,
 SENSOR & DEMODULATOR

FIGURE 8-8

8.4.3 Sensitivity and Output. The sensitivity of a differential transformer is usually stated in terms of millivolts/.001 inch/volt input.

Sensitivity and output generally increase with frequency, especially in the low frequency portion of the range specified for a particular differential transformer.

8.4.4 Resolution. The output voltage variation of the differential transformer is stepless. Therefore, the effective resolution depends entirely on the minimum voltage or current increment which can be sensed by the associated recording system. The output can readily be resolved to within 0.1% of the full range output by a suitable null balancing indicating system.

8.4.5 Excitation. The fundamental inductive arrangements of the differential transformer with a straight movable magnetic core can be designed for operation at any A.C. frequency in the range below 60 cps up into the radio frequency region. Standard differential transformers which are readily commercially available are in the range from 60 cps to 20,800 cps.

Accurate response to vibration and rapid mechanical motions requires the use of an excitation frequency at least two times the highest frequency present as a component of the mechanical motion.

When a differential transformer is excited at a fixed voltage, the primary current will vary downward with increasing frequency. As the heating effect is proportional to the square of the current for all practical purposes, the maximum input voltage may be increased at higher frequencies by the amount required to maintain the primary current at a fixed value, up to the absolute maximum voltage limit for the winding and circuit insulation.

A constant current power source, rather than a constant voltage source, is preferable for accurate operation, particularly when using an input level which produces a substantial temperature rise in the transformer. A constant current source eliminates any output variation directly due to the normal primary resistance variation with temperature. This primary resistance variation is important at low frequencies but may be insignificant at high frequencies where the impedance is principally inductive.

8.4.6 Phase Characteristics. The phase angle of the output voltage with respect to the input voltage has two values differing by 180° , depending on whether the core is on one side of null or the other.

Generally the phase angle as described above is between -20° and $+75^{\circ}$ depending on the type of transformer, the frequency, load and other factors. The calculation of the phase angle can be made by taking the input voltage as a

reference, the phase of the primary current is the angle whose tangent is $\frac{-2\pi f L_P}{R_P}$

where f = frequency
 L_P = primary inductance
 R_P = primary resistance.

The negative sign indicates the current lags the voltage. The e.m.f. generated in the secondary, leads the primary current by 90° ; hence, the phase of this e.m.f. is readily calculated. If the output load is a very high impedance, the output voltage is practically equal to the e.m.f. both in amplitude and in phase. If not, the phase of the output voltage appearing in the load can be calculated by eliminating AC circuit theory if the secondary resistance and inductance are known.

Displacement of the core causes a shift in the output phase angle, this shift is very small (approximately 1°) within the linear range.

In many applications, the output phase angle is not important. In some applications however, it is desirable to make the angle small or zero. The phase angle can be minimized by inverse of frequency or simple circuit modifications.

The correction for phase is dependent on application, where maximum sensitivity, minimum variation of phase with frequency or minimum variation of phase with core displacement.

Typical circuits for reduction of phase angles are shown below.

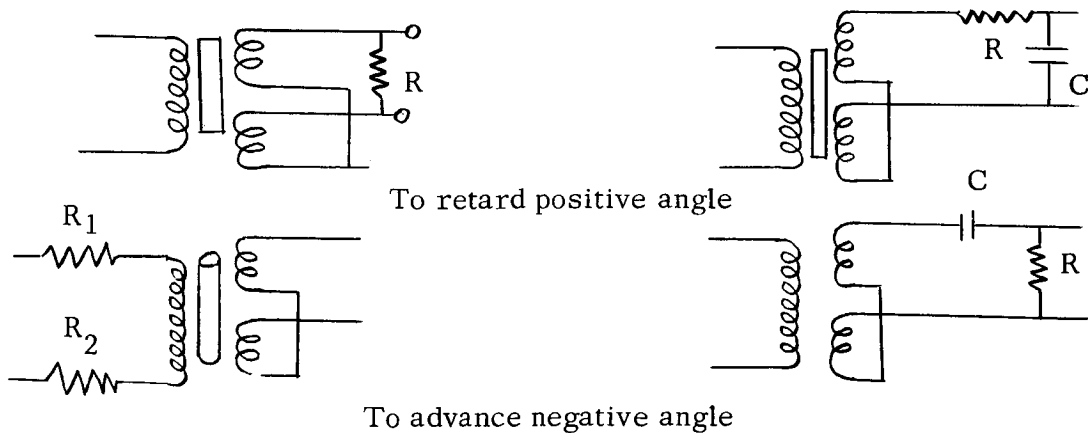


Figure 8-9

8.4.7 Mounting the Transformer Body. The transformer body must be mounted so that there are no nonsymmetrical stresses on the transformer case. Rigidly damping the body of the transformer at one end will, for example, introduce nonsymmetrical stress patterns which may affect null voltage magnitudes and position as well as output linearity. The construction of this assembly in the deflection block is consistent with the necessity of minimizing error due to thermal expansion. The body of the differential transformer is also positioned centrally so that any stress applied to the transformer core is applied at the axial center.

8.4.8 Mounting the Transformer Core. Each core is matched to its transformer by the manufacturer and marked for proper orientation with respect to the transformer. If this orientation is reversed the voltage at null will not be the minimum for which the transformer is designed. Also, maximum linearity may not be attained. The core can not be subjected to any mechanical stress which will affect its magnetic properties. The cores are supplied by the manufacturer with standard typed threads for core extension assemblies. The core assemblies will be constructed of nonmagnetic material. To maintain a highly precise balance of magnetomotive force the core extension can be either fabricated from brass or annealed Type 310 or Type 316.

It is expected that after the core is properly mounted into the assembly and locked mechanically a bonding agent or cement will be used to prevent it from vibrating loose.

There are many epoxies commercially available which will meet the mechanical and thermal requirements in this application.

8.4.9 Elevated Temperature. Manufacturers make available differential transformers for use at elevated temperatures up to 1000^oF. These units are designed in terms of their electrical and mechanical characteristics. For example, high temperature insulation and ceramic bobbin materials are used. The transformer body is also made of nonmagnetic stainless steel.

The mounting of the L.V.D. T. in deflection blocks with the transformer at the precise block center and the core attached at the two flexure legs minimize affects of any thermal gradients.

It is also intended that a constant current source be used to further reduce the thermal effects.

APPENDIX IX ELECTRICAL CIRCUITRY

The electrical circuitry associated with the performance of the LVDT must consist of an oscillator (2000 cps) for excitation, a demodulation to obtain a d. c. signal to the telemetry system. If the 5 volt full scale system is used rather than the 30 millivolt full scale an amplifier will be necessary.

Figure 9-1 shows an instrument block diagram required for each deflection block (4 deflection blocks in the system) if the 5 volt telemetry system is used.

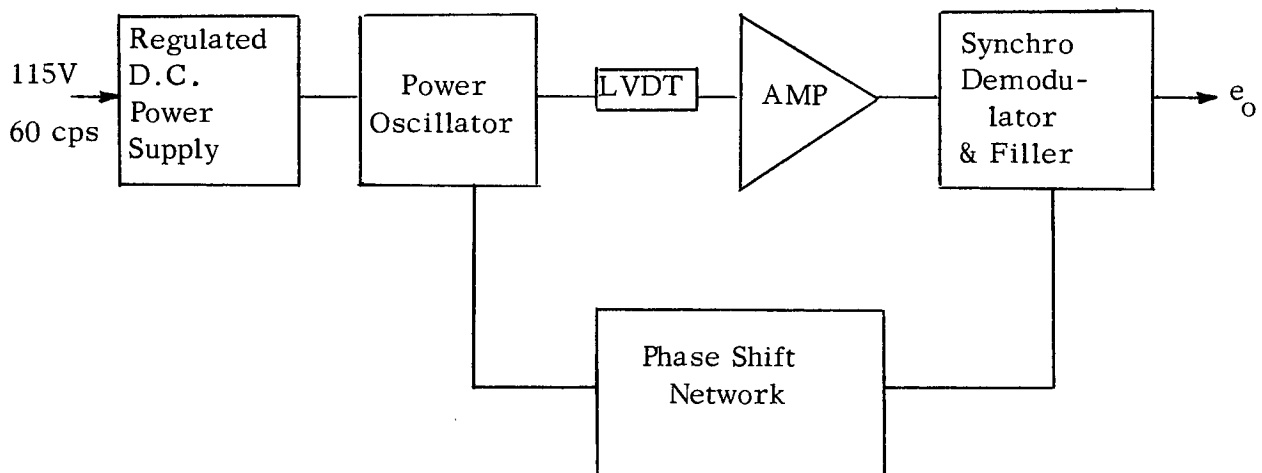


Figure 9-1

The carrier, amplifier, demodulator system as shown in Figure 9-1 is commercially available in packages of approximately 48 cubic inches.

A Schaetvitz Engineering, Pennsauken, J. J., Model CAS-2500 or equivalent generally have the following specifications.

Power Requirement	- 105 - 130V - 60 cps - 7W
Output Voltage	- \pm 2.5 vdc.
Transducer Excitation	- 1.25V rms.
Frequency Response	- DC - 250 cps.
Sensitivity	- AC amplifier gain 1-100

Output (Z) Impedance - 1000 ohms.
Operating Temperature - 0°F to 130°F
Thermal Coefficient of Sensitivity - 0.04% per °F
Gain Stability Long-term - 0.5% after 15 min.
Weight - 2.5 lbs.

Also available from manufacture on special request, a vehicle DC power supply for the oscillator and a fixed gain A. C. amplifier for the two thrust/drag ranges (6000 and 500 lbs.). This would reduce overall weight of the electronic system.

[†] 15 Millivolt Telemetry System

The [†] millivolt telemetry channel is attractive from the view point of circuitry simplicity and weight reduction. It is expected that the sensor may have sufficient sensitivity (1V/.001" at 26 volt excitation) for the motion expected (6000# approximately .0014"). The configuration shown in our design also allows for electrically adding the signals from the two fixed deflection blocks, and the two flexible deflection blocks independently. This then should result in an output of approximately 2.8 volts for full scale 6000# and approximately 0.23 volts for 500#. The output would not be sufficient for the 5 volts channel. However, this voltage would be more than adequate for the .030 volt channel.

When considering this instrumentation circuitry there is less flexibility in the data recording.

Sensor Outputs

It is recommended that the d. c. output voltages from the two fixed deflection blocks (aft) be summed and introduced into one channel of telemetry. Also the two d. c. output voltages from the two flexible deflection blocks (forward) be summed and introduced into a second channel of telemetry. To record two thrust ranges it will be necessary to top off the two fixed gains on the amplifier. A minimum of four channels for the measurement of thrust force is then necessary.

Corrections for friction force developed at the flexibility mounting should be accomplished in the data reduction.

The inertial acceleration also requires a total of four channels of telemetry with use of the range extender described in Appendix XI.

It is then necessary to resume at least eight channels of telemetry for this data acquisition.

A compromise to reduce the number of channels would be as follows.

1. Design an electronic circuit to sum each pair of deflection blocks (fixed and flexible) and then subtract the output voltage from the deflection block. The result will be the corrected output voltage due to friction force developed in the system. This reduces the number of channels by a factor of 2.
2. Record acceleration force on accelerometer which would be mounted on the engine. The number of channels required also be reduced by a factor of 2.

Calibration

A careful calibration of the complete measuring system comprising of the deflection blocks (forward and aft) and the inertial accelerometer is necessary to achieve an accuracy of 0.1% full range.

Thrust/Drag Device

The individual deflection blocks should be calibrated in the laboratory after the sensors are mounted and the null established. Load can be applied with a laboratory hydraulic testing machine and a calibration constant established.

Prior to a test flight the complete system can be re-calibrated and checked out by pushing or pulling against the ramjet structure. It is recommended that a special calibration fixture be incorporated on the ramjet for this purpose.

An in-flight calibration of the sensors and telemetry system can be accomplished by a step input voltage change to the sensors.

Accelerometers

A calibration constant will be supplied by the manufacturer of the accelerometer, however this calibration constant should be checked by the standard techniques.

Pre-flight and in-flight calibration can be made by introducing an external current into the servo loop. Since the accelerometer is a closed loop servo system, inertial acceleration inputs can be simulated by standard current techniques. The electro-mechanical servo cannot differentiate between an electrical (simulated acceleration) input and a true inertial input.

APPENDIX X ACCELEROMETER

Various types of accelerometers have been considered to measure the magnitude of the inertial force of the ramjet engine. The strain gage type and piezo-electric type are not suitable because of either sensitivity or response. Table 10-1 shows a comparison of the common type of accelerometers. It can be noted that the servo or pendulous type fulfills most of the requirements for this application.

The servo accelerometer similar to the Donner 4310 or G.E. LB-1 provides an analog signal proportional to applied linear acceleration. Figure 10-1, shows the principal components of a servo accelerometer. A force due to applied acceleration a , acts upon the pendulous mass M .

M displaces through angle θ producing error signal at pick-off, P . The error signal is amplified by a D. C. amplifier A which produces a servo current i_s . The servo current i_s is returned through the torque coil, T. C. which is attached to the pendulous element. The action of the coil carrying the servo current i_s , in the permanent magnetic field H produces a restoring force, closing the loop.

Acceleration analog output, E_o , is obtained by passing i_s through a load resistor, R_L .

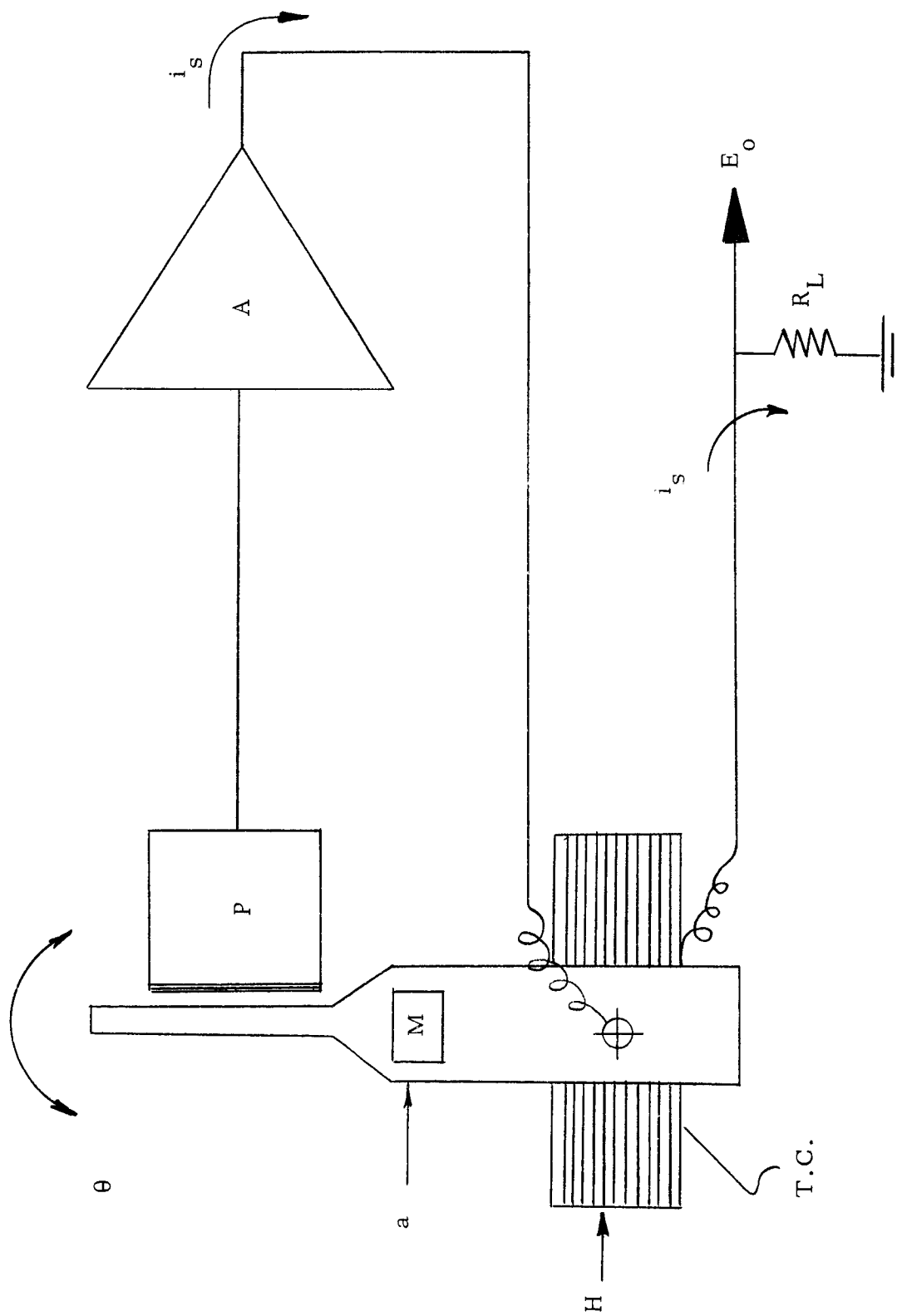
Electrical loading is a very important consideration in applying an accelerometer to a system since the output load impedance is common to both the accelerometer servo loop and the system input. The nature of the load will affect both the calibration accuracy and the stability of the accelerometer. The available servo type accelerometers normally have a standard internal load resistance of 5000 ohms. With the full scale servo amplifier output current of ± 1.5 m. a., a standard unit, therefore has an output voltage of ± 7.5 volts full scale regardless of the acceleration range. The external load is placed in parallel across the internal load and ideally then would be an infinite impedance so as not to change the calibration factor. If the external impedance is known precisely beforehand, the accelerometer can be calibrated initially with the same load attached, or the scale factor can be computed from the factoring calibration based upon the 5000 ohm internal load.

The accelerometer is calibrated originally by using a nominal value of internal load and then degaussing the saturated permanent magnet to obtain the pressure calibration level. Any change of load will change the calibration in terms of volts/g of acceleration. To maintain calibration accuracy, the load must be stable with time and temperature.

COMPARISON OF COMMON ACCELEROMETERS

Characteristic	Piezo-Electric	Potentiometer	Strain Gage	Variable Reluctance	Servo or Pendulous Type
Size	Small	Large	Small	Large	Small
Weight	Light	Medium	Light	Heavy	Medium
Over-all Accuracy	2-5%	1-3%	0.5%	1%	.1%
Ruggedness	Very good	Poor	Very good	Good	Good
Frequency Response	Very high	Low	High	Low	Medium
Cross-Axis Sensitivity	Very poor	Very poor	Poor	Poor	Very good
Temperature Sensitivity	Poor	Good	Poor	Good	Very good
Output level	Very low	High	Very low	High	High
Excitation	None	Regulated A.C. or D.C.	Regulated A.C. or D.C.	A.C.	Unregulated D.C.
Cost	\$50-500	\$65-250	\$250 to 400	\$200 to 400	\$450 to 1000
Peculiarities	Cannot measure gravity poor frequency response	Poor resolution	Poor linearity	Sensitive to stray magnetic fields poor linearity	Sensitive to angular accelerations
Application	Shock and vibration instrumentation	General purpose control and instrumentation	General purpose airborne instrumentation	Telemetry control and instrumentation	High accuracy D.C. measurements, control and instrumentation

Table 10-1



Servo-Accelerometer
Figure 10-1

The general specifications for the accelerometers are as follows:

Non-linearity	- less than .05% full range
Hysteresis	- less than .02% full range
Resolution	- better than .0001% full range
Non-repeatability	- less than .01% of full range
Zero-output	- less than .05% of full range
Output noise in volts (RMS)	- less than .05% of full range
Cross axis sensitivity	- less than .002 g/g referred to true sensitive axis.
Temperature sensitivity	- 0.01%/deg F.
Natural frequency	- electrically damped 185-300 cps.
Damping ratio	- electrically damped 0.4 to 0.7 \pm 0.1
Temperature	- operating -40°F to +200°F
Shock	- 120g momentary impact
Vibration	- 15g rms - 20 - 2000 cps 0.12g ² /cps.
Ambient pressure	- 0 - 5 atmospheres absolute.
Range	- \pm .001g +5g.
Input power	- \pm 15 volts D. C. \pm 15% - \pm 28 volts D. C. \pm 15% (Max. 10 m. a.)
Voltage output	- \pm 7 1/2 volts
Current output	- \pm 1.5 m. a.
Case alignment	- \pm 1° to true sensitive axis.
Weight	- approx. 4 oz.
Electrical connectors	- 6-7 solder terminals

The above specifications can be improved by the manufacturer by special order and at an additional cost.

APPENDIX XI RANGE EXTENDER

It is expected that the measurement of acceleration due to the inertial forces is necessary in order to obtain the necessary accuracy requirements of the system. This ratio may be as high as 3000 to 1. Assuming the X-15 acceleration is 3g and the ramjet acceleration is .001g, the acceleration measurement system must detect a range of 3000 to 1.

To maintain a voltage level for the data acquisition at both of these levels it will be necessary to record on at least two telemetry channels. The first channel divides the total range of the transducer signal into 24 equal voltage steps, each step scaled 1/24th of 5 volts. This step output varies in incremental voltage steps until it attains the level closest to that of the transducer signal. The second channel amplifies the difference between the step channel output and the signal input with a fixed loop gain. This second channel, which provides the Vernier Output, is constrained between 0 and 5 volts and has a range of \pm one base step. Thus the Vernier Output represents a gain of 12-1.

The purpose of the range extender similar to the Donner model 4100 is to amplify the low level signal while automatically step re-biasing to maintain the output signal excursion within present voltage limits.

Figure 11-1 shows a block diagram of the functional components of the range extender.

A signal input E_s is amplified by a precise ratio in amplifier A, to produce vernier output V. The high and low voltage comparators VC's monitor the vernier voltage and produce a logic output when either high or low voltage limits are reached. If a high limit is reached, add pulse A is applied to digital register, DR, which drives digital-to analog converter D/A.

The DR will step to one count higher, producing a precise step of bias voltage from base amplifier, A, which when fed back into the vernier amplifier, causes V to return to zero as shown on the graph.

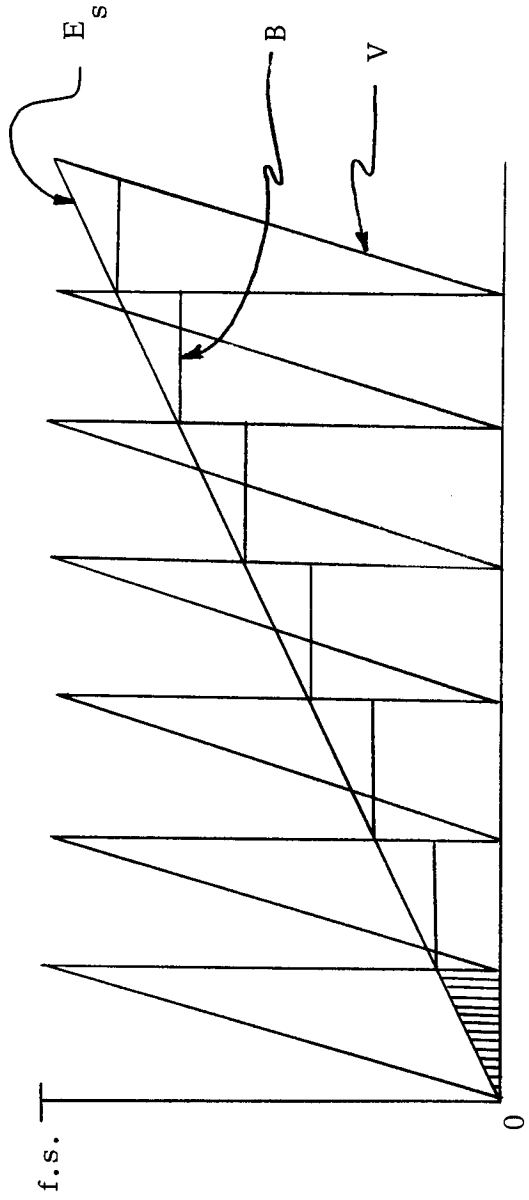
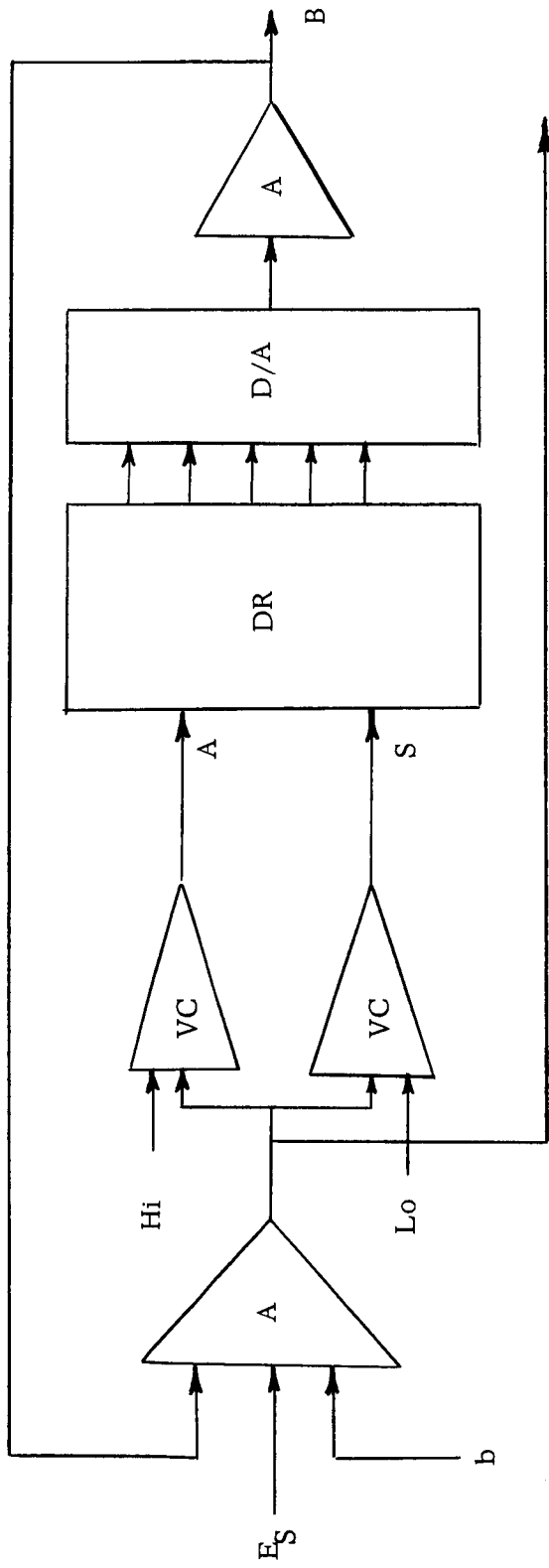


Figure 11-1 Vernier Range Extender

Base output B will have discreet values (in stair step fashion) indicating which value of the bias is being fed into the vernier amplifier.

When the signal hits the low limit, it will cause a subtraction operation (s) and reverses the above operation. A bias signal (b) may be used to offset the range of operation of the extender if desired. A continuous closed-loop re-biasing will result. The amplified signal V is always contained between the low and high voltage limits. The original input signal can be reconstructed from base output B and voltage output V since these indicate the amplification factor and the value of each base step. For convenience, the amplified high step is shown equal to the full scale vernier output. Where opposite polarity inputs exist, voltage V will go negative and the base step will result in positive re-biasing.

The range extender is similar in principle to a vernier caliper or micrometer.

The general specifications for the vernier range extender are as follows:

Range	-	Any accelerometer range.
Output	-	Two channels.
Step	-	0-5 volts, equally divided into 24 incremental steps, so that 0V = minus full g range, 2.5V = 0g and 5 volts = plus full g range.
Response	-	Zero to full scale output in less than 0.01 second (as low as 0.001 second)
Input	-	28 volts D.C. 200 m. a. maximum
Operating temperature	-	+30 degrees to + 170 degrees F.
Vibration survival	-	10g rms (5 to 2000 cps).
Shock	-	60g for 11 msec.
Weight	-	2 lbs. /37 cu. in.

The above specifications can be modified to comply with any variations for the environment, performance, accelerometer selected or for other type of transducer.

The range extender or amplifier, whichever is used, would be mounted with the data acquisition instrumentation within the X-15 aircraft. The environment would not be as severe as if mounted in the ventral fin area.

APPENDIX XII

HYPERSONIC FLIGHT

THRUST, DRAG AND MEASUREMENTS

A Selective Literature Search

Periodicals

1964

Anonymous

Gaseous oxygen rocket rig for demonstration and research.

Aircraft Engineering, v. 36, n. 2, February 1964, p. 43

Engineering Index, June 1964, p. 164

Thrust measurement equipment with indicator, combustion chamber pressure gage, water cooling system.

Anonymous

Measuring strain at 7000°F.

Iron Age, v. 193, n. 12, March 19, 1964, p. 89

Applied Science and Technology Index, v. 52, n. 6, June 1964, p. 332

An electro-optical extensometer measures strain remotely at temperatures up to 7000°F. Measures two targets elongation on test bar. Resolution is 0.025% of full scale. Strain rates are variable from static to 2000 in./in/ sec.

Anonymous

Project Gemini.

Spaceflight, v. 6, n. 1, January 1964, p. 2-11

Engineering Index, June 1964, p. 180

Objectives of project. Details of crew, instrument control, data gathering, etc. systems.

Avery, A.H., Dugger, G.L.

Hypersonic Airbreathing Propulsion.

Astronautics and Aeronautics, v. 2, n. 6, June 1964, p. 42-47

Hypersonic-ramjet configurations and discussion of performance. 9 references

Bailey, A.B., Potter, J.L.

Pressures in the stagnation regions of blunt bodies in rarefied flow.

AIAA Journal, v. 2, April 1964, p. 743-745

Applied Science and Technology Index, v. 52, n. 6, June 1964, p. 5

Discussion of instrumentation, probes etc. appears in Arnold Engineering Development Center TDR-63-168, Sept. 1963.

(Noted in ref. 4 of this article)

Bartlett, E.P.

Effective heat of ablation of graphite.

AIAA Journal, v. 2, January 1964, p. 171-173

Applied Science and Technology Index, v. 52, n. 3, March 1964, p. 332

- 1964 Bennett, L., Stadler, J.
Drop size sensor.
Review of Scientific Instruments, v. 35, January 1964, p. 17-21
Applied Science and Technology Index, v. 52, n. 3,
March 1964, p. 325
Measurement of moisture droplets.
- Brown, H.S.
Rotary wing flight testing.
Canadian Aeronautics and Space Journal, v. 10, n. 2,
February 1964, p. 33-39
Engineering Index, June 1964, p. 82
Areas are discussed from standpoint of evolutionary test
requirements and measuring methods; current problems and
test demands.
- Bynum, D.J. etc.
Surface strains in case-bonded models of Rocket motors.
AIAA Journal, v. 2, n. 2, February 1964, p. 343-347
Engineering Index, May 1964, p. 160
Strain measurements made with electric-resistance type strain
gages on rocket engine models.
- Casey, J.J., Grimes, J.
Dynamic stability testing with ablation at mach 14 in a long-duration
wind tunnel.
AIAA Bulletin, v. 1, n. 1, January 1964, p. 65
Tests recently conducted in blow-down wind tunnel at re-entry
mach numbers. Wind tunnel uses a zirconia capacitance heater
to provide long-run times at high stagnation temperatures.
Model fastened to shielded transverse strut.
- Chicklis, C.K.
Polymeric heat shields in space.
Rubber World, v. 149, February 1964, p. 82
Applied Science and Technology Index, v. 52, n. 6, June 1964,
p. 319
Abstract of original article.
- Cosenza, C. J.
Program for hypersonic flight testing in areas of structures,
aerothermodynamics and structural dynamics.
AIAA Bulletin, v. 1, n. 1, January 1964, p. 68
(AF Flight dynamics laboratory, Wright-Patterson, AFB, Ohio)
Six vehicles to be placed into equilibrium hypersonic glides
from 170,000 to 225,000 ft at velocities from 13,000 to
19,500 fps. Details given in such areas as telemetry systems;
instrumentation for aerodynamic forces, pressures and heating
rates, flight control and structural data; and structural
processes and materials.

1964

Eisenlohr, A.

Impregnated tungsten for rocket nozzles.

Metal Progress, v. 85, n. 4, April 1964, p. 94-95

Engineering Index, July 1964, p. 163

Discussion of 6 cooling systems and advantages and disadvantages of each. Systems include ablative, convective, and radiation cooling, pool boiling, transpiration cooling and vaporization cooling techniques.

Ferri, A.

Supersonic combustion progress.

Astronautics and Aeronautics, August 1964, p. 32-37

Hypersonic airbreathing engines, combustion, engine performance and cooling, fuel injection problems.

Fradenburgh, E.A., Kiely, E.F.

Development of dynamic model rotor blades for high speed helicopter research.

American Helicopter Society Journal, v. 9, n. 1, January 1964,

p. 3-20

Engineering Index, June 1964, p. 82

Scale model rotor blades which are dynamically and structurally similar to full scale blades. Testing experience and information gained.

Higson, G.R.

Recent advances in strain gages.

Journal of Scientific Instruments, v. 41, July 1964, p. 405-414

Main Library Card File, (Measurement-Instruments-Strains and Stresses)

Jaroudi, R., Heard, D.E.

Optimum geometric factors for semicircular fins in radiation-cooled nozzles.

AIAA Journal, v. 2, January 1964, p. 146-148

Applied Science and Technology Index, v. 52, n. 3, March 1964

p. 315

Kovacs, A., Mesler, R.B.

Making and testing small surface thermocouples for fast response.

Review of Scientific Instruments, v. 35, April 1964, p. 485-488

Kyser, J.B.

Tracer spark measurement technique for velocity mapping of hypersonic flow fields.

AIAA Journal, v. 2, n. 2, February 1964, p. 393-394

Applied Mechanics Reviews, v. 17, n. 7, July 1964, p. 547

Although the initial spark is diffuse, the two subsequent sparks are sufficiently well defined to yield accurate displacement data. Technique appears capable of measuring the velocity in a uniform hypersonic stream but resolution must be improved to map complex flow fields.

1964

Lakshminarayana, B.

Effects of chordwise gap in aerofoil of finite span in free stream.
Royal Aeronautical Society Journal, v. 68, n. 640, April 1964
p. 276-280

Engineering Index, July 1964, p. 4

Attempt is made to extend Glauert's analysis to predict increase in induced drag and decrease in lift due to split in aerofoil of finite span placed in free stream. Analysis is for incompressible, inviscid flow around split aerofoil.

Lees, L.

Hypersonic wakes and trails.

AIAA Journal, v. 2, March 1964, p. 417-428

Applied Science and Technology Index, v. 52, n. 6, June 1964, p. 4

Lewis, C.H., Carlson, D.J.

Normal shock location in underexpanded gas and gas-particle jets.

AIAA Journal, v. 2, April 1964, p. 776-777

Lion, K.S.

Nonlinear twin-T network for capacitive transducers.

Review of Scientific Instruments, v. 35, n. 3, March 1964
p. 353-356

Engineering Index, May 1964, p. 192

Circuit described which converts capacitance variation to analogous voltage and current signals.

Meieran, S.

Temperature sensor for strain-gage transducer.

Electronics, v. 37, n. 15, May 4, 1964, p. 77-78

Applied Science and Technology, v. 52, n. 7, July 1964, p. 86

Monitoring the current change through a dropping resistor between the voltage source and the transducer, a signal is available with a magnitude many times that of a thermocouple output. Change in current with temperature is nearly linear. (Illustrated circuit)

Miller, D.S., Hijman, R.

Mach 9 to 22 studies of flow separations due to deflected control surfaces.

AIAA Journal, v. 2, n. 2, February 1964, p. 312-321

Engineering Index, May 1964, p. 3

Measurements of separation phenomena obtained during hypersonic aerodynamic test program. Pressure and heat-transfer measurements are correlated with Schlieren photography, temperature sensitive paint and oil-streak flow visualization data.

1964

Parkinson, D.H.

Superconductors in instrumentation

Journal of Scientific Instruments, v. 41, February 1964, p. 68-77
Applied Science and Technology Index, v. 52, n. 6, June 1964 p. 302
Some applications both suggested and actual are reviewed.
Superconducting bolometer, galvanometers, switches, infrared detectors, flux pumps.

Rubin, I., Imber, M.

Optimization study of space radiators.

AIAA Journal, v. 2, n. 2, February 1964, p. 353-358
Engineering Index, May 1964, p. 176
Method is developed for optimizing rectangular fin with variable root temperature along tube length.

Sanchez, J.C.

Low-pressure marvells-solid state transducers.

Astronautics and Aeronautics, v. 2, n. 4, April 1964, p. 50-53
Applied Science and Technology Index, v. 52, n. 6, June 1964, p. 267
Piezo-resistive strain gage features negligible hysteresis and plastic deformation at temperatures below 1000°F. It can be doped to give substantial resistance in extremely small gage lengths.

Shaw, J.M.

Hypersonic test facilities at Royal Aircraft establishment.

Royal Aeronautical Society Journal, v. 68, n. 639, March 1964 p. 179-188
Engineering Index, June 1964, p. 210
Design aspects of 7x7-in. hypersonic tunnel; instrumentation; description of shock tunnel and shock tube; other hypersonic facilities. 24 refs.

Sheer, R.E., Nagamatsu, H.T.

Vibrational relaxation and recombination of nitrogen and air in hypersonic nozzle flows.

AIAA Bulletin, v. 1, n. 1, January 1964, p. 16
(General Electric Co., Schenectady, N.Y.)
Effects of vibrational relaxation and recombination of high temperature nitrogen and air investigated in hypersonic shock tunnel at high-flow mach. numbers.

Wan, K.S.

Turbulent wake characteristics with different eddy viscosity coefficients.

AIAA Journal, v. 2, January 1964, p. 121-122
Applied Science and Technology Index, v. 52, n. 3, March 1964, p. 5

- 1964 Wang, C.Y.
Contours for stagnation-point mass injection in hypersonic flow.
AIAA Journal, v. 2, January 1964, p. 178-179
Applied Science and Technology, v. 52, n. 3, March 1964, p. 5
- Webb, W.H., Hromas, L.A.
Turbulent diffusion of a reacting wake.
AIAA Bulletin, v. 1, n. 1, January 1964, p. 16
(Space Technology Laboratories, Redondo Beach, Calif.)
An integral solution for the diffusion of species in the wake developed for hypersonic turbulent wake. Essentially an extension of method proposed by Lees and Hromas for equilibrium wake.
- 1963 Anonymous
AIAA simulation for aerospace flight conference.
American Institute of Aeronautics Conference, August 26-28, 1963, Columbus, Ohio, New York, 1963
Main Library Card File, (Aerodynamics)
A370 page report. Located in A.T.L. Library
- Anonymous
Unusual thermocouples and accessories
Instrument Control Systems, v. 36, n. 6, June 1963, p. 110-113
Applied Mechanics Reviews, v. 17, n. 1, January 1964, p. 60
First of a series of brochure-type reviews of commercial thermocouples available in U.S.
- Black, F.S., Wilken, H.W.
High temperature sensors for re-entry research vehicle.
Society of Automotive Engineers, Paper 750K, meeting September 23-27, 1963, 15 p.
Engineering Index, January 1964, p. 177
ASSET re-entry vehicle program. Temperature profile at various portions of vehicle, testing of thermocouples, their coatings, materials selected are Mo, Cb, Pt-20%. Rh sheaths, Mg and Be oxide insulation, and W-5% Re vs. W-26% Re and Pt v Pt-10% Rh thermoelements.
- Bolling, F.
4300°F Thermocouples for re-entry vehicle applications.
Society of Automotive Engineers, Paper 750E, September 23-27 meeting, 1963, 12 p.
Engineering Index, January 1964, p. 177
Research, design and development of sensors for local dynamics surface temperatures. Transducer concepts and sensor assembly configurations considered.
(First paper of two. Second by Pustell, R.A. (G.E.) on component evaluation and design development on nose cap temp. sensor. Probe utilized sintered iridium high temp. sheath.)

1963

Borden, W.T.

Calorimeters - Heat rate sensors for space vehicle boosters.
Society of Automotive Engineers - Paper 750G, September 23-27,
1963, 5 p.

Engineering Index, January 1964, p. 177

Methods of measuring radiation and convective heating;
different modes require special gages. Types of gages,
capabilities and factors influencing accuracy. (One of
a number of papers concerning measuring instruments
presented at SAE meeting)

Broadfoot, K.D., Belin, R.E.

Method for the remote measurement of force in a moving machine
member.

Journal of Scientific Instruments, v. 40, December 1963, p. 589-591

Applied Science and Technology Index, v. 52, n. 3, March 1964, p. 358

Chen, Y.

Vibration of beams or rods carrying a concentrated mass.

ASME Transactions, series E, v. 30, June 1963, p. 310-311

Applied Science and Technology Index, 1963, p. 1165

Cruise, W.B.

Strain gaging studs for Saturn.

Instrument Society of America Journal, v. 10, December 1963,
p. 70-71

Applied Science and Technology Index, v. 52, n. 3, March 1964,
p. 316

D'Appolonia, E., Romualdi, J.P.

Load transfer in end-bearing steel H-piles.

American Society of Civil Engineers, Proceedings, v. 89

(SMZ No. 3450), March 1963, p. 1-25

Applied Science and Technology Index, 1963, p. 745

Deresiewicz, H.

On transmission of thermoelastic plane waves across plane boundary.

Journal of Mechanics and Physics of Solids, v. 11, n. 1, January -
February, 1963, p. 35-39

Engineering Index, 1963, p. 534

Dilatational waves propagating in thermally conducting solid
which are transmitted into contiguous solid having, in general,
different elastic and thermal properties.

Ferri, A., Vaglio-Laurin, R.

External hypersonic flows.

Aerospace Engineering, v. 22, n. 1, January 1963, p. 23-31

Applied Mechanics Reviews, v. 17, n. 4, April 1964, p. 312

Account of solved and unsolved questions bearing on the analysis
of flows about practical hypersonic vehicles. Also, recent
investigations of trails left behind vehicles upon re-entry
into atmosphere are considered.

1963

Foster, G.B.

Non-contacting, self calibrating vibration transducer.

Instruments and Control Systems, v. 36, December 1963, p. 83-84

Applied Science and Technology Index, v. 52, n. 3, March 1964, p. 123

Non-contact capacitance sensing detects amplitude of vibrating member by change in capacitance between sensing head and vibrating member.

Hellan, K.

Study of damping properties of metals.

Acta Polytechnica Scandinavica - Physics including Nucleonics

Ser Ph 27, 1963, 40 p.

Engineering Index, August 1964, p. 86

Purpose of investigation is to explain some properties of damping and establish basis for engineering design of vibrating parts. 22 refs.

Inger, G.R., Meis, D.A.

Shock polars for dissociating gases.

AIAA Journal, v. 1, n. 8, August 1963, p. 1771-1775

Applied Mechanics Reviews, v. 17, n. 2, February 1964, p. 135

Shock-polar equations derived for a dissociating and vibrationally excited diatomic gas, extremes of frozen and equilibrium conditions behind the shock.

Julien, Y.G.

Exact solution of the response of a damped rod to random excitation.

ASME Transactions, ser. E, v. 30, June 1963, p. 312

Applied Science and Technology Index, 1963, p. 1164

Leath, P.L., Marshall, T.

Electromagnetic probe for the measurement of hypersonic flow velocity at a point.

AIAA Journal, v. 1, April 1963, p. 948-950

Applied Science and Technology Index, 1963, p. 15

Levensteins, Z.J.

Hypersonic wave characteristics behind spheres and cones.

AIAA Journal, v. 1, December 1963, p. 2848-2850

Applied Science and Technology, v. 52, n. 3, March 1964, p. 5

Lezberg, E.A., Franciscus, L.C.

Effects of exhaust nozzle recombination on hypersonic ramjet performance. Part I-Experimental measurements.

AIAA Journal, v. 1, n. 9, September 1963, p. 2071-2076

Applied Mechanics Reviews, v. 17, n. 2, February 1964, p. 136

Experimental temperature measurements in supersonic nozzles with cone exit half angles of 10.5° and 7° for hydrogen-air and methone-air combustion products at stagnation temp. up to 5400°R and press. up to 4.5 atmos.

(Part II follows in same issue "Analytical Investigations")

- 1963 Linzer, F.D., Kaplan, E.
Considerations in design of calorimeters for project "Fire"
superorbital re-entry test vehicle.
Society of Automotive Engineers, Paper 750L, September 23-27,
meeting, 1963, 8 p.
Engineering Index, January 1964, p. 177
Function, location and design of Be calorimeters for forebody
and gold calorimeters for afterbody, methods of achieving 1-
dimensional heat flow in forebody calorimeter design; optimum
design for afterbody calorimeter is thermally isolated, small
diameter, thin disk of high thermal conductivity; thermo-
couple size, placement, heat losses etc.; accuracy of sensors.
- McGowan, J.W., etc.
Materials for thermal protection.
Transactions of the Eighth Symposium on Ballistic Missile and
Space Technology, October 16-18, 1963, p. 245-395
A series of four papers covering refractory metal sandwich
structures, resin-impregnated zirconia foam, and Pyrolytic
graphite. 54 refs.
- Merril, H.J.
Light and heat sensing.
MacMillan Co., 1963, N.Y.
Main Library Card File (Sensors) (E38AD96)
Report of sixth AGARD Avionics Panel meeting in Paris, July
1962.
- Moen, W.K
Significance of errors in high temperature measurement.
Society of Automotive Engineers, Paper 750F, meeting September 23-27
1963, 7 p.
Engineering Index, January 1964, p. 177
Magnitude and sources of errors in temperature meas. by
thermocouples, range of errors related to craft design and
placement. Specific heat, wire diameter, welding and
cementing techniques.
- Rhodes, J.E.
Transducers measure transient motion in shock tests.
Society of Automotive Engineers Journal, v. 71, August 1963,
p. 96-98
Applied Science and Technology Index, 1963, p. 1231
- Sanchez, J.C.
Semiconductor strain-gage pressure sensors.
Instruments and Control Systems, V. 36, November 1963, p. 117-120
Applied Science and Technology Index, v. 52, n. 3, March 1964
p. 358

- 1963 Schultz, A.B.
Nonlinear response of a beam to a shock pulse.
Franklin Institute Journal, v. 276, November 1963, p. 385-393
Applied Science and Technology Index, v. 52, n. 3, March 1964
p. 333
- Seiff, A.
Ames hypervelocity free-flight research.
Astronautics and Aerospace Engineering, v. 1, December 1963
p. 16-23
Applied Science and Technology, v. 52, n. 3, March 1964, p. 5
- Smith, J.E.
Tension tests of metals at strain rates up to 200 sec.
Materials Research and Standards, v. 3, September 1963, p. 713-718
- Stankevics, J.O., Rose, P.H.
Stagnation-point heat-transfer measurements in partially ionized air.
AIAA Journal, v. 1, December 1963, p. 2752-2763, (bib. p. 2762-2763)
Applied Science and Technology Index, v. 52, n. 3, March 1964, p. 5
- Taylor, R.L., Keck, J.C., etc.
High-speed scanner for traverse radiation measurements of luminous
hypersonic wakes.
AIAA Journal, v. 1, n. 9, September 1963, p. 2186-2188
Applied Mechanics Reviews, v. 17, n. 3, March 1964, p. 238
- Valentine, E.F.
Some pressure-drag effects of rounding the leading edges of hyper-
sonic inlets.
AIAA Journal, v. 1, August 1963, p. 1918-1919
Applied Science and Technology Index, 1963, p. 16
- Walker, M., Roschen, J., Schlegel, E.
Infrared scanning technique for determination of temperature profiles
in microcircuits.
IEEE-Transactions on Electron Devices, VED-10, n. 4,
July 1963, p. 263-267
Engineering Index, February 1964, p. 225
Direct, rapid nondestructive method of thermal profiling
which does not effect readings; effects of heat sinks, heat
sources. Heart of system is photosensitive single-crystal
In Sb cell with long wave cutoff near 6μ .

1963

Weeks, T.M., Dosanjik, D.S.

Interaction between an advancing shock wave and opposing jet flow.

AIAA Journal, v. 1, n. 7, July 1963, p. 1527-1533

Applied Mechanics Reviews, v. 17, n. 4, April 1964, p. 312

Interaction experimentally studied in shock tube, using schlieren and interferometric methods. Distorted shock wave shape resembles the jet velocity profile. Behind the shock a series of attenuating density fluctuations has been revealed.

Wheeler, W.H.

Ceramic radiative heat shields.

Ceramics Age, v. 79, n. 10, October 1963, p. 161-164

Engineering Index, January 1964, p. 177

Promising materials are low density ceramic foams, laminated composites, high density materials with high strength and high refractories, and resin impregnated porous ceramics.

Whetstone, C.R.

Miniature closed-cycle cooler produces 25°K reliably.

Electronics, v. 36, December 27, 1963, p. 46-47

Applied Science and Technology Index, v. 52, n. 6, June 1964 p. 318

Works on modified Stirling cycle; closed-cycle system has cooling capacity of 12 watts at 77°K with rotary input of 100 watts. Illustrated well.

Zumwalt, G.W., Tang, H.H.

Mach number independence of the conical shock pressure coefficient.

AIAA Journal, v. 1, n. 10, October 1963, p. 2389-2391

Applied Mechanics Reviews, v. 17, n. 2, February 1964, p. 135

Examination of computed ratios of pressure rise to dynamic shocks attached to the vortex of an unyawed cone shows that hypersonic similitude persists down to Mach 3 for cone angles of 42 degrees or even lower for smaller angles.

1962

Anonymous

Strain Gage Readings.

Stein Engineering Services Publication, v. 5, April 1962-March 1963,

Stein Engineering Services, Inc., 5602 East Monte Rosa, Phoenix 18, Arizona

Publication devoted to resistance strain gages, strain gage based transducers and associated instrumentation. Contains reviews and digests of latest literature, articles on technology and Index.

1962

Bertram, M.H., etc.

Aerodynamics of hypersonic cruising and boost vehicles.

NASA-University Conference on Science and Technology of Space
Exploration-Proceedings, v. 2, November 1962, p. 215-234
Engineering Index, May 1964, p. 3

Problems of efficient hypersonic flight of boost glide
and air breathing vehicles in areas of aerodynamics,
stability and control, heating, and air ingestion; problems
of interference between major vehicle components.

Burke, A.F., Curtis, J.T.

Blunt-cone pressure distributions at hypersonic Mach numbers.

Journal of Aerospace Science, v. 29, Feb. 1962, p. 237-238
Applied Science and Technology Index, 1962, p. 13

Gardner, A.R.

Beat the heat with pyrolytic graphite.

Product Engineering, V. 33, January 22, 1962, p. 72-75
Applied Science and Technology Index, 1962, p. 556

Geiger, R.E.

Experimental lift and drag of a series of glide configurations
at Mach numbers 12.6 and 17.5.

Journal of Aerospace Science, v. 29, April 1962, p. 410-419
Applied Science and Technology Index, 1962, p. 14

Greenberg, R.A.

Correlation of nose-bluntness-induced pressures on cylindrical
and conical afterbodies at hypersonic speeds.

Journal of Aerospace Science, v. 29, March 1962, p. 359-360
Applied Science and Technology Index, 1962, p. 14

Jonash, E.R., Tomazic, W.A.

Current research and development on thrust chambers.

NASA-University Conference on Science and Technology of Space
Exploration, Proceedings, v. 2, Nov. 1962, p. 43-52
Engineering Index, May 1964, p. 154.

Present state of art of chemical rocket thrust chamber. One
of principle problems covered is adequate cooling to maintain
structural stability of chamber. 24 refs.

Korkan, K.D.

Stagnation point velocity gradient on two-dimensional and axisymmetric
bodies in hypersonic flow.

ARS Journal, v. 32, December 1962, p. 1924-1925
Applied Science and Technology Index, 1963, p. 16

1962

Levin, A.D.

Influence of drag during boost on rocket vehicle performance.
American Rocket Society Journal, October 1962, p. 1620-1621
STAR Reports, v. 1, p. 1, January 8 to March 23, 1963, p. 150
Complete investigation covered the range of (thrust-to-weight ratio) 1. from 1.25 to 2.00 and (thrust-to-weight ratio) 2. from 0.75 to 2.00. Effect of drag during boost reduced payload-to-gross-weight ratio by about 0.002

Roberts, L.

Ablating materials for atmospheric entry.
NASA-University Conference on Science and Technology of Space Exploration, v. 2, Nov. 1962, p. 461-8
Engineering Index, May 1964, p. 177
Some of more important concepts of thermal protection by ablation described and extent of progress made in materials research. Some of materials successfully flight tested are listed. 30 refs.

Rozycki, R.C., Fenster, S.J.

Stagnation-point heat transfer in partially ionized air.
Journal of Aerospace Science, v. 29, December 1962, p. 1490
Applied Science and Technology Index, 1963, p. 632

Sparrow, E.M., Eckert, R.G.

Radiant interaction between fin and base surfaces
ASME Transactions, ser C, v. 84, February 1962, p. 12-18
Applied Science and Technology Index, v. 962, p. 556

Wan, K.S.

The inviscid flow field in the wake of hypersonic bodies.
Journal of Aerospace Science, v. 29, n. 12, December 1962, p. 1488-1489
Applied Mechanics Reviews, v. 17, n. 3, March 1964, p. 230

White, F.M.

Hypersonic laminar viscous interactions on inclined flat plates.
ARS Journal, v. 32, May 1962, p. 780-781
Applied Science and Technology Index, 1962, p. 14

Wilson, M.R., Wittliff, C.E.

Low density stagnation point heat transfer measurements in the hypersonic shock tunnel.
ARS Journal, v. 32, February 1962, p. 275-276
Applied Science and Technology Index, 1962, p. 14

- 1961 Hauser, R.L.
 Abaltive coatings.
 Materials in Design Engineering, v. 54, November 1961, p. 135-137
 Applied Science and Technology Index, 1962, p. 556
- Holt, M.
 Direct calculation of pressure distribution on blunt hypersonic nose shapes with sharp corners.
 Journal of Aerospace Science, v. 28, November 1961, p. 872-876
- Pitts, J.W., Moore, D.G.
 Development of high temperature strain gages.
 National Bureau of Standards Monograph, n. 26, March 17, 1961, 20 p.
 Main Library Card File
 Ceramic and metal components evaluated in the program for improvement of strain gages. 18 refs.
- 1959 Portnoy, H.
 The drag of ducted bodies with annular or side intakes in supersonic flow.
 Aeronautical Quarterly, v. 10, August, 1959, p. 283-295
 Main Library Card File (Supersonic Speeds)
- 1958 Fay, J.A., Riddell, F.R.
 Theory of stagnation point heat transfer in dissociated air.
 Journal of Aerospace Science, v. 25, February 1958, p. 73-85, 121
 Main Library Card File (Aerodynamics)
 Process at hypersonic velocities complicated by two features not normally present at low velocities.
- 1956 Cartright, E.M., Jr.
 Some aerodynamic considerations of nozzle-afterbody combinations.
 Aeronautical Engineering Review, v. 15, September 1956, p. 59-65
 Main Library Card File (Aerodynamics)
 Review of manner in which jet-stream interactions affect thrust and drag of various nozzle installations. 9 refs.
- 1955 Graham, E.W. etc.
 Drag of non-planer thickness distributions in supersonic flow.
 Aeronautical Quarterly, v. 6, May 1955, p. 99-113
 Main Library Card File (Supersonic speeds)
 Thickness drag is considered and the interference effects caused by lift and side force are discussed.
- 1953 Ripperger, E.A.
 The propagation of pulses in cylindrical bars-an experimental study.
 First Midwestern Conference on Solid Mechanics Proceedings, 1953, p. 29-39
 Main Library Card File.
 Measurements of the pulse amplitudes as a function of time at selected points along the length of a bar were made by means of piezoelectric strain gages.

PAMPHLETS

- 1964 Blackstock, T.A., Ladson, C.L.
Comparison of the hypersonic aerodynamic characteristics of some simple winged shapes in air and helium.
NASA Technical Notes, June 1964, 40 pp. (TND-2328)
Investigation made at Mach numbers of 6.8 and 9.6 in air and 10.9 and 18.0 in helium. Planforms were square and delta with angle of attacks from 0° to 25° . Experimental values of lift and drag coefficients and lift-drag ratio.
- Bogdan, L.
High-temperature, thin-film resistance thermometers for heat transfer measurement.
NASA Contractors Report, April 1964, 24 pp. (CR-26)
Thin-film resistance thermometer of platinum-alloy film deposited on a pyrex substrate.
- Bogdan, L.
Measurement of radiative heat transfer with thin-film resistance thermometers.
NASA Contractors Report, March 1964, 39 p.p. (CR-27)
The use of a dual-element thin-film resistance thermometer for simultaneous measurement of convective and radiative components of heat transfer. Platinum alloy films deposited on substrates of fused quartz.
- Fischel, J., Webb, L.D.
Flight-information sensors, display and space control of the X-15 airplane for atmospheric and near-space flight.
NASA Technical Notes, August 1964, 32 p.p. (TND-2407)
- Garcia, F.S.
An aerodynamic analysis of Saturn I Block I flight test vehicles.
NASA Technical Notes, February 1964, 57 p.p. (TND-2002)
Evaluation of telemetered data included axial force calculations stability analysis, and environmental steady-state and fluctuating pressure data analysis.
- Graves, R.A., Jr., Walton, T.E., Jr.
Free-flight test results on the performance of cork as a thermal protection material.
NASA Technical Notes, September 1964, 40 p.p. (TND-2438)
Series of flight tests conducted aboard NASA flight vehicles in the low-heating-rate environment of the afterbody regions at altitudes of 482,000 ft. and velocities to 17,900 fps.

- 1964 Haller, G.C.
Comparison of heat-rejection and weight characteristics of several radiator fin tube configurations.
NASA Technical Notes, July 1964, 34 p.p. (TND-2385)
Configurations consisting of central fin and tube, an open-sandwich fin and tube without fillet, two open-sandwich designs with fillets, and closed sandwich fin with tube.
Radiator planform area and fin thickness also investigated.
- Hicks, R.M., Hopkins, E.J.
Effects of spanwise variation of leading-edge sweep on the lift, drag, and pitching moment of a wing-body combination at Mach numbers from 0.7 to 2.94.
NASA Technical Notes, April 1964, 53 p.p. (TND-2236)
Four wing-body combinations used. Ogee, modified trapezoidal, triangular and trapezoidal configurations.
- Howe, J. T., Shaaffer, Y.S.
Mass addition in the stagnation region for velocity up to 50,000 fps.
NASA Technical Report, August 1964, 52 p.p. (TRR-207)
Main Library Card File.
- Keyes, J.W.
Longitudinal aerodynamics characteristics of blunted cones at Mach numbers of 3.5, 4.2 and 6.0.
NASA Technical Notes, February 1964, 62 p.p. (TND-2201)
Complete table of drag coefficient, lift coefficient etc. for various forms and Mach numbers.
- Lyon, R.H., Maidanik, G.
Review of some recent research on noise and structural vibration.
NASA Technical Notes, April 1964, 47 p.p. (TND-2266)
Noise transmission through structural panels, sound radiation from a machine housing and transmission of vibrational energy from one structural element to another.
- Penland, J.A.
A study of the stability and location of the center of pressure on sharp, right circular cones at hypersonic speeds.
NASA Technical Notes, May 1964, 33p.p. (TND-2283)
Data obtained on various models at Mach number of 6.8 and a Reynold's number of 0.22×10^6 /in. Results of tests are in the -3° to 30° angle-of-attack range and include lift, drag, lift-drag ratio, pitching moment, normal force and axial force.
- Pride, R.A., etc.
Design, tests and analysis of a hot structure for lifting re-entry vehicles.
NASA Technical Notes, April 1964, 149 p.p. (TND-2186)
Instrumentation consisted of strain gages, thermocouples, load cells, deflectometers and a transit.

1964

Raper, J.L., etc.

Detailed description and flight performance of Ram B vehicle.

NASA Technical Notes, September 1964, 97 p.p. (TND-2437)

Total of 75 measurements taken of transverse acceleration, thrust and drag acceleration, skin temps., differential pressure for angle of attack, vibration etc.

Saltzman, E.J.

Base pressure coefficients obtained from X-15 airplane for Mach numbers up to 6.

NASA Technical Notes, August 1964, A5 p.p. (TND-2420)

Power-off and power-on base pressure measured on X-15 compared with wind-tunnel data, semi-empirical estimates and theory.

Spencer, B. etc

Supersonic aerodynamic characteristics of a series of bodies having variations in fineness ratio and cross-section ellipticity.

NASA Technical Notes, August 1964, 76 p.p. (TND-2389)

Series of 2/3-power low-wave-drag bodies at Mach numbers of from 1.50 to 2.86. Reynolds number per foot was held at constant 2.75×10^6 .

Stallings, R.L., Jr., Burbank, P.B. etc.

Heat transfer and pressure measurements on delta wings at Mach numbers of 3.51 and 4.65, angles of attack from -45° to 45°

NASA Technical Notes, August 1964, 176 p.p. (TND-2387)

Staylor, W.F., Goldberg, T.J.

Afterbody pressures on two-dimensional boattailed bodies having turbulent boundary layers at Mach 5.98.

NASA Technical Notes, July 1964, 36 p.p. (TND-2350)

Modification and extensions of previous work and gives good estimate for existing base-pressure data. Empirical estimation of boattail pressures made possible predictions of afterbody drag. Models tested at free stream Mach number of 5.98, surface Mach numbers ranging from 3 to 7.

Suddath, J.H., Oehman, W.I.

Minimum drag bodies having cross-sectional ellipticity.

NASA Technical Notes, September 1964, 26 p.p. (TND-2432)

Newtonian flow theory and the calculus of variations were used to study minimum drag shapes at hypersonic speeds and zero angle of attack.

Walton, T.E., Jr.

Free-flight investigation of mass-transfer cooling on a blunt cone to a Mach number of 10.6.

NASA Technical Notes, April 1964, 36 p.p. (TND-2197)

Nitrogen coolant allowed to flow tangentially back over conical afterbody to cool stagnation region. Telemetry monitored pressure, temperature; normal, transverse, thrust and drag accelerations.

1963

Charczenko, N., Hayes, C.

Jet effects at supersonic speeds on base and afterbody pressures of a missile model having single and multiple jets.

NASA Technical Notes, November 1963, 40 p.p. (TND-2077)

Tests performed at Mach numbers of 2.30, 2.95, 4.00 and 4.65, angles of attack of 0° . Pressure measurements on afterbody from orifices through scanning press. valves with $5\#/in^2$ transducers and jet exit pressures measured with $25\#/in^2$ transducers.

Charczenko, N., Hennessey, K.W.

Investigation of a retrorocket exhausting from the nose of a blunt body into a supersonic free stream.

NASA Technical Notes, D751, September 1961, 30 p.p.

Space Science and Technology, v. 1, 1963, John Wiley & Sons Inc., New York.

Pressure distribution and pressure drag of a blunt body with a supersonic jet issuing upstream from its center. Mach numbers of 1.60, 2.00 & 2.85.

Clark, F.L., Johnson, C.B.

Real-gas hypersonic nozzle flow parameters for nitrogen in the thermodynamic equilibrium.

NASA TND-2019, November 1963, 19 p.p.

Applied Mechanics Reviews, v. 17, n. 1, January 1964, p. 48

Study covered a range of stagnation pressures up to 1000 atmospheres and stagnation temperatures from 1800° to $5000^\circ R$.

Glawe, G.E., etc.

A steady-state, stagnation-point, heat-transfer-rate measuring device.

NASA Technical Notes, May 1963, 16 p.p. (TND-1704)

Immersion type device made up of three disks sandwiched together, two end disks are of different material than center disk forming thermocouple junctions.

Lucas, J.G., Golladay, R.L.

An experimental investigation of gaseous-film cooling of a rocket motor.

NASA Technical Notes, October 1963, 30 p.p. (TND-1988)

Hot-gas velocities encountered by the film at the injection point were in the range 600 to 700 fps and along nozzle wall 3000 fps in throat region. Hot-gas total temp. at injection point was about $4760^\circ R$.

1963

Maglieri, D.J., etc.

In-flight shock-wave pressure measurements above and below a bomber airplane at Mach numbers from 1.42 to 1.69.

NASA Technical Notes, October 1963, 46 p.p. (TND-1968)

Applied Mechanics Reviews, v. 17, n. 1, January 1964, p. 57

Measurements made at 1,300 to 2,000 feet above and below and also 4,600 to 9,100 feet below. Detailed description of unique instrumentation probe used along with corresponding static and wind-tunnel calibrations.

Spencer, B., Jr., Phillips, W.P.

Effects of cross-section shape on the low-speed aerodynamic characteristics of a low-wave-drag hypersonic body.

NASA Technical Notes, October 1963, 38 p.p. (TND-1963)

Investigations have indicated considerable improvement in maximum lift-drag ratio and lift-curve slope.

Tereniak, W.B., Clevenson, S.A.

Flight shock and vibration data of the Echo A-12 application vertical tests.

NASA Technical Notes, October 1963, 22 p.p. (TND-1908)

Main Library Card File

Data as measured at base of spacecraft adapter during the flights of Echo A-12. Also included are data obtained from a vibration survey performed on equipment prior to flight.

1962

Crandall, S. H.

On scaling laws for material damping.

NASA Technical Notes, December 1962, 25 p.p. (TND-1467)

STAR Reports, v.1. p. 1, Jan. 8 to March 23, 1963, p. 141

Similarity analysis made to provide scaling laws which indicate the effects of amplitude, frequency, and material properties on the resonant damping of structural members due to internal material properties. Data on steel, brass and aluminum cantilever beams.

1961

Shea, J.T., Baumann, R.C.

Vanguard I Satellite structure and separation mechanism.

NASA Technical Notes, March 1961, 15 p.p. (TND-495)

Space Science & Technology Guide, (016.629F945G), p. 61

Test results for both satellite and separating mechanism are considered.

Stoney, W.E., Jr.

Collection of zero-lift drag data on bodies of revolution from free-flight investigations.

NASA Technical Report, 1961, 188 p.p. (TRR-100)

Main Library Card File.

Mach number range extends from 0.6 to approximately 2.0 and Reynolds numbers based on body length from 2×10^6 to 100×10^6 .

1960

Eldridge, E.A., Deem, H.W.

Physical properties of metals and alloys.

ASTM Special Technical Publication #296, 1960, 206 p.p.

American Society for Testing Materials, 1916 Race St.

Philadelphia 3, Penn.

Main Library Card File (P165T296)

Report on physical properties from cryogenic to elevated temperatures.

(ASTM-ASME joint committee on effect of temp. on properties of metals)

Roberts, L.

An analysis of ablation shield requirements for manned re-entry vehicles.

NASA Technical Report 1960, 25 pp. (TR-62)

Main Library Card File.

Problem of sublimation of material and accumulation of heat in an ablation shield analysed. 10 refs.

1959

Bertram, M.H.

Boundary-layer displacement effects in air at Mach numbers of 6.8 and 9.6

NASA Technical Reports, 1159, 32 p.p.

STAR Reports, v. 1, p. 2, April 8 - June 23, 1963, p. 811

Measurements are presented for pressure gradients induced by laminar boundary layer on a flat plate in air for a Mach number of 9.6 and for the drag of thin wings at a Mach number about 6.8 and zero angle of attack.

Cummings, H.N.

Qualitative aspects of fatigue of materials

WADC Technical Report, September 1959, 250 p.p. (P3249T59-230)

Main Library Card File.

Review of literature covering period May 1, 1958 to April 30, 1959

Krzywoblachi, M.Z.

Aerodynamic studies.

WADC Technical Note, January 1959, 101 p.p. (P3249N56-360 pt. 21)

Main Library Card File

A review of literature on the forces acting on an air vehicle covering the period July 1954 to September 1954. (pt. 19 covers July 1956 to Sept. 1956, pt. 24 covers Oct. 1957, to December 1957)

Books

- 1961 Shapiro, A.H.
Shape and flow; the fluid dynamics of drag.
Anchor Books, 1961, Garden City, N.Y.
Main Library Card File.
- 1958 Hoerner, S.F.
Fluid dynamic drag.
Published by Author, 1958, Midland Park, N.J.
Main Library Card File (Aerodynamics) (629.142H671F)
Practical information on aerodynamic drag and hydrodynamic
resistance.

REFERENCES AND BIBLIOGRAPHY

1. Finch, Thomas W., and Matranga, Gene J.: Launch, Low-Speed, and Landing Characteristics Determined From the First Flight of the North American X-15 Research Airplane. NASA TM X-195, 1959.
2. McKay, James M.: Measurements Obtained During the First Landing of the North American X-15 Research Airplane. NASA TM X-207, 1959.
3. Flight Research Center: Aerodynamic and Landing Measurements Obtained During the First Powered Flight of the North American X-15 Research Airplane. NASA TM X-269, 1960.
4. Walker, Harold J., and Wolowicz, Chester H.: Theoretical Stability Derivatives for the X-15 Research Airplane at Supersonic and Hypersonic Speeds Including a Comparison with Wind-Tunnel Results. NASA TM X-287, 1960.
5. Saltzman, Edwin J.: Preliminary Full-Scale Power-Off Drag of the X-15 Airplane for Mach Numbers From 0.7 to 3.1. NASA TM X-430, 1960.
6. Stillwell, Wendell H., and Larson, Terry J.: Measurement of the Maximum Speed Attained by the X-15 Airplane Powered With Interim Rocket Engines. NASA TN D-615, 1960.
7. Stillwell, Wendell H., and Larson, Terry J.: Measurement of the Maximum Altitude Attained by the X-15 Airplane Powered With Interim Rocket Engines. NASA TN D-623, 1960.
8. Matranga, Gene J.: Launch Characteristics of the X-15 Research Airplane Determined in Flight. NASA TN D-723, 1961.
9. Reed, Robert D., and Watts, Joe D.: Skin and Structural Temperatures Measured on the X-15 Airplane During a Flight to a Mach Number of 3.3. NASA TM X-468, 1961.
10. McKay, James M., and Scott, Betty J.: Landing-Gear Behavior During Touchdown and Runout for 17 Landings of the X-15 Research Airplane. NASA TM X-518, 1961.
11. Holleman, Euclid C., and Reisert, Donald: Controllability of the X-15 Research Airplane With Interim Engines During High-Altitude Flights. NASA TM X-514, 1961

12. Saltzman, Edwin J.: Preliminary Base Pressures Obtained From the X-15 Airplane at Mach Numbers From 1.1 to 3.2. NASA TN D-1056, 1961.
13. Matranga, Gene J.: Analysis of X-15 Landing Approach and Flare Characteristics Determined From the First 30 Flights. NASA TN D-1057, 1961.
14. Taylor, Lawrence W., Jr.: Analysis of a Pilot-Airplane Lateral Instability Experienced with the X-15 Airplane. NASA TN D-1059, 1961.
15. Yancey, Roxanah B., Rediess, Herman A., and Robinson, Glenn H.: Aerodynamic-Derivative Characteristics of the X-15 Research Airplane as Determined From Flight Tests for Mach Numbers From 0.6 to 3.4. NASA TN D-1060, 1962.
16. Kordes, Eldon E., and Noll, Richard B.: Flight Flutter Results for Flat Rectangular Panels. NASA TN D-1058, 1962 .
17. Taylor, Lawrence W., Jr., and Merrick, George B.: X-15 Airplane Stability Augmentation System. NASA TN D-1157, 1962.
18. Jordan, Gareth H., McLeod, Norman J., and Guy, Lawrence D.: Structural Dynamic Experience of the X-15 Airplane. NASA TN D-1158, 1962.
19. Hoey, Robert G., and Day, Richard E.: Mission Planning and Operational Procedures for the X-15 Airplane. NASA TN D-1159, 1962.
20. Banner, Richard D., Kuhl, Albert E., and Quinn, Robert D.: Preliminary Results of Aerodynamic Heating Studies on the X-15 Airplane. NASA TM X-638, 1962.
21. McKay, James M., and Kordes, Eldon E.: Landing Loads and Dynamics of the X-15 Airplane. NASA TM X-639, 1962.
22. Kordes, Eldon E., Reed, Robert D., and Dawdy, Alpha L.: Structural Heating Experiences on the X-15 Airplane. NASA TM X-711, 1962.
23. Keener, Earl R., and Pembo, Chris: Aerodynamic Forces on Components of the X-15 Airplane. NASA TM X-712, 1962.
24. Hopkins, Edward J., Fetterman, David E., Jr., and Saltzman, Edwin J.: Comparison of Full-Scale Lift and Drag Characteristics of the X-15 Airplane With Wind-Tunnel Results and Theory. NASA TM X-713, 1962.

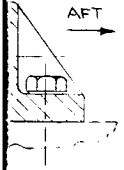
25. Walker, Harold J., and Wolowicz, Chester H.: Stability and Control Derivative Characteristics of the X-15 Airplane. NASA TM X-714, 1962.
26. White, Robert M., Robinson, Glenn H., and Matranga, Gene J.: Resume of Handling Qualities of the X-15 Airplane. NASA TM X-715, 1962.
27. Peterson, Forrest S., Rediess, Herman A., and Weil, Joseph: Lateral-Directional Control Characteristics of the X-15 Airplane. NASA TM X-726, 1962.
28. Weil, Joseph: Review of the X-15 Program. NASA TN D-1278, 1962.
29. Tremant, Robert A.: Operational Experiences and Characteristics of the X-15 Flight Control System. NASA TN D-1402, 1962.
30. Larson, Terry, J., and Webb, Lannie D.: Calibrations and Comparisons of Pressure-Type Airspeed-Altitude Systems of the X-15 Airplane From Subsonic to High Supersonic Speeds. NASA TN D-1724, 1963.
31. Noll, Richard B., and Halasey, Robert L.: Theoretical Investigation of the Slideout Dynamics of a Vehicle Equipped with a Tricycle Skid-Type Landing-Gear System. NASA TN D-1828, 1963.
32. Watts, Joe D., and Banas, Ronald P.: X-15 Structural Temperature Measurements and Calculations for Flights to Maximum Mach Numbers of Approximately 4, 5, and 6. NASA TM X-883, 1963.
33. Noll, Richard B., Jarvis, Calvin R., Pembo, Chris, Lock, Wilton P., and Scott, Betty J.: Aerodynamic and Control-System Contributions to the X-15 Airplane Landing-Gear Loads. NASA TN D-2090, 1963.
34. Pyle, Jon S.: Comparison of Flight Pressure Measurements With Wind-Tunnel Data and Theory for the Forward Fuselage of the X-15 Airplane at Mach Numbers from 0.8 to 6.0. NASA TN D-2241, 1963.
35. Quinn, Robert D., and Kuhl, Albert E.: Comparison of Flight-Measured and Calculated Turbulent Heat Transfer on the X-15 Airplane at Mach Numbers from 2.5 to 6.0 at Low Angles of Attack. NASA TM X-939, 1964.
36. Holleman, Euclid C.: Piloting Experience During the Boost of the X-15 Airplane to High Altitude. NASA TN D-2289, 1964.

37. Maher, James F., Jr., Ottinger, C. Wayne, and Cepasso, Vincent N., Jr.: YLR99-RM-1 Rocket Engine Operating Experience in the X-15 Aircraft. NASA TN D-2391, 1964.
38. Saltzman, Edwin, J.: Flight Base Pressure Coefficients Obtained from the X-15 Airplane for Mach Numbers Up to 6. NASA TN D-2420, 1964.
39. Fischel, Jack, and Webb, Lannie D.: Flight-Information Sensors, Display, and Space Control of the X-15 Airplane for Atmospheric and Near-Space Flight Missions. NASA TN D-2407, 1964.
40. Schaevitz Engineering - Pennsauken, N. J.: A Flight Thrustmeter for Turbojet Engines. TR-100 - Nov. 27, 1961.
41. Flui Dyne Engineering Corporation - Minneapolis, Minnesota.: Force Measurements with the Flex-Cell. M-3519-2-5M-61.
42. Fox, G. R., and Sneck, H. J.: Gaseous Slider Investigation for High Speed Track Vehicles, TIS Report 60GL195, September 30, 1960.
43. Rippel, H. C.: Cost Bronze Hydrostatic Bearing Design Manual, Franklin Institute Laboratories, Philadelphia, Pa., 19103.
44. Mains, R. M.: The Practical Problems of Generating Large Stiffness or Flexibility Materials, ASME Paper 63WA268.

421D9

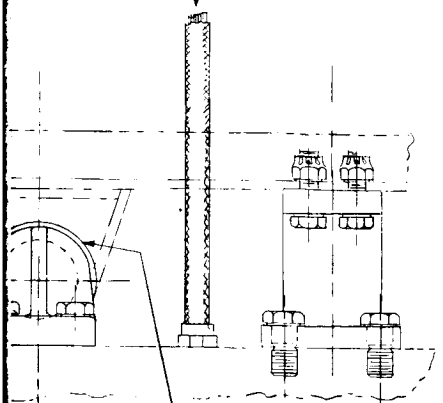
REVISIONS			
SYM	ZONE	DESCRIPTION	DATE
①		REMOVED ACCELEROMETERS	4 JAN 1962

ARGE
CYLINDER
SPACE FOR THERMAL EXPANSION



G
F
E
D
REV
421D905
D

RAMJET
INSTRUMENTATION
ELECTRICAL WIRES



NOTES:
1-ARRANGEMENT SHOWN REFERS TO
G.E. DWG. 587E430.

W AT C
NG FWD.)

JETTISON
CYLINDER

UNLESS OTHERWISE SPECIFIED DIMENSIONS ARE IN INCHES— TOLERANCES ON: 2-PLACE DECIMALS ± 3-PLACE DECIMALS ± ANGLES ± ALL SURFACES ✓ MATE JAL — GOVT OR COME GE	SIGNATURES		DATE	GENERAL ELECTRIC ADV. TECH. LABS. DEPT. LOC. SCHDY. TITLE (PRELIM. DESIGN CONCEPT) AFT DEFLECTION BLOCK ASSY. ARRANGEMENT I FIRST MADE FOR: X-15 RAMJET THRUST/DRAG INSTRUMENTATION CONTRACT NO. CODE IDENT NO. SIZE DWG NO. D 421D905 SCALE: HALF SIZE WT. CALC. ACTUAL SHEET OF
	DRAWN BY <i>R. H. Lewis</i>		BY <i>R. H. Lewis</i>	
	CHECKED	ISSUED	DATE	
	ENG'G	APPROVED	DATE	

5

4

3

2

1

G

F

E

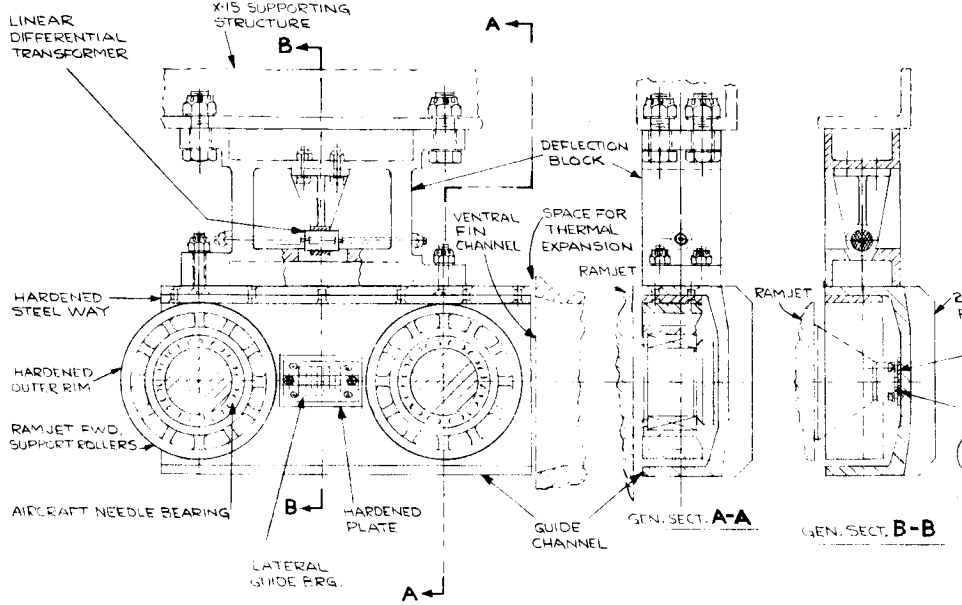
D

C

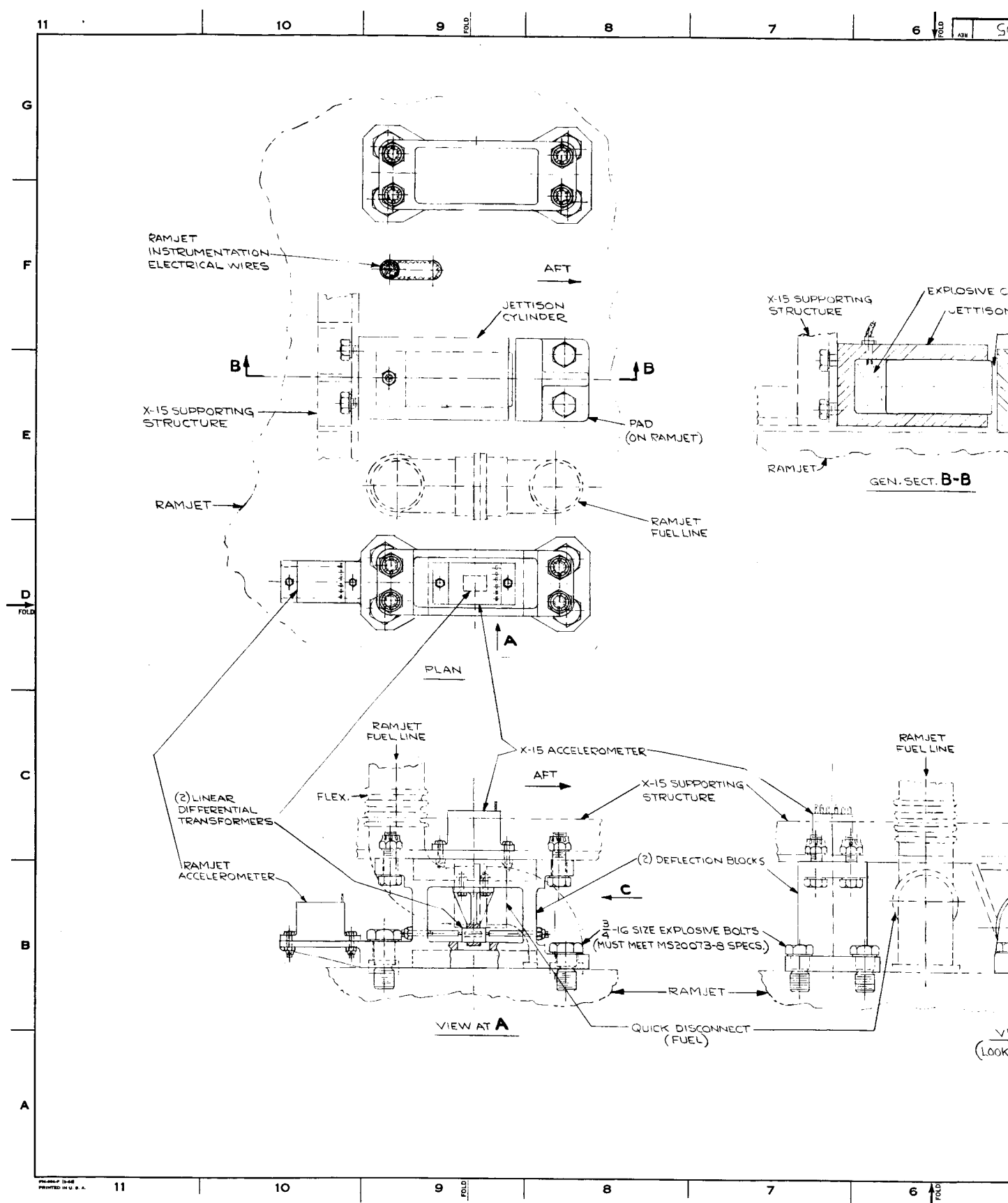
B

A

AFT
→



FWD. DEFLECTION BLOCK ARRANGEMENT

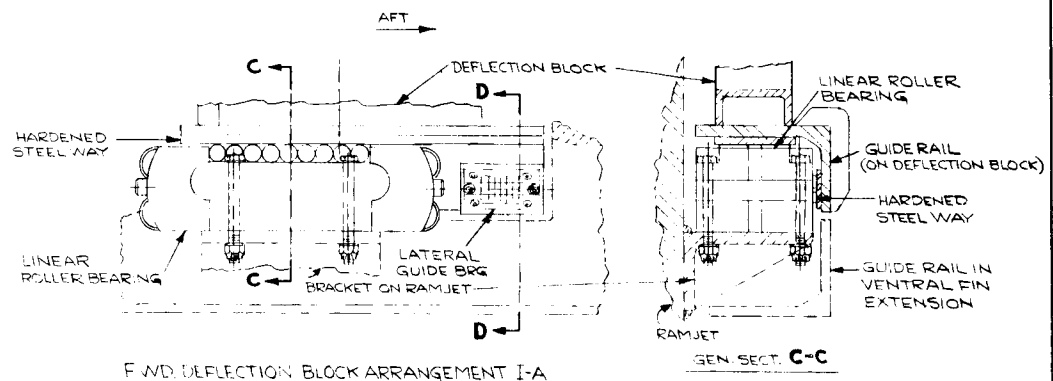


6 FOLD 4210892 D 325

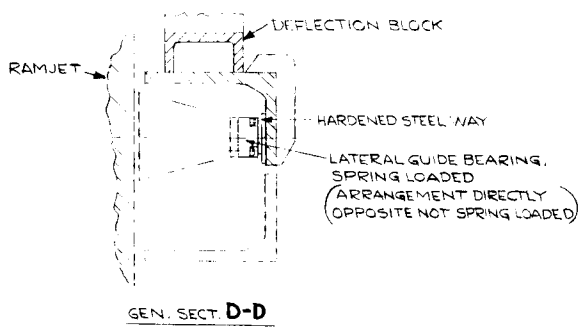
4 FOLD 3

2 1

REVISIONS				
SYM	ZONE	DESCRIPTION	DATE	APPROVED
1		REMOVED ACCELEROMETERS	4 JAN. 1965	<i>[Signature]</i>



FWD DEFLECTION BLOCK ARRANGEMENT I-A
(USING LINEAR ROLLER BEARING OTHERWISE)
SAME AS ARRANGEMENT I



GEN. SECT. D-D

NOTES:
1. ARRANGEMENTS SHOWN REFER TO
G.E. DWG. 587E430.

UNLESS OTHERWISE SPECIFIED DIMENSIONS ARE IN INCHES— TOLERANCES ON: 2-PLACE DECIMALS ± 3-PLACE DECIMALS ± ANGLES ± ALL SURFACES ✓ MATERIAL— GOVT OR COM.— GE—	SIGNATURES		DATE	GENERAL ELECTRIC	
	DRAWN <i>[Signature]</i>	CHECKED <i>[Signature]</i>	4 DEC. 1964	ADV. TECH. LABS., DEPT. LOC. SCHDY.	
	ISSUED <i>[Signature]</i>	ENGR. <i>[Signature]</i>	23 DEC. 1964	TITLE (PRELIM. DESIGN CONCEPT) FWD DEFLECTION BLOCK ASS'YS. ARRANGEMENT I	
	DATE	DATE	1964	First Max. Pos. X-15 RAMJET THRUST/DRAG INSTRUMENTATION	
CONTRACT NO.			CODE IDENT NO.	SIZE	DWG NO.
				D	4210892
SCALE: 1/2" SIZE			WT. CALC. ACTUAL	SHEET	OF

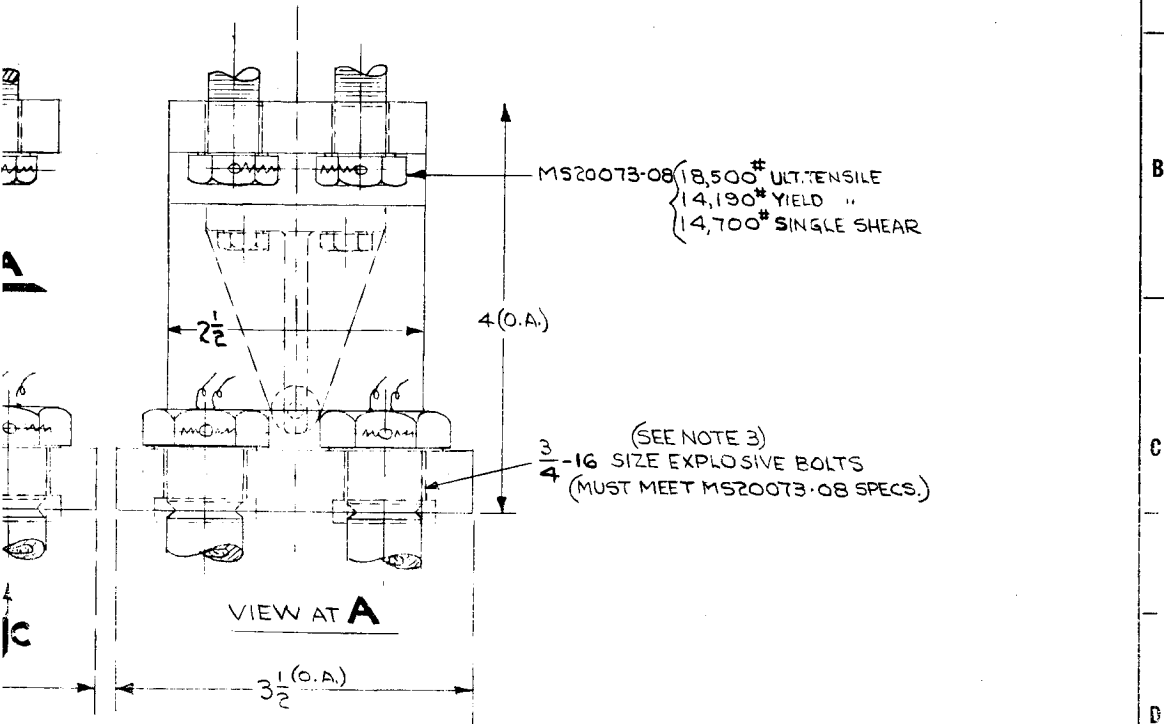
6 FOLD 5

4 FOLD 3

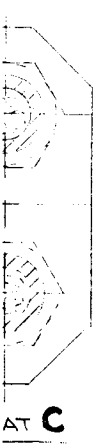
2 1

NOTES:

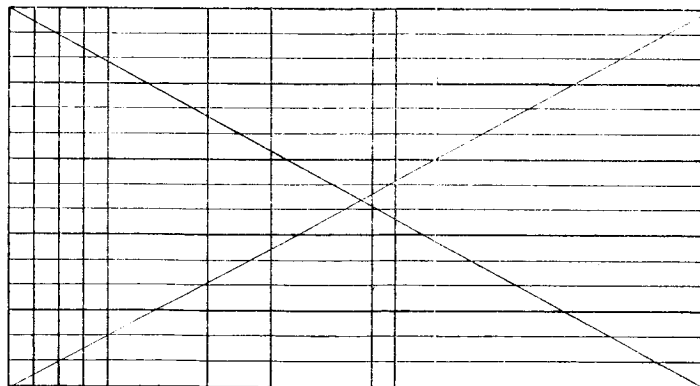
1. AFT DEFLECTION BLOCK SHOWN IS FOR ARRANGEMENT I ON G.E. DWG. 587E430.
2. MATERIAL REMOVAL FOR WEIGHT REDUCTION IS CONCEPTUAL (TO BE OPTIMIZED IN PHASE II STUDY).
3. VERTICAL MOVEMENT OF HEADS SHALL BE RESTRAINED WHEN BOLTS ARE EXPLODED TO PREVENT DAMAGE TO SURROUNDING COMPONENTS.



SCALE: FULL SIZE

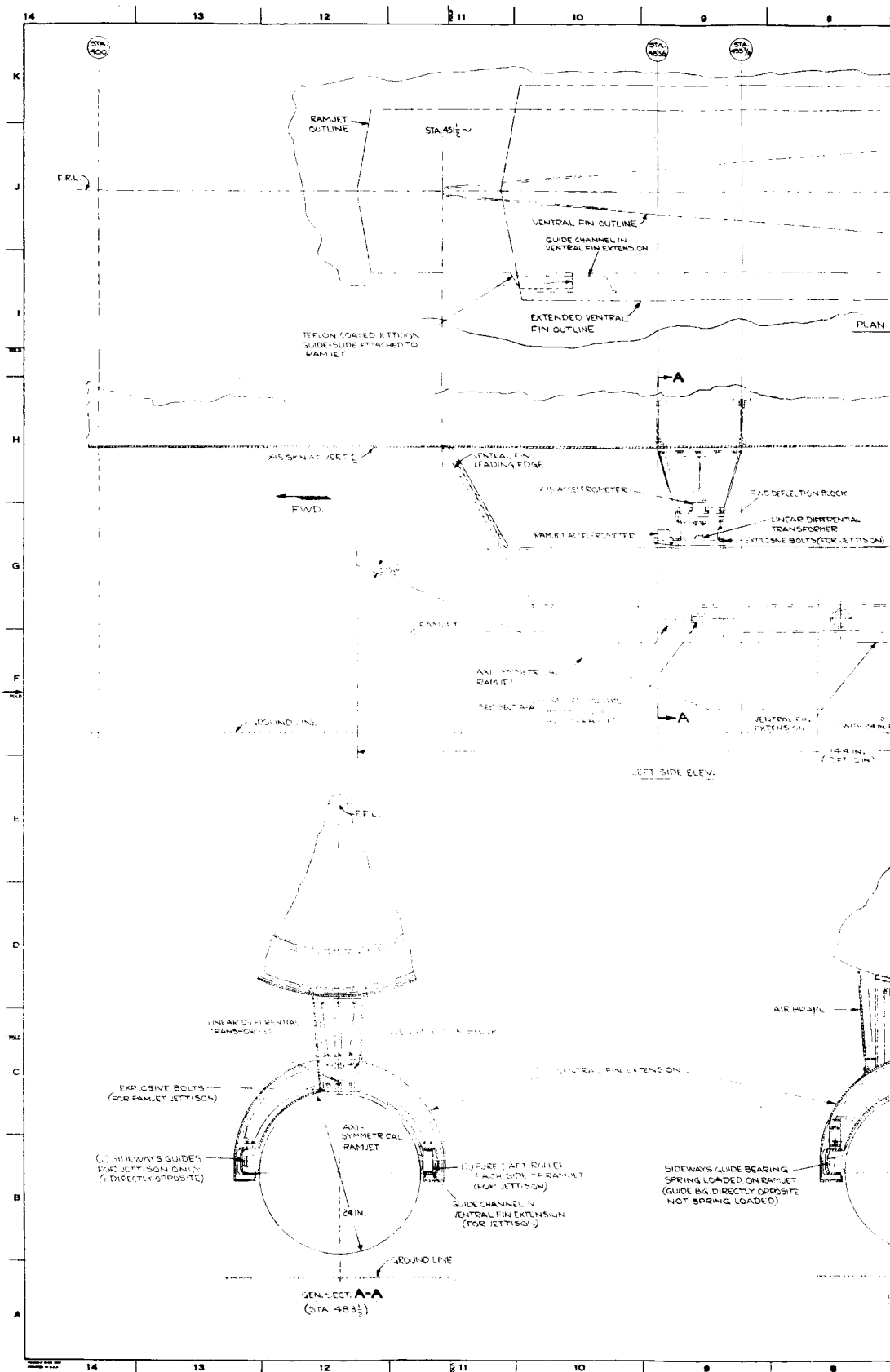


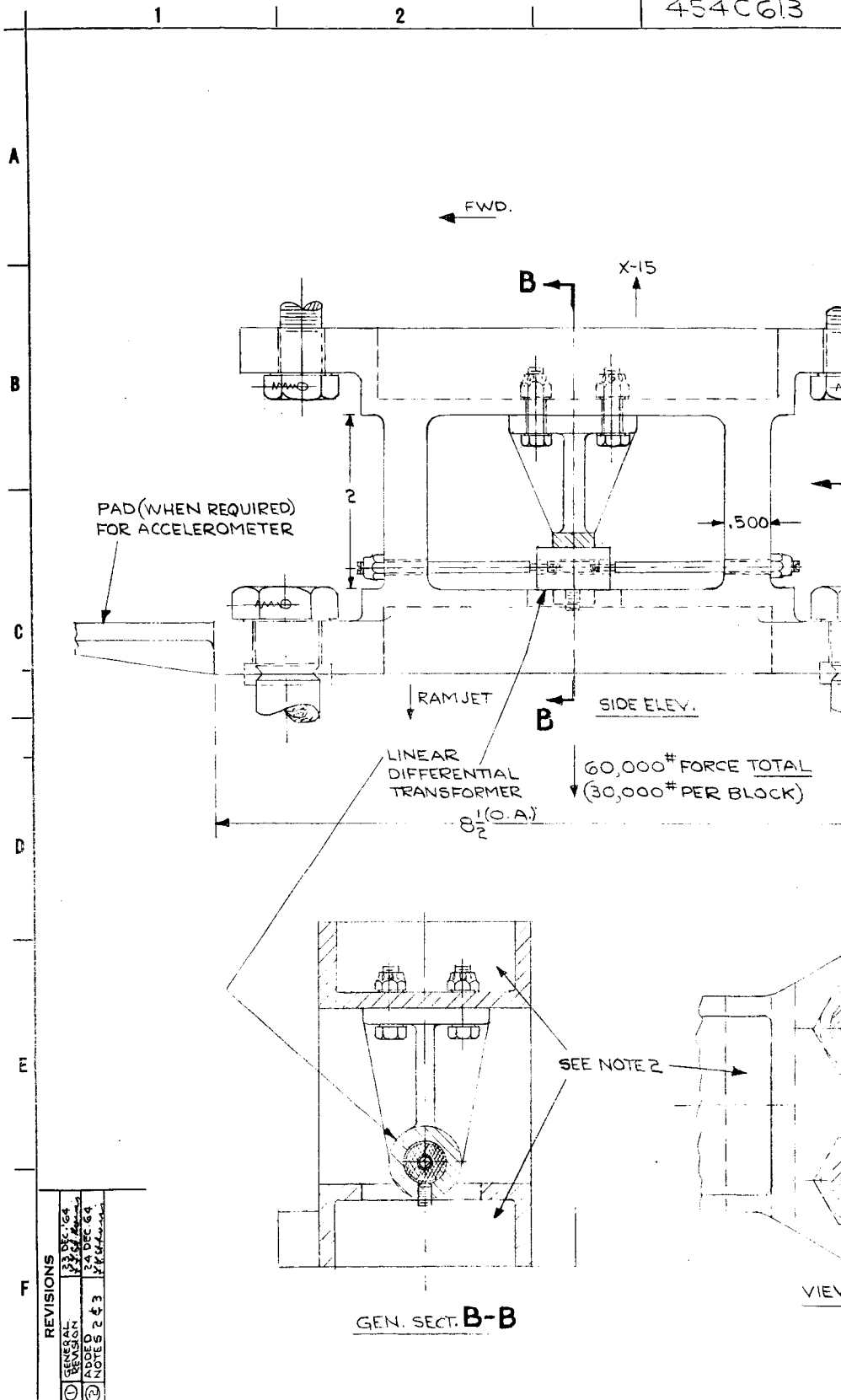
AT C



GROUP DESCR.	B. NO.	PRELIM. DESIGN CONCEPT AFT DEFLECTION BLOCK ARRANGEMENT (ARRANGEMENT I)	
	FIRST MADE FOR X-15 RAMJET THRUST/DRAG INSTRUMENTATION		
	BEGUN BY <i>J. J. Lewis</i> 24 NOV. 64 TRACED BY _____ FINISHED BY <i>J. J. Lewis</i> 1 DEC. 64 INSPECTED 1 DEC. 64 <i>MS</i> SF-2272		
GENERAL ATL-SCHDY		ELECTRIC WORKS	454CG13

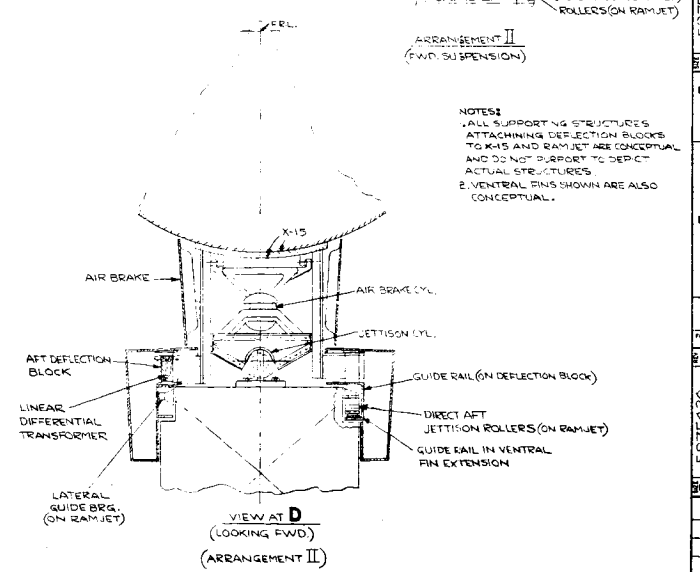
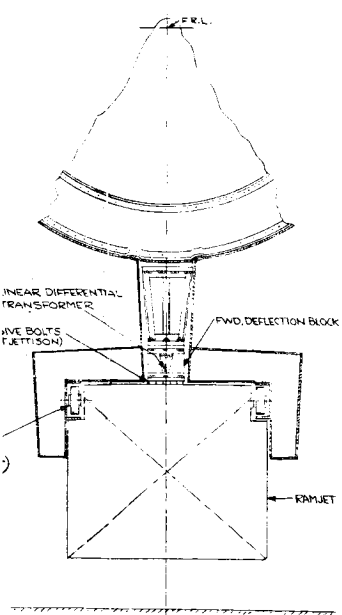
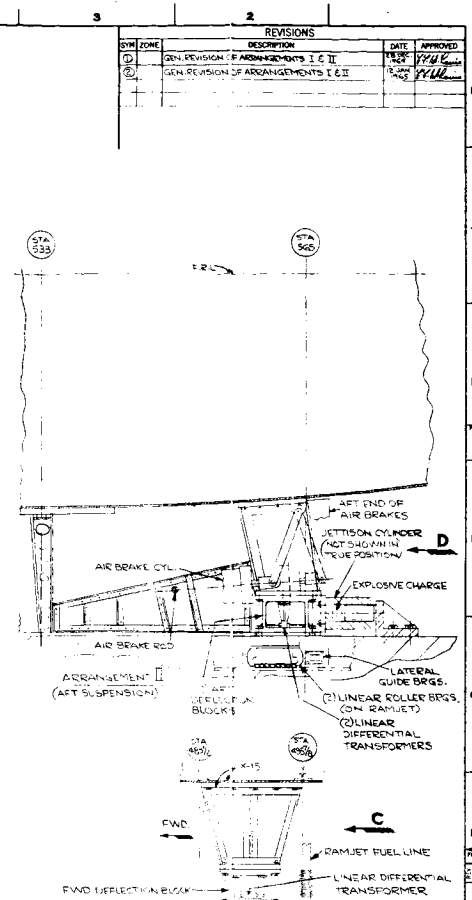
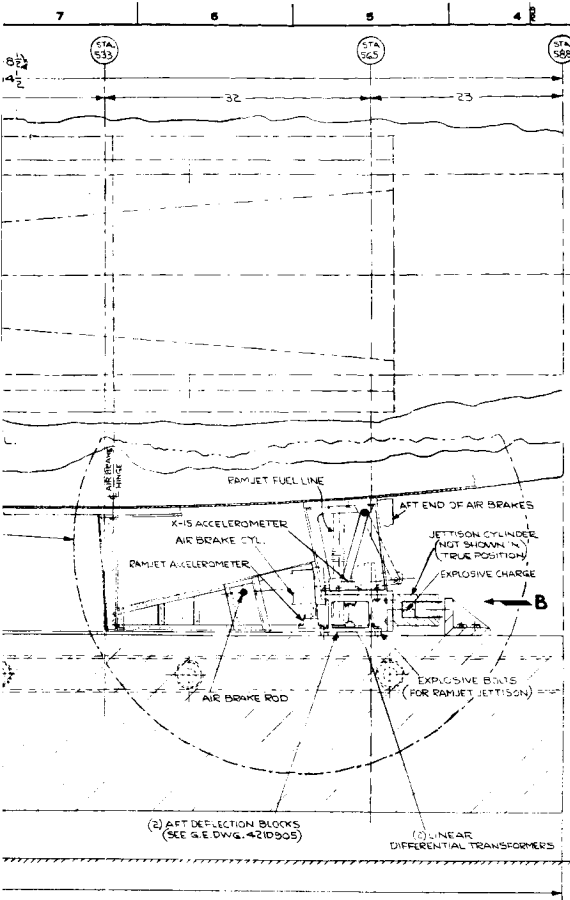
FIGS
11





REVISIONS	
①	GENERAL REVISION 13 DEC 64
②	NOTES 2 & 3 17 JAN 65

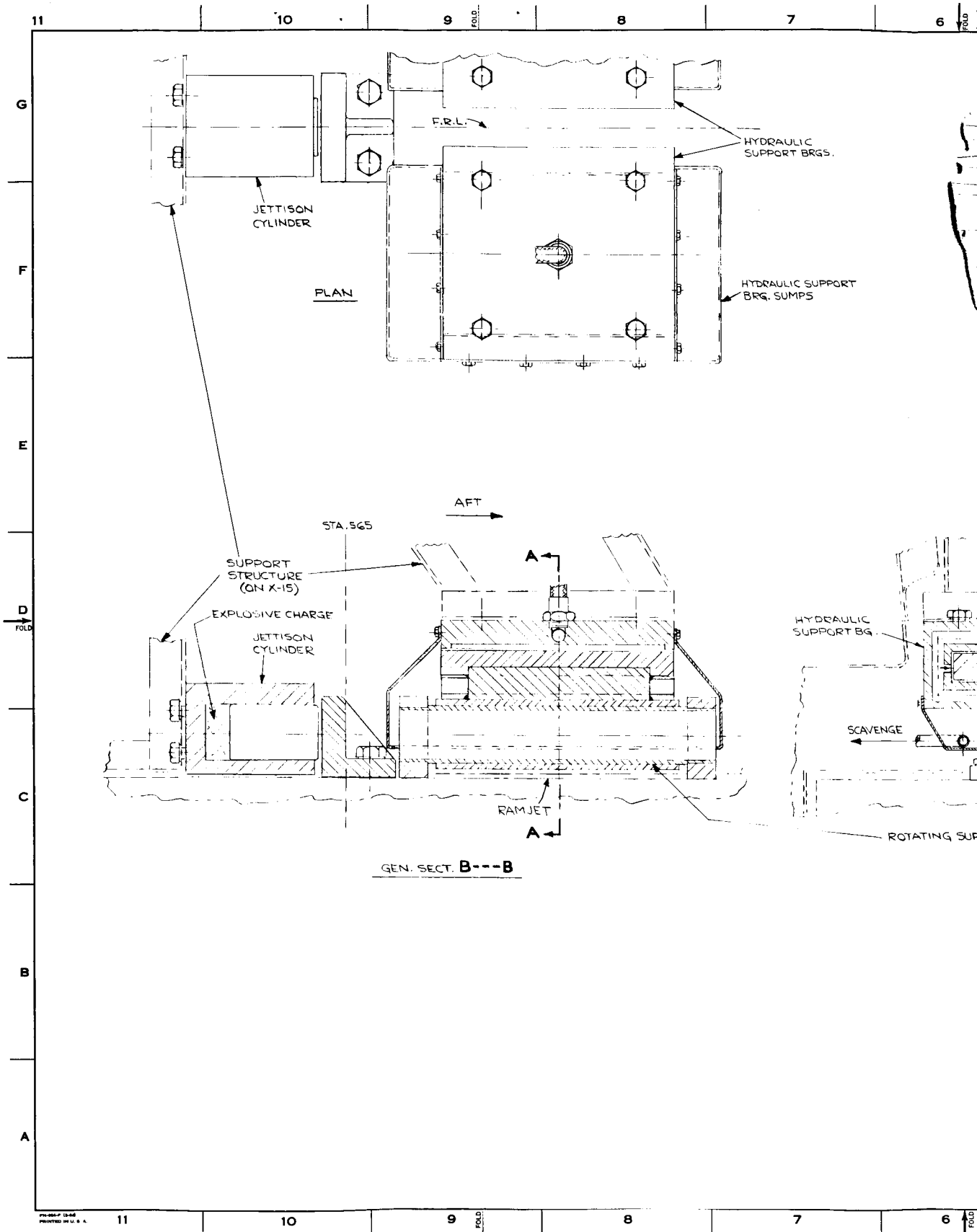
GEN. SECT. B-B

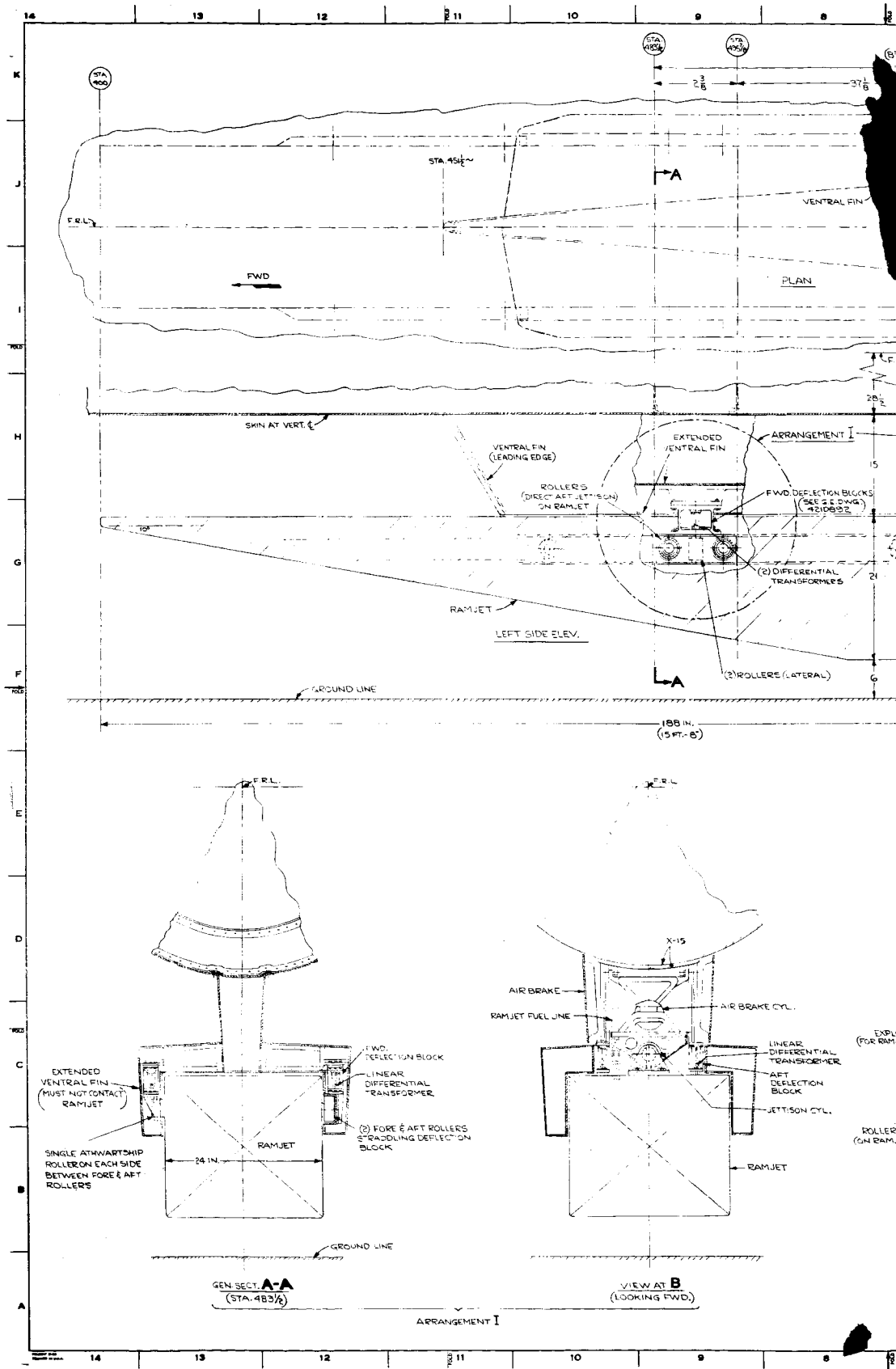


REV	ZONE	DESCRIPTION	DATE	APPROVED
1		GEN PHYSICAL ARRANGEMENTS I & II	1/24/54	[Signature]
2		GEN REVISION OF ARRANGEMENTS I & II	1/24/54	[Signature]

NOTES:
 1. ALL SUPPORTING STRUCTURES ATTACHING DEFLECTION BLOCKS TO X-15 AND RAMJET ARE CONCEPTUAL AND DO NOT PURPORT TO DEPICT ACTUAL STRUCTURES.
 2. VENTRAL PINS SHOWN ARE ALSO CONCEPTUAL.

UNLESS OTHERWISE SPECIFIED DIMENSIONS ARE IN INCHES—TOLERANCES ON PLACES DECIMALS ± ANGLES ±		SIGNATURES		DATE	GENERAL ELECTRIC AVIATION LABS. INC. SCH. BY
MATERIAL: 6061-T6 ALUM. PART OR SIM.		[Signature]		1/24/54	
CONTRACT NO.		TITLE		X-15 RAMJET THRUST/DRAG INSTRUMENTATION (DIRECT AFT JETTISON)	
CODE / REV. NO.		SIZE		DRAWING NO. 587E430	
SCALE 2 IN. = 1 FT.		BY		SHEET OF	





421D904

D 3216

4

3

2

1

REVISIONS				
SYM	ZONE	DESCRIPTION	DATE	APPROVED

G

F

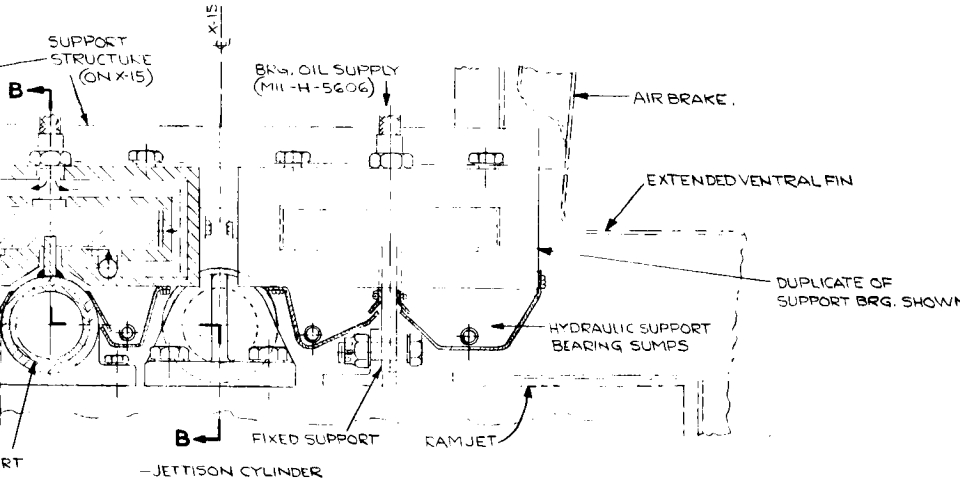
E

D

C

B

A



GEN. SECT. **A-A**
(LOOKING FWD.)

D 3216

D 3216

D 3216

D 3216

UNLESS OTHERWISE SPECIFIED DIMENSIONS ARE IN INCHES TOLERANCES ON: 2-PLACE DECIMALS ± 3-PLACE DECIMALS ± ANGLES ± ALL SURFACES ✓	DRAWN BY CHECKED BY <i>[Signature]</i>	DATE 18 DEC 1969	GENERAL ELECTRIC ADV. TECH. LABS. DEPT. LOC. SCH. DY. TITLE (PRELIM. DESIGN CONCEPT) AFT HYDRAULIC SUPPORT BEARING ARRANGEMENT FIRST MADE FOR X-15 RAMJET THRUST/DAG INSTRUMENTATION CONTRACT NO. CODE IDENT NO. SIZE DWG NO. D 421D904 SCALE: HALF SIZE WT. SAME AS ACTUAL SHEET OF
	ISSUED BY ENGRG. APPR. FILE	DATE 23 DEC 1969	
	MATERIAL - GOVT OR COM.	GE	
	SIGNATURES	DATE	

5

4

3

2

1

D 3216